ANL-6760
Instruments
(TID-4500, 22nd Ed.)
AEC Research and
Development Report

ARGONNE NATIONAL LABORATORY
9700 South Cass Avenue
Argonne, Illinois 60440

Mn^{56} COINCIDENCE COUNTING FACILITY

by

A. DeVolpi and K. G. A. Porges
Reactor Physics Division

and

R. N. Larsen
Electronics Division

August 1963

Operated by The University of Chicago
under
Contract W-31-109-eng-38
with the
U. S. Atomic Energy Commission

DISCLAIMER

This report was prepared as an account of work sponsored by an agency of the United States Government. Neither the United States Government nor any agency Thereof, nor any of their employees, makes any warranty, express or implied, or assumes any legal liability or responsibility for the accuracy, completeness, or usefulness of any information, apparatus, product, or process disclosed, or represents that its use would not infringe privately owned rights. Reference herein to any specific commercial product, process, or service by trade name, trademark, manufacturer, or otherwise does not necessarily constitute or imply its endorsement, recommendation, or favoring by the United States Government or any agency thereof. The views and opinions of authors expressed herein do not necessarily state or reflect those of the United States Government or any agency thereof.

DISCLAIMER

Portions of this document may be illegible in electronic image products. Images are produced from the best available original document.

TABLE OF CONTENTS

		Page
ABSTRACT		7
I.	INTRODUCTION	7
II.	DETECTION APPARATUS	11
	A. Gamma-Gamma System	11
	B. Beta-Gamma System	14
	C. Shielding	16
III.	SIGNAL CIRCUIT CONCEPTS	18
	A. Gamma-Gamma	18
	B. Beta-Gamma	21
IV.	SIGNAL CIRCUIT OPERATION	23
	A. Gamma-Gamma	23
	B. Beta-Gamma	26
V.	ELECTRONIC DESIGN	29
	A. Digital Circuits	29
	B. Detector Signal Circuits	35
	C. DC and AC Power Supplies	38
VI.	EQUIPMENT OPERATION	41
	A. Daily Checkout	41
	1. Gamma-Gamma	41
	2. Beta-Gamma	47
	B. Counting Routine	47
	1. Intercalibration	47
	2. Manganese Bath	49
	3. Other Radioisotopes	49
	4. Background and Environment	51

TABLE OF CONTENTS

		Page
VII.	DISCUSSION	53
	A. Equipment Performance	53
	1. Gamma-Gamma	53
	2. Beta-Gamma	58
	B. Comments on Design and Performance	63
VIII.	SUMMARY	69
APPENDICES		
	A. Geometry, Gain Stability, and Decay-scheme Dependence of Coincidence Counting	71
	B. Corrections for Dead Time and Coincidence Resolving Time	86
	C. Literature Survey	90
	D. Data Collection and Processing	91
	E. Mn^{56} Decay Tables	99
	F. Sample Preparation	106
REFERENCES		109
ACKNOWLEDGMENTS		113

LIST OF FIGURES

No.	Title	Page
1.	Decay Scheme after Low-energy Neutron Activation of Mn^{55}	8
2.	Details of Liquid Counter Construction	11
3.	Exploded View of Detector Assembly for 4 x 5-in. NaI(Tl) Crystals Used in Liquid Counting	12
4.	Shielding and Liquid Flow Arrangement for $\gamma\gamma$ Counter	13
5.	Pyrex Liquid Scintillation Cell	14
6.	$\beta\gamma$ Coincidence Arrangement	15
7.	Liquid Scintillation Cell Housing (a) Holder and (b) Spacer	15
8.	Full-capability Single-channel Detection Using Four Analyzers and Two Amplifiers	19
9.	Delay-mixing-splitting Technique Using Two Amplifiers	20
10.	Delay-mixing-splitting Technique with Only One Amplifier	20
11.	Simplified Pulse History for Delay-mixing-splitting-repeating Scheme	20
12.	Complete Signal-processing Network for $\gamma\gamma$ and $\beta\gamma$ Coincidence Counting	23
13.	Photographs of $\gamma\gamma$ Signal Circuit Operation	24
14.	Photographs of $\beta\gamma$ Signal Circuit Operation with Mn^{56} Source	27
15.	Digital Repeater	29
16.	Front-panel Arrangement of Dual Fast-slow Coincidence Circuit	30
17.	Chassis Layout of Dual Fast-slow Coincidence Circuit	30
18.	Fast-slow Coincidence Circuit	32
19.	Tunnel Diode Discriminator	34
20.	Mixer-splitter	36
21.	$\gamma\gamma$ NaI(Tl) Voltage-division System	39
22.	$\beta\gamma$ Voltage-division System	40
23.	Counting System Check List	42
24.	Counting System Daily Checkout	43
25.	Mn^{54} Spectra Used in Checkout	44

LIST OF FIGURES

No.	Title	Page
26.	Comparison of Mn^{54} and Mn^{56} Spectra (Mn^{54} Normalized in Pulse Height)	44
27.	Mn^{56} Spectrum in Amplifier B.	45
28.	$\gamma\gamma$ Disintegration Rate as a Function of Channel 1 High Voltage	53
29.	$\gamma\gamma$ Disintegration Rate as a Function of Channel 2 High Voltage	54
30.	$\gamma\gamma$ Delay Plateau	54
31.	Insensitivity of $\gamma\gamma$ Counter to Liquid Volume (Capacity 2.00 Liters)	55
32.	Disintegration Rate as Affected by Changes in Common High Voltage	55
33.	$\gamma\gamma$ Decay Curves for 12 Half-lives	56
34.	$\gamma\gamma$ Disintegration Rate Computed for Mn^{56} Sample Decaying for 10 Half-lives	57
35.	Decay of 10-g/liter Manganese Bath Sample (Disintegration Rate Initially about 800 d/s)	57
36.	$\beta\gamma$ Disintegration Rate in Vicinity of Normal γ High Voltage Setting	58
37.	$\beta\gamma$ Discrimination Rate in Neighborhood of Normal Operating γ Discriminator Level	59
38.	$\beta\gamma$ Disintegration Rate vs β Discriminator Level.	59
39.	$\beta\gamma$ Disintegration Rate as a Function of γ Channel-window Width	60
40.	$\beta\gamma$ Delay Curve	60
41.	$\beta\gamma$ Delay Plateau	61
42.	Mn^{56} Decay in $\beta\gamma$ Coincidence System	61
43.	Coincidence Rate Computed for $\beta\gamma$ Counting of Mn^{56} Decay	62
44.	Some Passive Network Concepts for Mixing, Splitting, and Repeating	64
45.	Delay-mixing-splitting-repeating Technique Applied to Single-channel Liquid Scintillation Counting	65

LIST OF FIGURES

No.	Title	Page
46.	Arrangement of Phototubes and NaI(Tl) Crystal for Mn^{56} Coincidence $\beta\gamma$ Counting with Cherenkov β Detection	67
47.	Absorbance of Manganous Sulphate Solution (Approximate Rendition)	67
48.	Cherenkov Counter Integral Bias Curves	68
49.	Abridged Mn^{56} Decay Schemes	82
50.	Timing of Events and Pulses Which Lead to Gains or Losses in Coincidence Count Rate	86
51.	"Ra-Be Irradiation History" Record Sheet	92
52.	Data Format for Reporting Counts Taken Manually.	93
53.	Format for Card Types Used in Both Manual and Automatic Compilation of Data	94
54.	Typical Computer Results for Mn^{56} Decay Corrections	96

LIST OF TABLES

No.	Title	Page
I.	Intercalibration Schedule	48
II.	Comparison of β Efficiencies	51
III.	Card Punch Code	95
IV.	Mn^{56} Decay Table: $e^{-\lambda t}$	100-102
V.	Mn^{56} Decay Tables	103, 104
	a. $e^{\lambda t}$	103
	b. $1/(1 - e^{-\lambda t})$	103
	c. $\lambda t/(1 - e^{-\lambda t})$	104
VI.	Counting Time for Equal Number of Counts: Mn^{56}	105

Mn^{56} COINCIDENCE COUNTING FACILITY

by

A. DeVolpi, K. G. A. Porges,
and R. N. Larsen

ABSTRACT

A two-stage absolute counting facility for large liquid samples of aqueous $Mn^{56}SO_4$, primarily intended for better than 1% precision measurements of neutron source strengths by the "manganese bath" technique, is described here. Two-liter samples are counted in a $\gamma\gamma$ coincidence arrangement which greatly improves long-term reproducibility at some sacrifice in counting statistics; this sacrifice is, however, lessened through a novel pulse-distribution scheme which allows full utilization of the output of each detector channel. The system is calibrated on an absolute scale through another unit which counts aliquots of strongly activated samples mixed with liquid scintillator in a $4\pi\beta/\gamma$ coincidence mode. The entire facility is designed to be readily adaptable to other radioisotope-counting requirements.

I. INTRODUCTION

As part of experiments which require the absolute determination of weak neutron intensities, a two-stage counting system has been developed chiefly to assay the activity of radioactive solutions obtained from integrating neutron detectors of the manganese bath type. When a precision of better than 1% is required of such a radioassay, long-term stability becomes an important consideration in determining the choice of detection system.

A survey of literature referring to the manganese bath technique has disclosed that customary counting methods do not offer much hope for the required precision. In principle, the Mn^{56} decay scheme (Fig. 1)[2,3] suggests several possibilities for activity analysis; however, when a 640-liter solution - as in the present case - is activated by a relatively weak neutron source, a large liquid sample is needed, which tends to rule out beta counting. Detection of light from Cherenkov radiation is reasonably efficient for upwards to 0.1 liter of 200-gm/liter manganous sulfate per 2-in. cathode diameter of a low-noise photomultiplier tube. Beta-scintillation counting through direct contact of the solution with plastic scintillators is complicated by light collection, surface area, and other

difficulties. Evaporation of a 2-liter sample yields almost 1 kg of powder for a 200-gm/liter concentration of $MnSO_4$. Use of the Szilard-Chalmers reaction to separate carrier-free activity suffers from an absolute uncertainty of about 2% and a range of nonreproducibility of about 2%.(1)

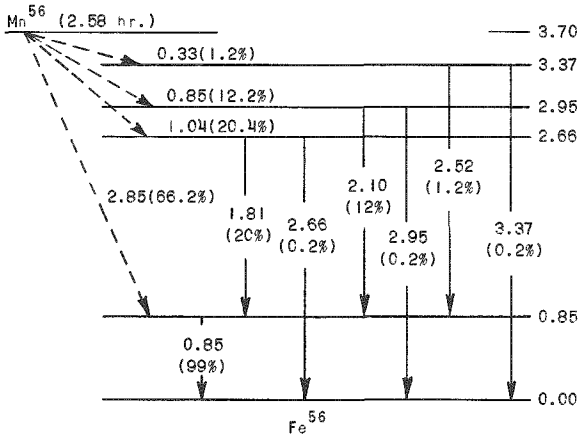

Fig. 1. Decay Scheme after Low-energy Neutron Activation of Mn^{55}.

Direct gamma counting of a liquid sample is feasible, though it has to contend with gain drifts, which are an inherent difficulty in scintillation counting. When the decay scheme is suitable, as is the case for Mn^{56}, the effect of amplitude drifts can be greatly reduced by requiring coincidence between two scintillation crystals at some sacrifice in efficiency. By computing the ratio of the product of the pulse-height-selected single-channel counts N_A and N_B to the gamma-gamma coincidence count N_{AB}, one obtains a quantity proportional to the disintegration rate N:

$$\frac{N_A N_B}{N_{AB}} = N(1 + \bar{\alpha})\bar{\mu} \quad .$$

This ratio depends on the detection efficiency largely through the small factor $\bar{\alpha}$, which is also a function of the decay branching fractions. A more thorough discussion of this factor, which in most situations amounts to less than 0.1, may be found in Appendix A, where the above equation is derived from very general considerations. The quantity $\bar{\mu}$ is chiefly dependent on geometry, with a small portion being sensitive to pulse-height spectrum.

The coincidence requirement, to be sure, results in considerably worse statistics of the overall measurement when single-channel efficiencies are low. Ordinary coincidence circuitry delivers useful counts only over a small part of its output spectrum, since one channel of pulse-height selection is associated with each detector. A pulse-distribution scheme, described in detail in this report, overcomes this limitation by making almost the full spectrum available. With the aid of this count rate doubling technique, less than 1% statistical error can be obtained, for instance, from activation of a 1-c Ra-Be neutron source in a 25-gm/liter $MnSO_4$ solution contained in a 42-in.-diameter sphere.

Gamma-gamma coincidence counting does not, however, result in an absolute measurement, partly because an unknown geometry factor is

introduced in order to obtain high counting efficiency from a 2-liter solution, and partly because branching in the decay of Mn^{56} is not known accurately enough. For this reason, the gamma-gamma counter is intercalibrated with another system by comparing disintegration rates from a source of high specific activity. The latter system, a 4π β/γ coincidence unit, is also described in this report.

The use of a two-stage measurement process affords a certain latitude in design of each unit. Thus, the gamma-gamma coincidence setup was designed for relatively low background, optimum efficiency, and long-term reproducibility; on the other hand, high counting rate capabilities, maximum efficiency, and appropriate precision have been incorporated into the other section, a beta-gamma coincidence unit. A major part of the electronic circuitry is common to both units, as will be described, effecting a considerable economy.

In the γ-γ system, two 4 x 5-in. sodium iodide crystals are mounted so that almost 2 liters of solution can surround the detectors in an annulus. The solution can be poured in through tubing which emerges from the lead shielding. Phototube signals are amplified and shaped in two doubly differentiating amplifiers, the pulses are timed from the zero crossing, selected in energy by two single-channel pulse-height analyzers, and finally placed in coincidence. Mn^{56} gammas have energies 0.845 Mev in coincidence with 1.8 or 2.1 Mev. A delay, mixing, splitting, and repeating artifice is used to permit counting the 0.845-Mev radiation from either crystal and still obtain valid coincidences with the lines of higher energy from the opposite detector.

The $\beta\gamma$ system takes advantage of the fact that β emission of Mn^{56} is 100% in coincidence with gamma emission, and that most of the beta particles have high energies (cf. Fig. 1). Aliquots of activated manganese solution are added to a liquid scintillator which has a beta-detection efficiency of about 98%, a background level (including noise) of about 1.3 cps, and can with high accuracy currently handle count rates up to 10^4 cps. The accompanying gamma channel features a 3-in. NaI(Tl) scintillator which makes use of the same electronic chain as the $\gamma\gamma$ detectors.

Convenient operation of the beta detectors at room temperature with adequately low noise rates was made possible by establishing a photoelectron coincidence requirement between two photomultiplier tubes observing the same scintillation event. The pulses are fed directly from high-gain phototubes into a pair of tunnel-diode discriminators, biased to accept pulses due to a single photoelectron, thence into a coincidence analyzer and subsequently into time analysis with the gamma channel.

Daily, thorough checkouts of gain, timing, scaling, and other aspects are utilized to ensure reliable operation. These procedures, as well as methods of intercalibration, of data accumulation and processing, and of

sample preparation, are incorporated in this handbook. In addition, results of testing and evaluation of the two systems are documented. All electronic and nonelectronic apparatus are described, including performance of the circuitry. Appendices contain (A) an examination of the coincidence equations, revealing the feasibility of high-stability $\gamma\gamma$ counting, (B) dead-time and resolving-time corrections, (C) a literature survey, (D) data-processing chain, (E) some useful tables concerning Mn^{56} decay, and (F) techniques of preparation of manganese samples.

II. DETECTION APPARATUS

A. Gamma-Gamma System

Two 4-in.-deep, 5-in.-diameter NaI(Tl) crystals are mounted as shown in Fig. 2. The arrangement was chosen to optimize coincidence efficiency while also allowing each detector to view as large a volume as possible. The container, plus tubing, holds 1.85 liters of fluid. Ordinarily, two-fold coincidence equipment is designed to allow either point-source geometry or 4π detection by one of the detectors for reasons covered in Appendix A. Here, however, absolute determination was sacrificed in order to have as high a coincidence efficiency as possible, given the use of two available inorganic crystals. The fact that coincidence efficiency in some regions of the container is noticeably lower than in the central volume enters into the result only to the extent of the Compton contribution to the 0.845-Mev spectrum; these conclusions are supported in Appendix A.

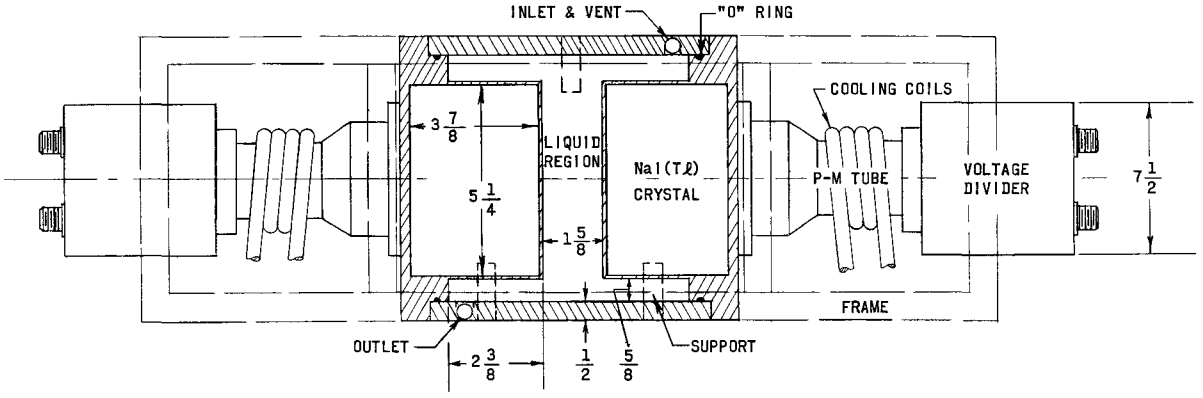

Fig. 2. Details of Liquid Counter Construction. (Dimensions in in.)

In order to optimize the geometry, the NaI(Tl) cylinders were removed from their original containers and repotted in 10-mil-thick stainless steel cans. The flange at the base of each can was designed to close one end of a section of $\frac{1}{2}$-in.-thick, $6\frac{1}{2}$-in.-ID, Type 304 stainless steel pipe. The stainless container and fittings, as well as Tygon tubing, were chosen to prevent corrosion by the acidic solution and to permit easy cleaning of the system by flushing. When repotted in the thin-walled steel can, a minimum amount of MgO reflecting powder was used in order to decrease the distance between solution and crystal (which originally had been over $\frac{1}{4}$ in.). The mounting flange from the aluminum Harshaw package was reused, but the top plate which mounts around the glass optical coupler was machined from stainless steel. Figure 3 shows the expanded sections composing the can. The glass coupling plate was secured with transparent adhesive, and the entire package was assembled and sealed with epoxy by Electronics Division personnel in their dry room. The two identical crystals were then inserted in the outer container. Finally, the entire rig is

mounted, as shown in Fig. 2, in a frame with shims that tilt the liquid container slightly to permit full drainage and filling, and further prevent air pockets from forming (which would result in unpredictable effective liquid volume).

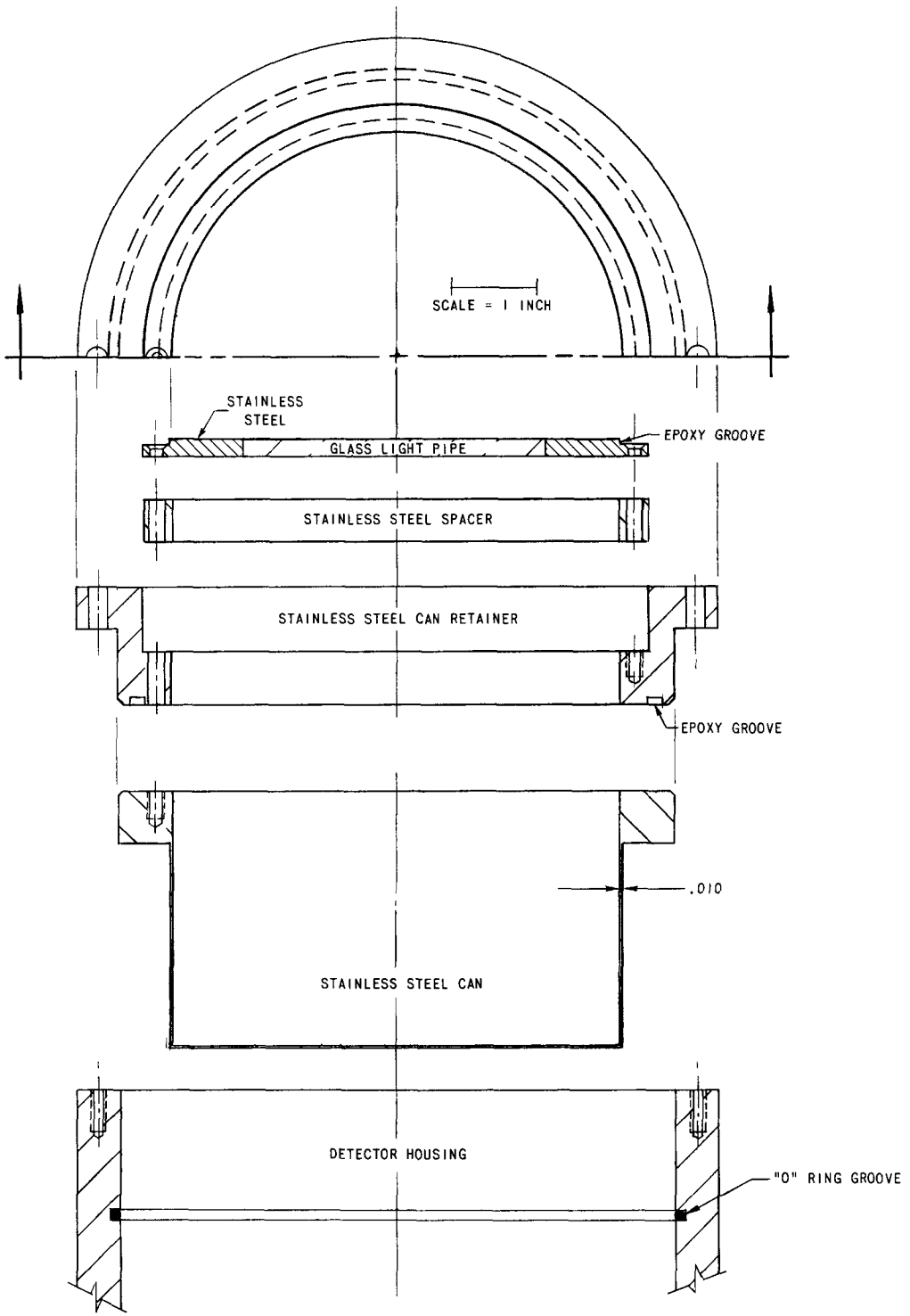

Fig. 3. Exploded View of Detector Assembly for 4 x 5-in. NaI(Tl) Crystals Used in Liquid Counting

The liquid counter frame, with phototubes mounted on each crystal, as well as voltage dividers at the base of each phototube, sits on a lead base and is entirely surrounded by about 8 in. of lead shielding, as described below.

The plumbing system is schematically indicated in Fig. 4. In preparation for a count, approximately 2 liters of solution are poured into the 2-liter stainless steel beaker, filling the counting volume by gravity flow. Air is vented through the standpipe, which also is used to measure the liquid level in the tubing. After counting, the solution is drained through the bottom valve into a 2-liter polyethylene container. The entire unit has been raised about 8 in. off the floor to allow run-off into a standing bottle. Although there should be no trapped pools after drainage, residual drops of liquid must be flushed out by at least two complete charges and discharges of ordinary water. The inside diameter of the entire plumbing system has been kept above $\frac{1}{4}$ in. to keep transfer times down to a minute or so. Thus, it takes about 5 min to empty, flush twice, and refill.

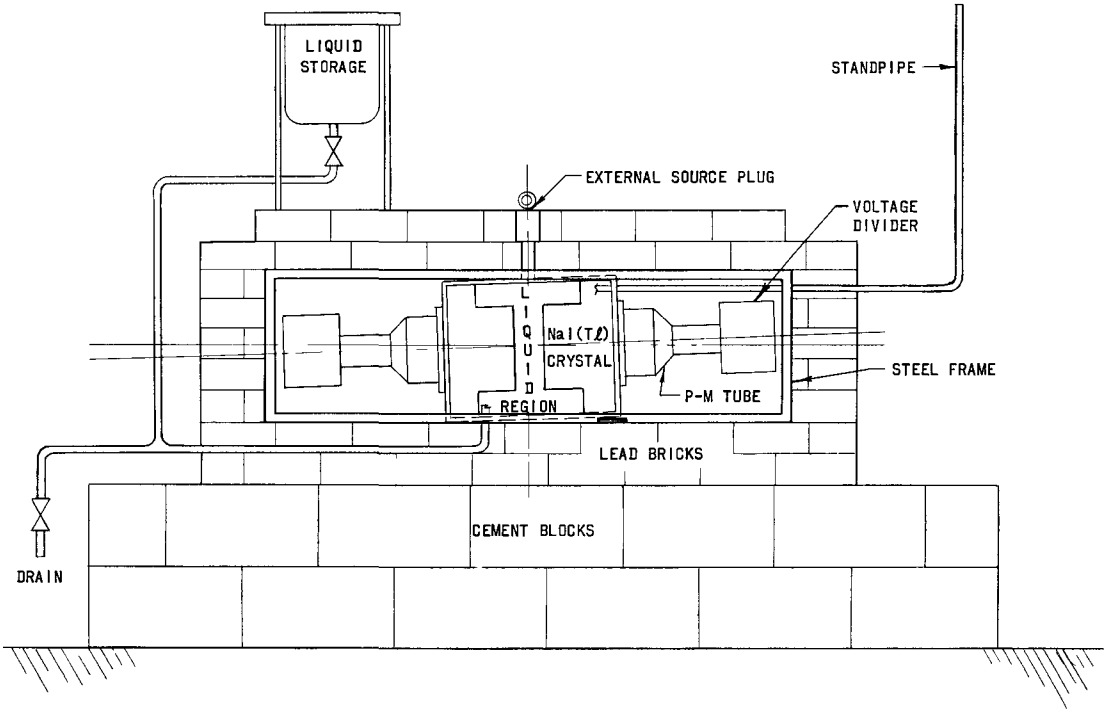

Fig. 4. Shielding and Liquid Flow Arrangement for $\gamma\gamma$ Counter

Provision was made for maintaining the detectors and photomultipliers at constant temperature by means of cooling coils which surround the dynode region of the photomultiplier tubes and may be connected through to a thermostat. The temperature of the counting room, which is ordinarily maintained within a few degrees by the air-conditioning system, has thus far been stable enough to dispense with temperature control.

Both in order to prevent heating and for accessibility reasons, no vacuum tubes or transistors are inside the shield. Coaxial cables convey DC voltages to dividers mounted close to the photomultiplier sockets; anode signals are transmitted directly to the preamplifiers through about 2 ft of low-capacity (RG-114U) cable.

B. Beta-Gamma System

After considering and testing various alternatives, a 4π liquid scintillation counter was chosen for the beta channel. In this device, aliquots of aqueous solution from an irradiated manganese sample are mixed with liquid scintillator and poured into a counting vial (shown in Fig. 5). Scintillations and Cherenkov light from this source are viewed by two phototubes, optically coupled to the vial.

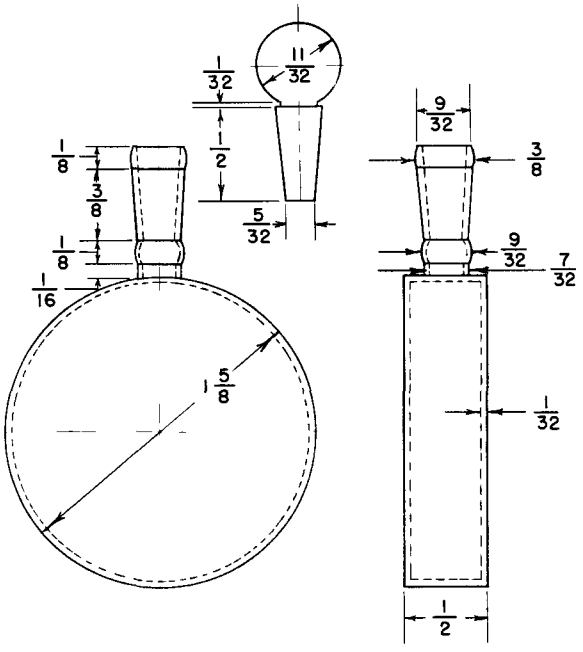

Fig. 5. Pyrex Liquid Scintillation Cell (Dimensions in in.)

Besides the two-tube liquid scintillation detector on a horizontal axis, there is a 3-in. NaI(Tl) crystal vertically under the scintillation sample, as shown in Fig. 6. The two EMI-6255S phototubes were canned in a special alignment jig with about 2 in. of glass protruding at the cathode end. The threaded portion of each can is screwed into the scintillation housing; depth of the penetration can be varied. The scintillation cell holder floats between the two phototubes in silicon fluid, large "O" rings being used to seal the phototube penetrations. The cell holder, shown in detail in Fig. 7, has a removable horseshoe-shaped spacer. When in place the spacer locates the cell on the same horizontal axis as the two photomultipliers; when removed it is possible to insert other types of phosphors, such as a plastic scintillator.

A foam-rubber-cushioned lid gives access into the housing through the top. The lid presses on a microswitch in series with the input to the DC supply for β-channel high voltage. Another such microswitch presses against the lead shielding plug which must be removed in order to reach the liquid sample cells. Both switches must be closed for the high voltage to be on, thus preventing accidental light damage to the sensitive phototubes.

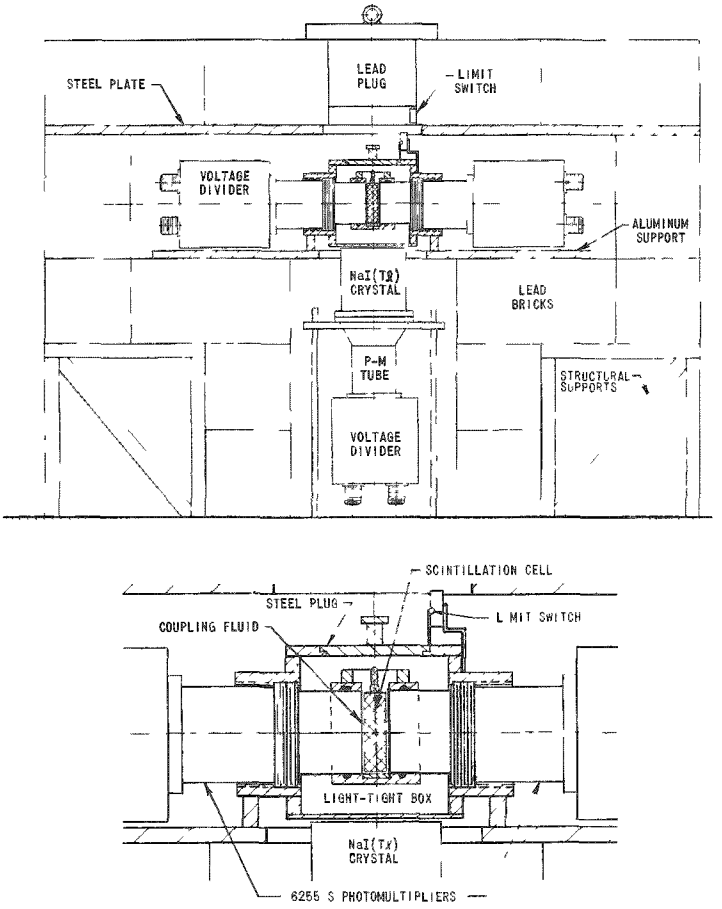

Fig. 6. $\beta\gamma$ Coincidence Arrangement

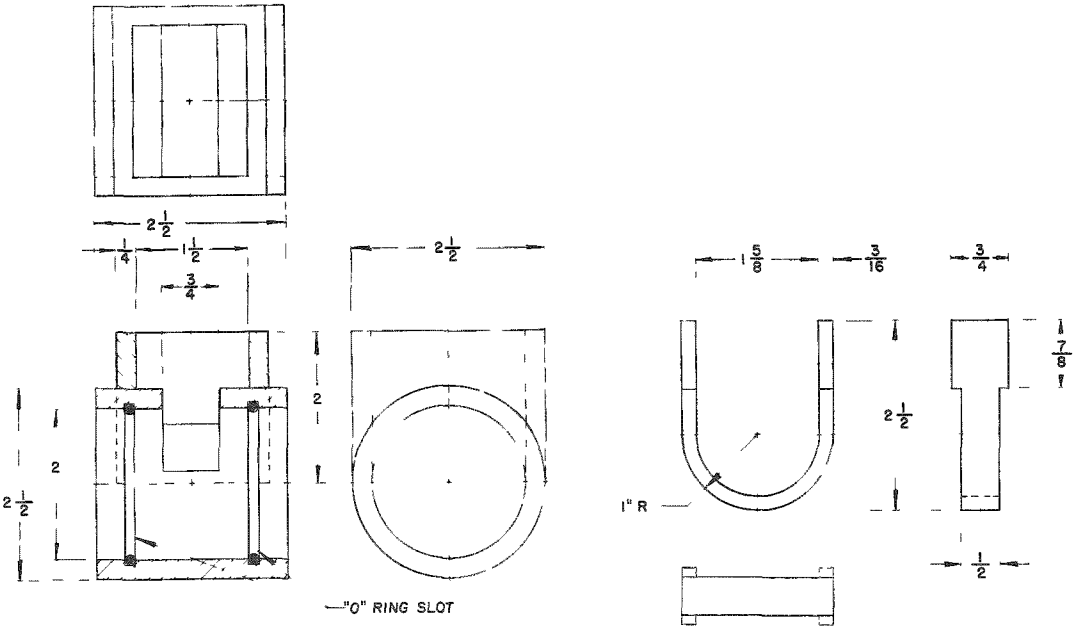

a. Holder b. Spacer

Fig. 7. Liquid Scintillation Cell Housing

Sufficient silicon oil (index of refraction close to 1.5 - about the same as the phototube glass, the scintillation cell, and the liquid scintillator) is introduced by means of a 20-ml hypodermic syringe into the scintillation cell holder to obtain good coupling between the vial and both phototube faces. A plenum is provided which maintains a reserve of oil against unavoidable depletion as sample vials are withdrawn repeatedly. In ordinary use, the chamber needs to be cleaned and refilled about once a week.

In order to circulate constant-temperature air in the vicinity of the temperature-sensitive scintillation cell, photocathode, and first dynode, the cell housing contains two threaded ports for connection to a thermostat. However, this step has not been indicated thus far by our experience.

Voltage bleeders in miniboxes are attached onto the phototube bases through Teflon sockets appropriate to this EMI tube. These boxes are sealed with black tape to safeguard the light-proofing. (Although the tube bases have been painted black, a few remaining pinholes make this external cover necessary.) For the same reason, the inside of the cell housing and the lid area has been coated with black, nonreflecting paint.

The 3 x 3-in. NaI(Tl) crystal, located directly under the housing, is in a standard package with a 3-in. photomultiplier tube and bleeder minibox

To place a sample cell in the counter, the following procedure is required:

(1) The 10-lb lead top plug is lifted out of its fitted channel. (A microswitch opens, disconnecting high voltage)

(2) The cell housing lid is removed (breaking the second microswitch connection).

(3) The vial may be placed in the holder by grasping the thin neck of the cell. (Silicon fluid is immediately displaced, making good optical contact.)

(4) The housing lid is replaced snugly (closing microswitch)

(5) The lead top plug is seated (restoring high voltage upon microswitch contact).

As in the other system, the phototubes and their respective voltage dividers are the only electronic devices included within the shield.

C. Shielding

Shielding design for either system was based on somewhat different requirements which are briefly discussed below. Potential local sources

of radiation background which had to be considered include: (a) critical facility located in the same building; (b) a multiple foil-counting facility located in the same room; (c) various other radioactive sources which might be brought into the room or building from time to time. Furthermore, gamma radiation "cross talk" between the $\gamma\gamma$ and $\beta\gamma$ detection units as well as added background in the relatively unshielded foil counters, mentioned above, had to be effectively prevented by proper shielding and location of each unit For the beta detector, the radiation shield was also required to improve overall integrity against light leakage; on the other hand, radiation background was relatively less important as this detector usually counts strong sources with high efficiency.

To meet these requirements the respective shields are located about 4 ft apart; the $\beta\gamma$ unit is surrounded by 4 in of lead, and the $\gamma\gamma$ unit by 8 in. The shields are constructed of standard 2 x 4 x 8-in. bricks, overlapped wherever possible; all cable and plumbing penetrations are angled or stepped in such a way as to avoid a "beam hole" directly into a detector crystal. The roof of the $\gamma\gamma$ shield is built over a steel plate which rests on the frame of the detector unit; the $\beta\gamma$ shield, on the other hand, is built over a "unistrut" skeleton which similarly supports the roof on a steel plate. Additional shielding of $\frac{1}{2}$-in.-thick steel pipe was placed around each of the gamma-detector photomultiplier tubes. Removable, stepped plugs of 1-in. diameter in the roof of the $\gamma\gamma$ unit, and through the side of the $\beta\gamma$ unit, allow the placement of various sources in the vicinity of the gamma detectors, for purposes of calibration or checkout. (In the $\gamma\gamma$ unit, the $\frac{1}{2}$-in. steel outer casing of the liquid source container is still interposed between the detectors and any source thus introduced.) The $\beta\gamma$ shield also has a removable plug through the roof through which scintillator vials are inserted, as described previously.

With this amount of shielding, gamma-detector backgrounds are down to the order of 1 cps per NaI crystal inside a 10-20% pulse-height channel This background level is adequate for counting manganese bath samples; hence no effort was made to bring down the background to a level comparable with the best current practice

III. SIGNAL CIRCUIT CONCEPTS

A. Gamma-Gamma

The purpose of the $\gamma\gamma$ counting system is to detect a relatively weak activity contained in a large liquid sample (approximately 2 liters) with high background discrimination and extremely constant detection efficiency. When a suitable decay scheme occurs, the last-mentioned requirement can be met most easily by requiring coincidence between two gamma detectors viewing the sample, as discussed in more detail in Appendix A. This makes the processed counting information (product of single-channel counts divided by coincidence count) almost entirely independent of inevitable fluctuations in detection efficiency, including electronic factors, but reduces the total efficiency very strongly, since it is necessary to exclude mutually the range of pulse heights accepted by the coincident channels. Ordinarily, this implies a corresponding restriction of the detector channels; the present system removes this restriction electronically by redistributing the pulses from both detectors into coincidence and single-channel output. The rationale of this pulse-redistribution system may become clearer from a brief exposition of the problems with a specific nuclide, Mn^{56}.

In the decay scheme of Mn^{56} (see Fig. 1), over one-third of all beta disintegrations leave the Fe^{56} nucleus in 3.3-, 2.9-, or 2.7-Mev excited states,* which then decay to the ground state almost exclusively through the 0.85-Mev level. The emitted gamma spectrum thus consists of a high-energy group and a low-energy group; just about all of the high-energy photons are emitted in time coincidence with low-energy photons; conversely 1/2 to 2/3 of the low-energy photons are not emitted in time coincidence with high-energy photons. The high-energy group can be readily separated by pulse-height selection; on the other hand, a channel which selects the low-energy peak also inevitably admits a certain fraction of the Compton "tail" of the high-energy group of radiations. From these various facts, it is readily apparent that, when weak sources are counted, the coincidence count rate of a straightforward coincidence system tends to be marginal. An improvement by a factor of two, achieved by making full use of the pulses delivered by both detectors, is therefore very useful.

In principle, several electronic schemes can be devised to sort pulses in such a way as to use all of the coincidence component. A straightforward scheme, for instance, is shown in Fig. 8. In that system there are two pulse-height selectors, one accepting the 2-Mev group and one set for 0.8 Mev, applied to each detector channel. The appropriate pulses are added and then presented to the coincidence circuit. This

*The fractional population of higher excited states varies roughly between 1/3 and 1/2, as reported in the literature.

scheme obviously demands careful alignment and excellent stability of all four analyzers, as well as requiring a large amount of electronic equipment. (Additional circuits, which would be required to allow short coincidence gates and thus suppress accidental coincidences, are not shown.)

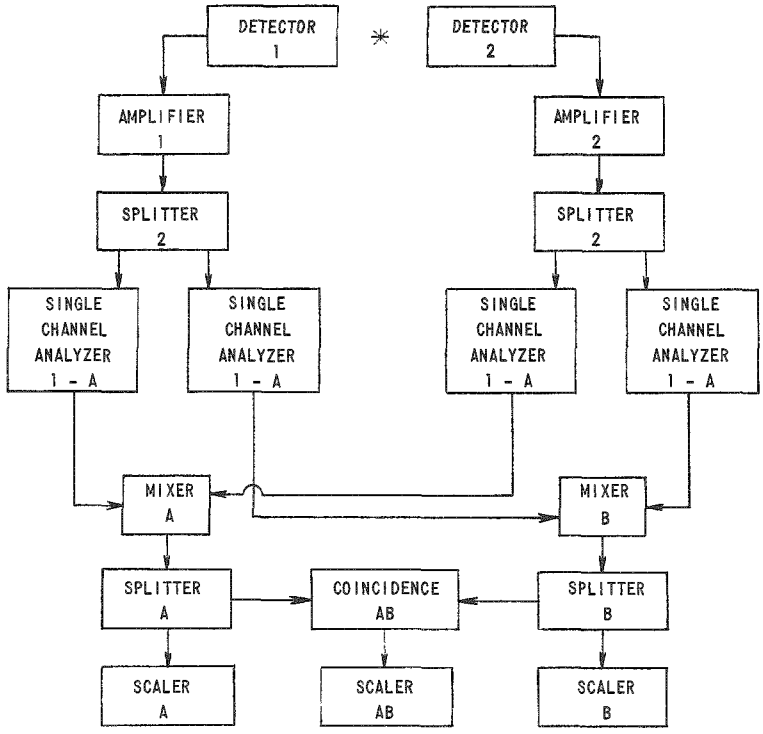

Fig. 8. Full-capability Single-channel Detection Using Four Analyzers and Two Amplifiers

If, on the other hand, one introduces sufficient delay into one of the detector channels, one can add the detector outputs and sort out pulse height groups in only two single-channel selectors; coincidence is then reestablished by repeating the pulses in concordance with the initial delay. A system of this type is depicted in Fig. 9; this is essentially the method described in this report. One should note that one of the two amplifiers may be omitted, as indicated in Fig. 10. Some comments concerning the relative advantages and defects of these schemes are made below and in Section VII-B.

A simplified pulse history for either of the two delay-mixing-repeating schemes is presented in Fig. 11. This figure specifically considers a situation in which coincidence is actually detected in the pair of NaI(Tl) crystals. Analyzer A is adjusted for 2-Mev amplitudes and analyzer B for the 0.8-Mev photopeak. The pulse from detector 2 is delayed enough to minimize overlap; the linear amplifier or amplifiers are assumed to be capable of handling this pulse train. Each analyzer fires when the proper pulse shows up; then we restore the time-coincidence

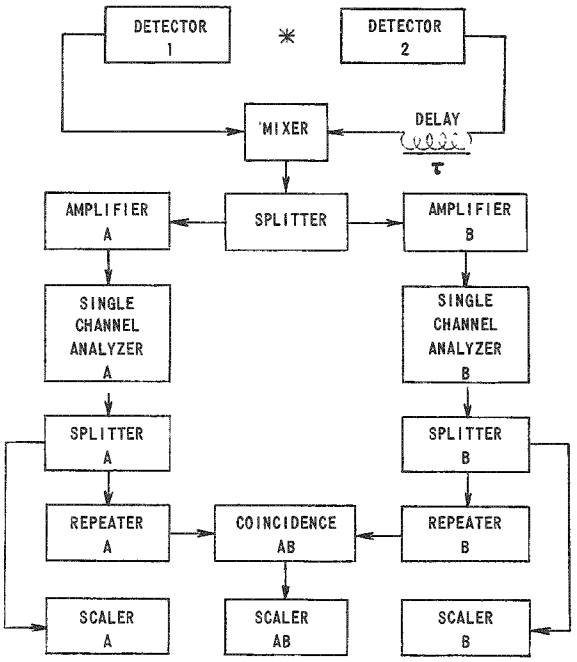

Fig. 9. Delay-mixing-splitting Technique Using Two Amplifiers

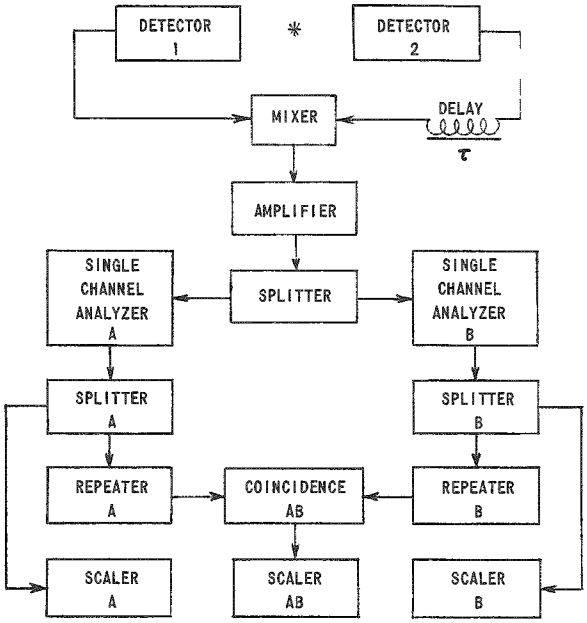

Fig. 10. Delay-mixing-splitting Technique with Only One Amplifier

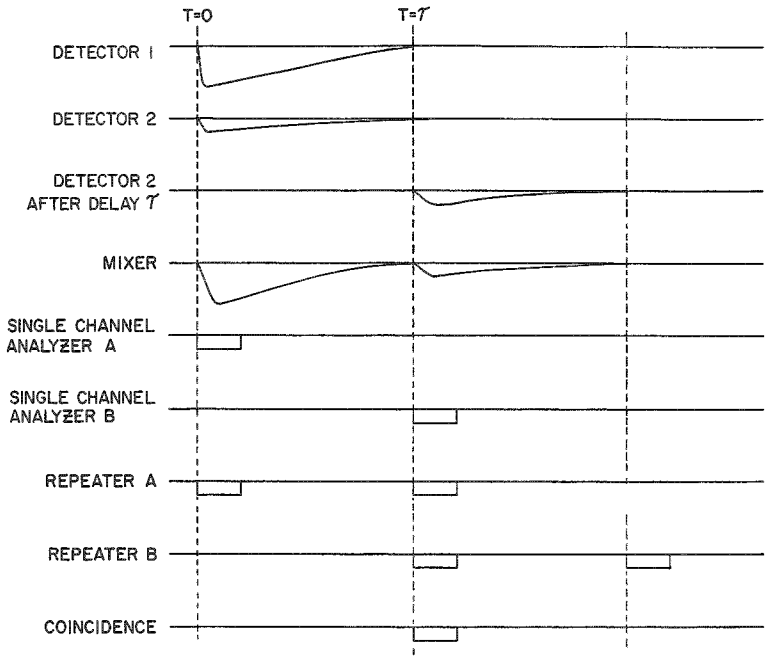

Fig. 11. Simplified Pulse History for Delay-mixing-splitting-repeating Scheme

information by repeating the pulse with a separation time identical to the initial delay. By virtue of symmetry, the reversed detection occurrence still yields a coincidence. The remainder of this section is devoted to detailed considerations influencing the electronic design of the present system, which uses two amplifiers; actual circuits are shown in Section V.

Being committed to two specific amplifiers, it was then also necessary to use an emitter-follower between the delay and the amplifier input, which is designed for a signal source of very low impedance (a condition which cannot be met by passive circuitry except at a large sacrifice of pulse height). Furthermore, the existing digital outputs were not sufficient to drive the necessary loads with a passive repeater. Thus, a chassis which contains the low-level mixer-splitter and a pair of pulse repeaters was designed to satisfy these two requirements. Another important advantage of the active repeater is that shape and height losses in cable reflection can be readily compensated. RG 176 ($Z_0 = 2200\,\Omega$) is used for the basic delay and repeating functions. Adjusting the repeating cables to the correct length is not difficult since they are open-ended delay lines, thereby permitting cutting and unpeeling from that end.

B. Beta-Gamma

The equipment for $\beta\gamma$ coincidence counting had to meet the following requirements: (1) absolute accuracy, the chief concern; (2) capability of sustaining high disintegration rates; (3) very high efficiency in the beta channel for Mn^{56}; (4) small correction factors for accidentals and dead-time effects; and (5) compatibility with the $\gamma\gamma$ system.

The physical arrangement has already been described in Section II-B. Signals from the photomultiplier anodes, after release of at least one photoelectron at both photocathodes, enter into fast coincidence. Thus, a beta source of relatively low energy should require photomultipliers of high conversion efficiency. Such tubes also generate a relatively strong thermal noise current and demand short coincidence gates to eliminate accidental coincidences; in turn, the anode pulse rise time and jitter must be somewhat shorter than this gate in order to avoid loss of true coincidences. Noise reduction through cooling of the photocathodes is limited by the adverse effect of low temperatures on the miscibility and optical properties of the scintillator mixture.

These difficulties can be avoided when the beta source has relatively high energy, as is the case with Mn^{56}, by trading off some loss in conversion efficiency against a considerable reduction in dark current with an "S" type photocathode. Available photomultipliers with "S" type response and 1.7-in. photocathode diameter, EMI-6255 S, were used in the present beta detector. These tubes have the further advantage of developing enough gain to allow direct connection of the anode to a tunnel diode discriminator (about 0.25-v threshold), but develop considerable timing

jitter, having "venetian blind" dynode structures. The dark current at room temperature ($\lesssim 0.01$ μa at 2000 a/lumen) is however low enough to permit almost complete suppression with 50-nsec coincidence gates; thus the timing jitter of the order of 20 nsec has no deleterious effect. Despite the enhanced noise level (1000 c/s) caused by relatively high voltage (2000 v) applied to each phototube, the beta-channel background rate (noise plus radiation) is down to 1 c/s after $\beta\beta$ coincidence.

A more serious difficulty with these tubes is the development of occasional satellite pulses, possibly from positive ion feedback. Such after-pulses were suppressed in the present system by imposing 13-μsec paralysis after each count accepted by the $\beta\beta$ coincidence circuit. This feature would begin to limit use of the equipment for disintegration rates in excess of those which obtain in its present application (at most 10^4 dps).

In order to match the RG-114 pulse cables, the phototube anodes have 185-ohm loads. Space-charge limiting between last dynode and anode thus occurs at about 8 v, which has the useful effect of preventing possible double triggering of tunnel diode discriminators with large pulses which occur without limiting. The discriminator output pulses are shaped with shorted 50-ohm cables and then applied to the coincidence circuit, whose input is paralyzed after every count for 5 μsec. A slow coincidence output is fanned out into the singles scaler; a fast output is delayed for about 1.8 μsec and then enters the final coincidence with the gamma channel.

The gamma detector consists of a NaI(Tl) crystal coupled to a photomultiplier whose anode pulses are fed through a short cable to the preamplifier of the undelayed $\gamma\gamma$ detector channel. By means of switches, further described below, the 0.8-Mev amplifier, pulse-height selector, and zero-crossing timer are "borrowed" from the $\gamma\gamma$ system; the final coincidence gate is thus approximately equal to the 50-nsec coincidence gate on the beta side plus the 300-nsec zero-crosser output.

Against the possibility that higher count rates might be required of the beta system, a 10-Mc prescaler has been provided in the beta singles count channel. With paralysis removed, the prescaler can yield an accurate count for low-energy beta emitters, where extensive satellite production is not likely to occur.

IV. SIGNAL CIRCUIT OPERATION

A. Gamma-Gamma

This section presents an exposition of signal routing in Fig. 12 and photographs of operation in Fig. 13, with explanatory comments.

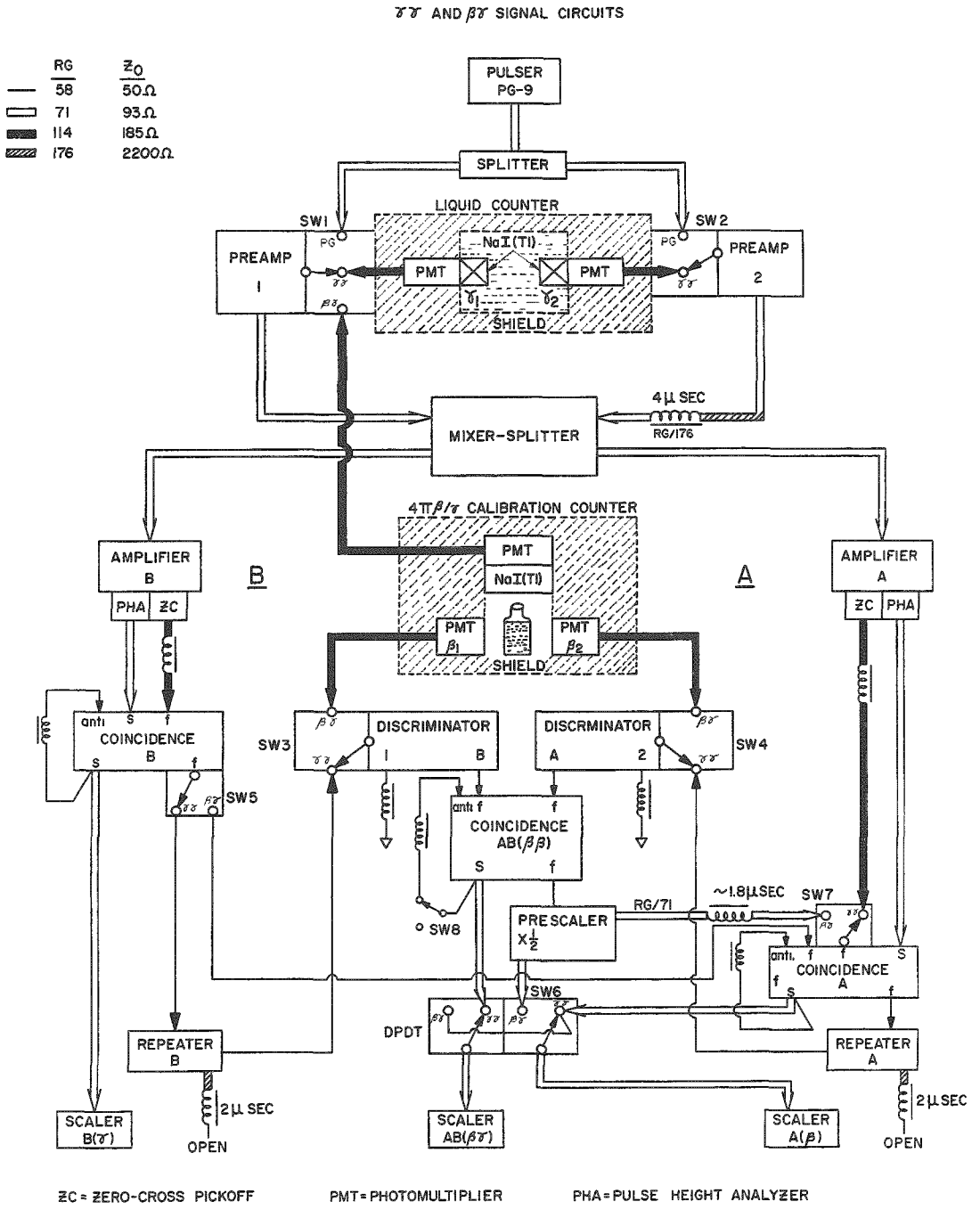

143-1344

Fig. 12. Complete Signal-processing Network for $\gamma\gamma$ and $\beta\gamma$ Coincidence Counting

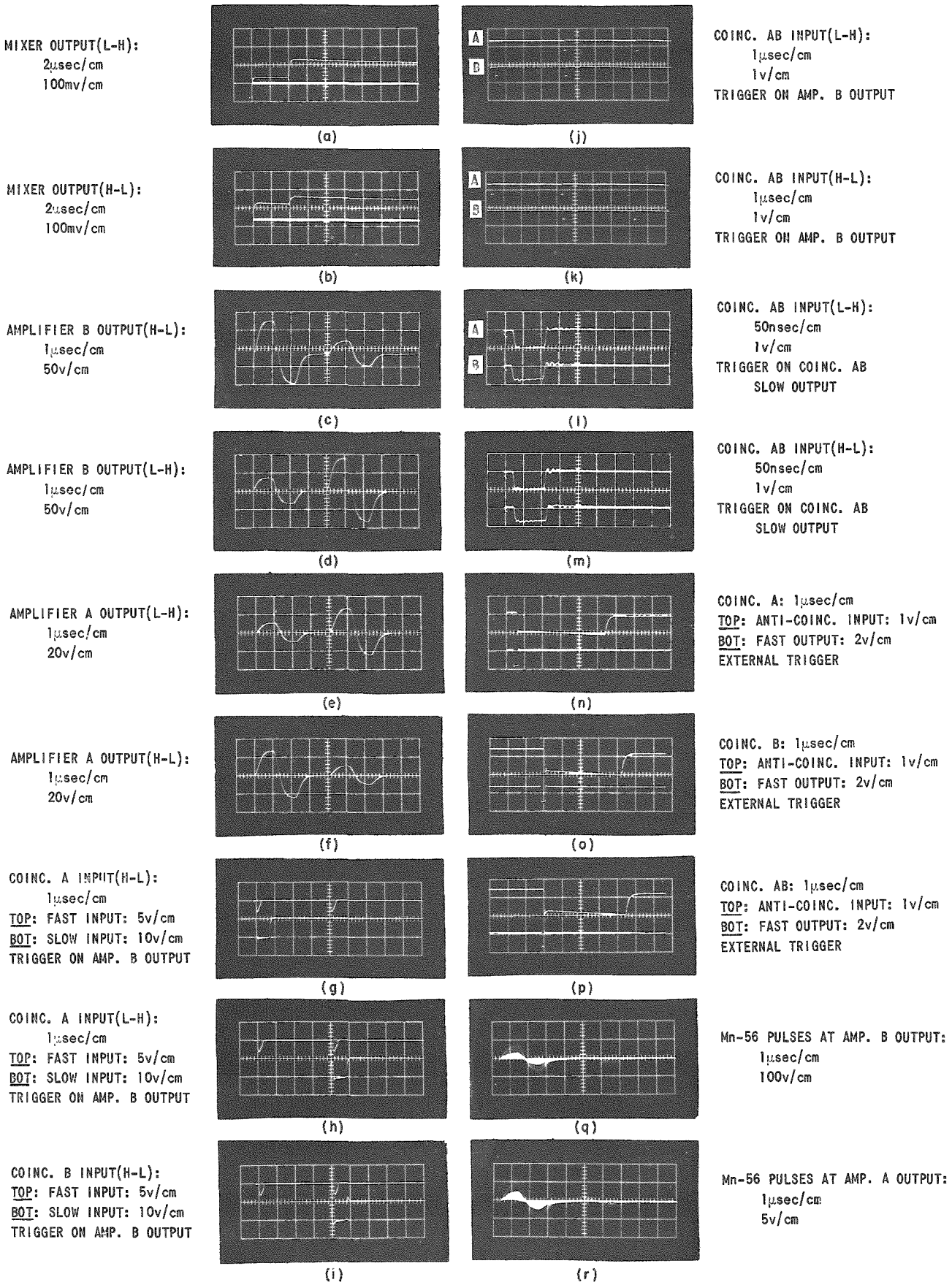

Fig. 13. Photographs of $\gamma\gamma$ Signal Circuit Operation

The entire $\gamma\gamma$ facility can be tested with an on-line pulse generator, a 60-cycle mercury relay type. The output of the pulse is attenuated and divided into two signals with pulse-height ratio corresponding to the approximate ratio between the 0.8-Mev photopeak and the 1.8-2.1-Mev high-energy group of Mn^{56}. The pulser signals may be introduced by switches to the preamplifier inputs; at the same time, high voltage is turned off to avoid feedthrough of cosmic ray pulses.

With the aid of a reversing switch, two pulse situations may be simulated: in the "high-low" position, a pulse of amplitude corresponding to the high-energy group is directed into preamplifier 1, while the pulse representing the low-energy photopeak is channeled into preamplifier 2; in the "low-high" position, the reverse situation applies - low into 1, high into 2.

Channel 2 contains a 4-μsec delay; channel 1 is undelayed. Input into side 1 is attenuated to match losses in channel 2 delay line.

After mixing, the signal is split into two identical output branches headed towards each amplifier Since the electronic circuitry throughout the mixer-splitter consists exclusively of emitter-followers to stabilize gain, there is some loss in pulse height. The output is shown in Figs. 13-(a) and (b). Pulse shapes are chosen to closely reproduce the charge-sensitive preamplifier outputs for actual NaI(Tl) scintillator input.

Single-channel analyzers and zero-crossing timers are integral components of the two double-delay line differentiating amplifiers While both amplifiers and zero-crossers process all pulses, the analyzer labeled "A" selects the high-energy group with a broad window and "B" the 0.8-Mev peak with a relatively narrow window. In order to obtain the best zero-crossing performance, gains in each amplifier are different. To improve overload conditions, the high-frequency response of the amplifiers was severely curtailed, as may be judged from Figs. 13 (c) through (f). One should note that, by careful tuning, the first pulse returns to the baseline well before the advent of the second. These photographs show the amplifier (which is identical with the pick-off circuit input) but not the actual discriminator input. There is an attenuator in front of the A analyzer; this permits the gain of amplifier B to be twice as great as A, allowing the A analyzer to be set about 10% with a 20% window and B at 33% with a 10% window.

A well-timed pulse in each channel is obtained from a coincidence between the zero-crosser and analyzer output These are shown in Fig. 13 (g) through (i) for the two arrival sequences. Because of inherent delay in the single-channel analyzer, the pick-off pulses have to be delayed at least 100 nsec to obtain reliable coincidences. To avoid loss of rise time, this delay is made in a long-pulse transmission cable (RG/114, 185 Ω) which

can be matched to the coincidence-circuit input without loss of pulse height. The fast-coincidence output has the duration and timing of overlap.

The fast output of the timing coincidence circuit is passed to the repeater which produces the pulses shown in Fig. 13, (j) and (k). Observe that the repetition interval is exactly the delay of channel 1 relative to 2. Actually, those pulses given in Fig. 13, (j) and (k) are first shunted through a pair of fast discriminators, where they are further "squared off" and then clipped with a 50-ohm echo line to about 90 nsec; this width eventually determines the final $\gamma\gamma$ coincidence gate.

Final adjustment of repeating time is made by carefully unwinding the end of the delay cable while observing pulses on the oscilloscope. As may be noted from photographs (l) and (m), this adjustment, if carefully made, can produce very satisfactory and stable matching. Balancing channel A with respect to channel B is possible by adjusting the length of transmission line which brings the zero-crosser signal into the timing-coincidence circuit. Interchange of the arrival sequence of the low- and high-pulse groups leads to only a small shift in the final coincidence alignment. This is a sensitive indication of baseline restoration in the amplifier and is the final arbiter as to whether delays are balanced and repeater clipping lines are cut to just one-half of the original delay in channel 2. To obtain photographs (l) and (m), the dual trace oscilloscope (Tektronix 581 with type 82 plug-in) was triggered with the final coincidence output "AB."

The three coincidence circuits used in the whole system are identical; each provides a 10-v "slow" output from a trigger pair which is used to drive 1-Mc scalers that require about 5-v signals. Use is also made of the anticoincidence input on each unit to provide a long paralysis. Photographs (n) through (p) show the attenuated and delayed "slow" output pulses which are fed back to the anticoincidence input, as well as the direct fast output for comparison. Thus, signals going into coincidence AB have pulse widths of about 90 nsec but have dead times close to 5 μsec. While this stratagem increases the dead time correction, it improves the overall accuracy of the system, as explained in Appendix B.

With a Mn^{56} solution in the liquid counter, the amplifier outputs appear as shown in (q) and (r). Here an effort was made to photograph some actual coincident events.

B. Beta-Gamma

When $\beta\gamma$ coincidence counting is to be conducted, one amplifier channel is "borrowed" from the $\gamma\gamma$ system, as well as the coincidence circuits, fast discriminators, and, of course, scalers. The two repeaters, the other amplifier channel, and the preamplifier with subsequent 4-μsec delay are

switched out of grid. As the $\beta\gamma$ mode has its own NaI(Tl) detector and high-voltage supply, the $\gamma\gamma$ high voltage is turned off to prevent background feedthrough.

The liquid scintillation detector at the input of the beta channel has already been discussed. In Fig. 14, photograph (a) exhibits the high-gain phototube outputs after the signals traverse about 8 ft of RG 114. Risetime is around 15 nsec (the tubes are inherently no faster than about 10 nsec). Note that signals are limited by space-charge effects; further, observe that the noise spectrum is visible in discriminator A input but is absent in discriminator B input: this is due to triggering the scope on discriminator A output, effectively displaying the envelope of coincident and noncoincident pulses. Although not noticeable on this photo, there are satellite pulses trailing along for several microseconds. A 13-μsec paralysis, imposed as described above on coincidence output $\beta\beta$, was found to be sufficient to reduce the satellites to less than 0.1% of acceptable pulses.

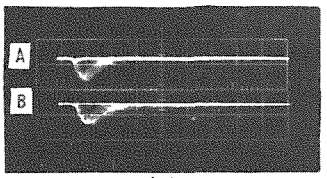

(a)

β DISCRIM. INPUT:
50nsec/cm
10v/cm
TRIGGER ON DISCRIM. A OUTPUT

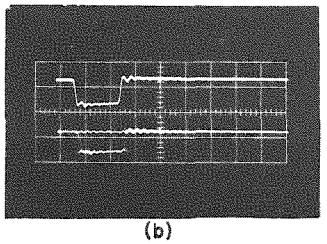

(b)

ββ COINC. INPUT:
50nsec/cm
1v/cm
TOP: DISCRIM. A INPUT
BOT: DISCRIM. B INPUT
TRIGGER ON DISCRIM. A OUTPUT

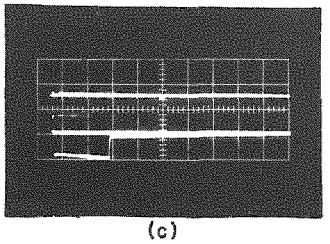

(c)

ββ COINC. INPUT:
2μsec/cm
1v/cm
TOP: DISCRIM. B OUTPUT WITH SATELLITE PULSES EVIDENT
BOT: ANTI-COINC. INPUT
TRIGGER ON DISCRIM. A OUTPUT

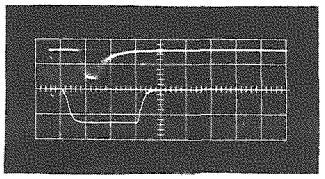

(d)

βγ COINC. INPUT:
100nsec/cm
TOP: β INPUT: 1v/cm
BOT: γ INPUT: 2v/cm
TRIGGER ON γ SLOW OUTPUT

Fig. 14. Photographs of $\beta\gamma$ Signal Circuit Operation with Mn^{56} Source

Some gauge of time jitter in the β channel may be obtained by examining the discriminator outputs synchronized with one of the signals, as shown in (b); time dispersal is not much more than that of the pulse risetime.

Figure 14 (c) depicts afterpulsing on the signal which enters the $\beta\beta$ coincidence, while the lower trace represents the dead time which blocks the $\beta\beta$ coincidence output.

The 100-nsec signals from the $\beta\beta$ coincidence go to a splitter located in the 10-Mc prescaler chassis. After scaling by 2, one branch goes via a switch box to a scaler-register. The other (unscaled) branch is amplified to 6 v, driving almost 2 μsec of RG 71, 93-Ω cable (over 1500 ft) in order to center the beta event within the confines of the gamma pulse emerging from coincidence B.

When the gamma photon is detected in the inorganic scintillator, its electronic representation is processed through preamp 1, the mixer-splitter, and then amplifier B, leading to a timed pulse coming out of coincidence B. This signal is then diverted to coincidence A, which accomplishes the final analysis of $\beta\gamma$ correlation. Photograph (d) of Fig. 14 exhibits such events being triggered on the slow γ output. Jitter here is of the order of 30 nsec. The coincidence circuit fires at a threshold of the order of $\frac{1}{3}$ v; thus, the total gate time ($\tau_\beta + \tau_\gamma$) is over 400 nsec.

Shifting from $\gamma\gamma$ to $\beta\gamma$ can be effected entirely by switching without reconnecting cables. In the interest of improved counting statics, it is also expedient to reset the upper and lower levels on single-channel analyzer B. The window is enlarged to about 20 v, while the 0.8-Mev photopeak is maintained at the same location as in $\gamma\gamma$ counting.

V. ELECTRONIC DESIGN

A. Digital Circuits

1. Digital Pulse Repeater

The pulse repeater uses the reflection from a delay line to produce a second (repeated) digital pulse. The circuit is shown in Fig. 15. At the input, the 1-kΩ bias resistor at Q_1 base also provides a termination for the sending cable. When a negative pulse appears at the input, it goes through diode D_1 and emitter followers Q_2 and Q_3. The pulse at this point has lost some amplitude and "squareness," so it is reshaped in the output stage. One-half of a pulse appearing at the emitter of Q_1 is propagated down the 2200-Ω delay line. Since this line is unterminated, the pulse is reflected uninverted from the open end and appears back at the sending end after a time of 2τ, where τ is the delay of the cable in one direction. This reflected pulse sees an approximate Z_0 termination of the cable (2.2 kΩ) because diode D_1 has become nonconducting and the reflected pulse is of the polarity to back bias it even further. The reflected pulse is reshaped and amplified in the output stage. The position of the second pulse relative to the first is determined by the length of the delay line.

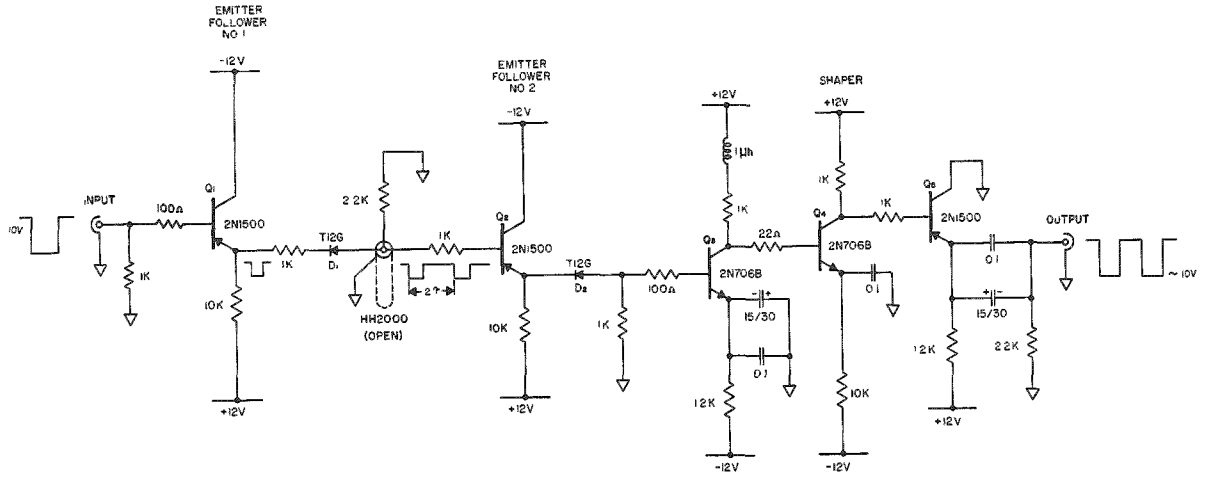

143-1204

Fig. 15. Digital Repeater

2. Coincidence Circuit

The coincidence circuit is based on a design by R. Epstein and L. Welter of Argonne National Laboratory.(38) This circuit has been developed as part of a system in which pulses to the coincidence circuit are generated by pulse standardizers. The circuit is not suitable for being driven by sources capable of producing large overload pulses.

The coincidence front panel is shown in Fig. 16. There are two coincidence circuits and 3 power supplies mounted on one $3\frac{1}{4}$-in.-high panel. A top view of the chassis is shown in Fig. 17. The printed circuit boards are mounted directly on the input connectors to provide minimum lead length between the connector and the input transistor.

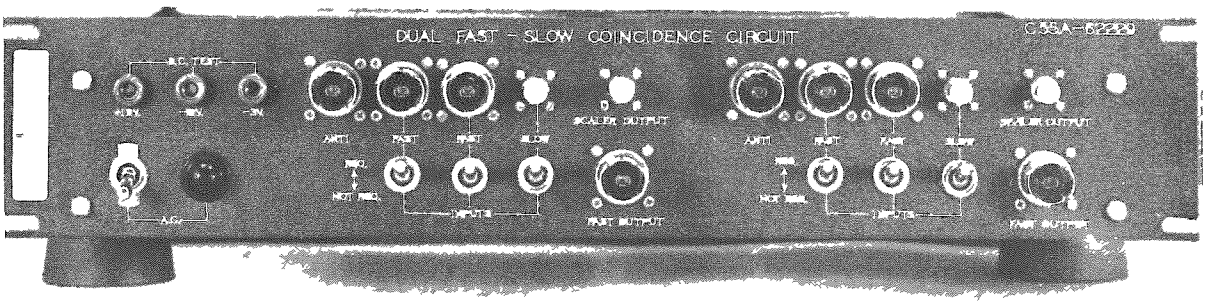

143-839

Fig. 16. Front Panel Arrangement of Dual Fast-slow Coincidence Circuit

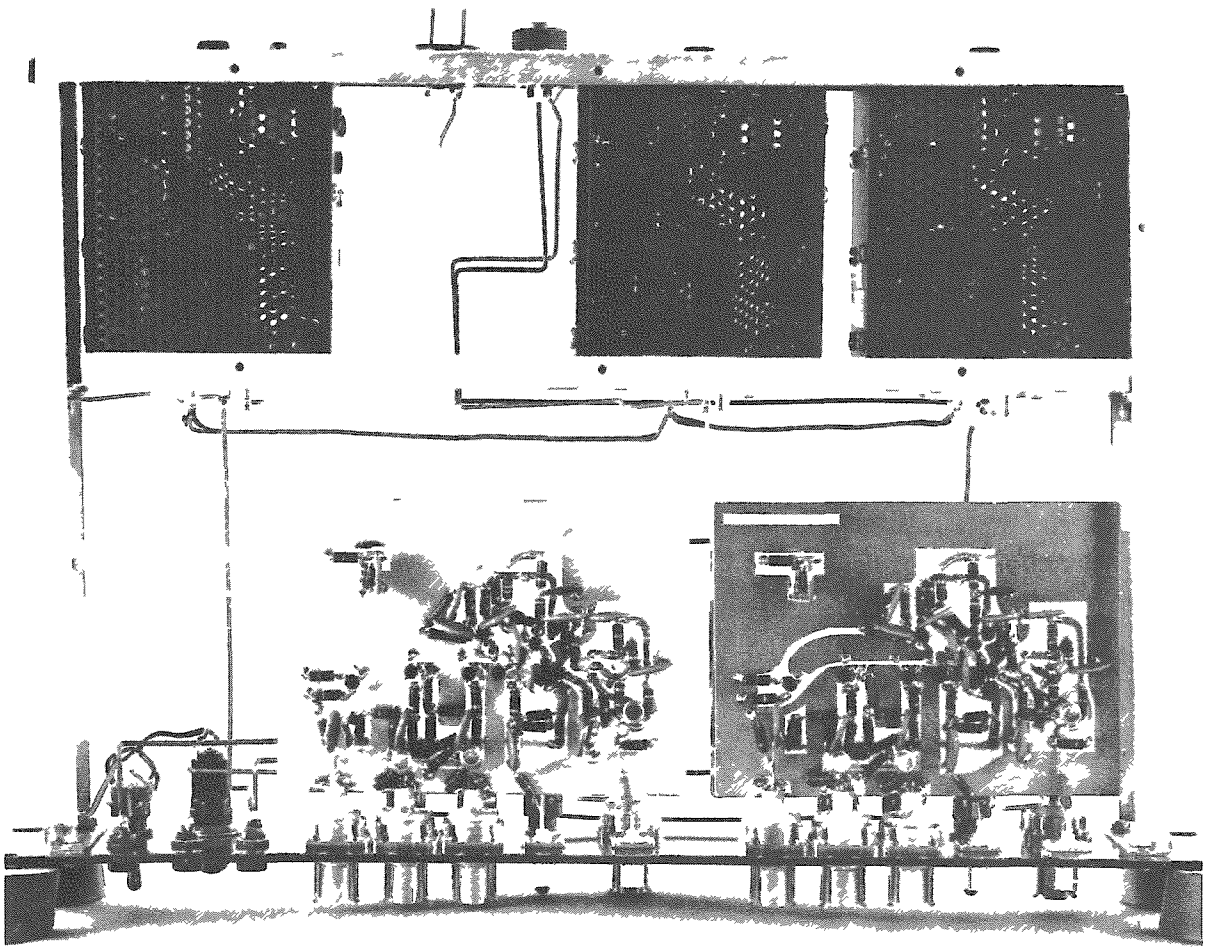

143-854

Fig. 17. Chassis Layout of Dual Fast-slow Coincidence Circuit

The circuit is shown in Fig. 18 and the operation is as follows:

Consider the tunnel diode (TD) and its 700-Ω load, which are connected across the -12-v and -3-v supply lines. In the absence of current from Q_1, Q_2, Q_3, or Q_4, the TD conducts sufficient forward current to be in the high-voltage state.

Q_2, Q_3, and Q_4 are current generators whose combined currents flow into the tunnel diode. This current flowing through the tunnel diode insures that the net TD current is in the reverse direction. Thus, the voltage across the tunnel diode is a small reverse voltage. If all of the currents are cut off, the tunnel diode switches to the high-voltage state. If all but one of the currents are cut off, the tunnel diode remains in the low-voltage state. Any of the inputs may be disabled by placing the input switch for that input in the "not required" position. This will quiescently cut off the current through the transistor instead of requiring that an input pulse cut it off.

The voltage pulse from the tunnel diode is transformer coupled (through emitter-follower Q_5) to the long tail pair Q_6 and Q_7. There is a small step-up in voltage through the pulse transformer (approximately 1.5:1).

Q_6 is normally off and Q_7 is on. A negative pulse reverses this condition, sending current to Q_8 and producing a fast output pulse at the collector of Q_7. This pulse is always of the same width as the input pulse. The function of Q_8 is to present a voltage pulse to the scaler drive circuits (Q_{10}, Q_9, Q_{11}, Q_{12}) without having a significant voltage pulse appear at the collector of Q_6. Such a pulse at this point is undesirable because it is coupled through the Miller Effect back to Q_6 base, which slows the circuit action.

Q_9 and Q_{10} form a trigger circuit. The output from this trigger drives cascaded emitter-followers Q_{11} and Q_{12}. These scaler-drive circuits are capable of operation at 4 Mc or less.

Q_1, upon receipt of a negative pulse (anticoincidence), drives additional backward current through the tunnel diode, preventing it from switching to the high-voltage state, even in the presence of coincidence inputs at transistors Q_2, Q_3, and Q_4.

Nominal values for the coincidence and anticoincidence input pulses are:

amplitude	-0.75 v
duration	10 nsec or greater
count rate	10 Mc or less
slow input amplitude	12 v

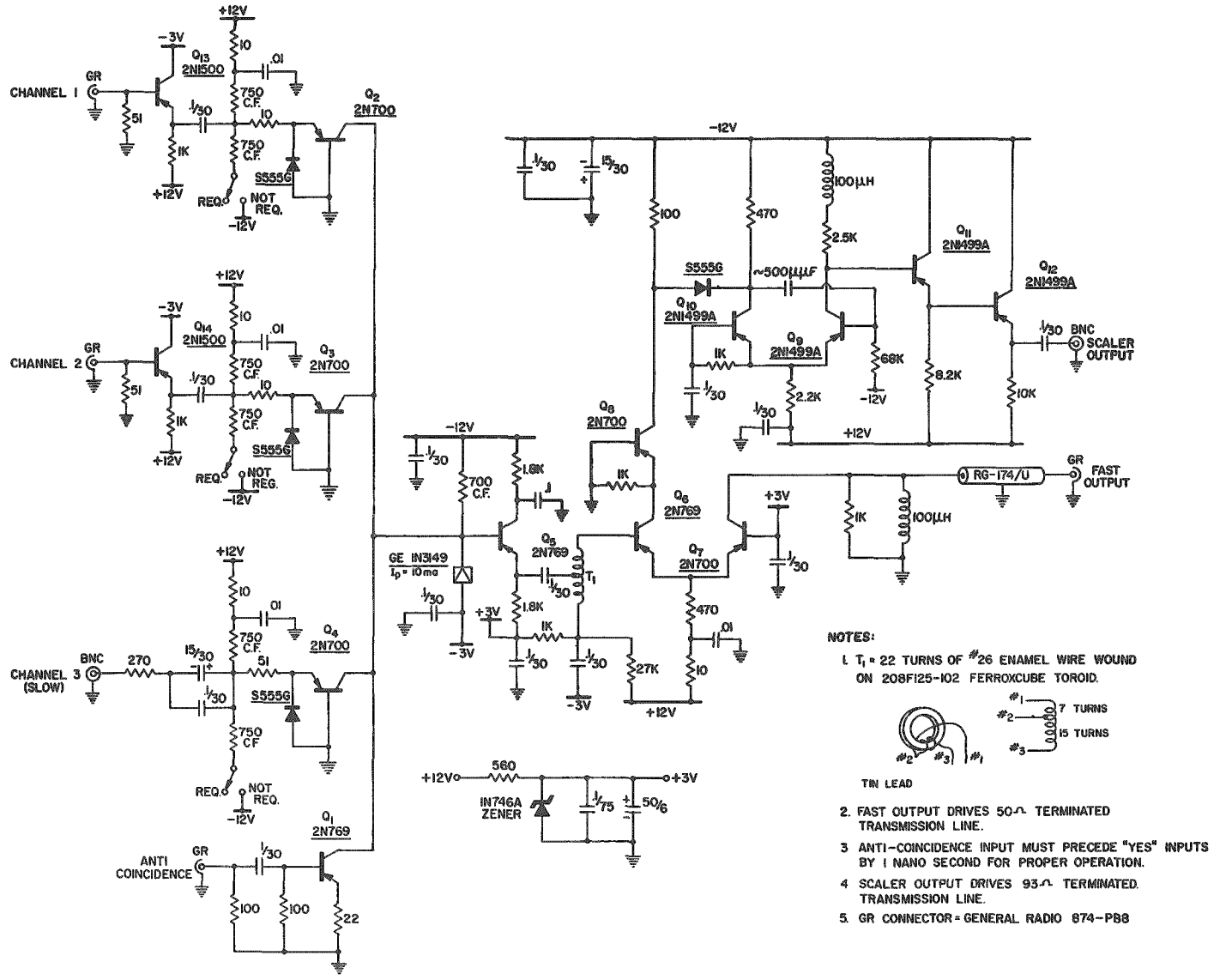

NOTES:

1. T_1 = 22 TURNS OF #26 ENAMEL WIRE WOUND ON 208F125-102 FERROXCUBE TOROID.
2. FAST OUTPUT DRIVES 50Ω TERMINATED TRANSMISSION LINE.
3. ANTI-COINCIDENCE INPUT MUST PRECEDE "YES" INPUTS BY 1 NANO SECOND FOR PROPER OPERATION.
4. SCALER OUTPUT DRIVES 93Ω TERMINATED TRANSMISSION LINE.
5. GR CONNECTOR = GENERAL RADIO 874-P88

143-1202

Fig. 18. Fast-slow Coincidence Circuit

The circuit will work for the following conditions as limits:

amplitude	-0.5 v
duration	5 nsec or greater
count rate	30 Mc or less.

3. Discriminator

The discriminator circuit is shown in Fig. 19. Its operation is as follows: when the discriminator level pot is set at zero percent, the emitter of Q_2 is approximately zero voltage. Since the tunnel diode No. 1 cathode is also at zero voltage there will be no quiescent current through the 600-Ω resistor. Q_1 quiescently conducts approximately 9.8 ma, which is in the direction such as to switch TD No. 1 to its high state. Therefore, when an additional signal current of 0.2 ma is provided, TD No. 1 will switch. However, if the discriminator level pot is set at 100%, all the quiescent current of Q_1 will flow into Q_2, which means that there will be zero current through TD No. 1. In this case, a signal current of 10 ma must be provided to switch TD No. 1 to its high state.

The input stage is designed to have an input impedance of 200 Ω This is provided by the 180-Ω resistor in series with approximately 20 Ω of the grounded base configuration of Q_1. The input signals are negative, which insures that Q_1 will always remain conducting, thus providing a relatively constant impedance at the input. Since the voltage on the emitter of Q_1 is quite constant under signal conditions, a voltage pulse at the input will be transformed to a proportional current signal at the collector of Q_1. This current is then used to switch the tunnel diode current discriminator TD No. 1.

TD No. 2 is a post discriminator and shaper. It is triggered each time that TD No 1 switches. The width of the pulse from TD No. 2 is determined by the 50-Ω clipping line. The 25-Ω resistor between the clipping line and TD No. 2 is needed to provide an approximate Z_0 termination for the clip line. The output from TD No. 2 is shaped in the following stages which are identical to the output stages of the coincidence circuit. It should be noted that the discriminator is not extremely linear, since this was not one of the requirements of this circuit. In order to provide better linearity, TD No. 1 must be biased by a constant-current source, which would involve the use of a few more transistors that should be temperature compensated.

The discriminator will operate with input pulses of 10 nsec. The maximum acceptable count rate is a function of the length of the clipping line, but the input stage is capable of operation at 10 Mc. The useful dynamic range of input pulses is approximately 0.1 to 2 v. It will tolerate a 50-v pulse at the input without producing after-pulses.

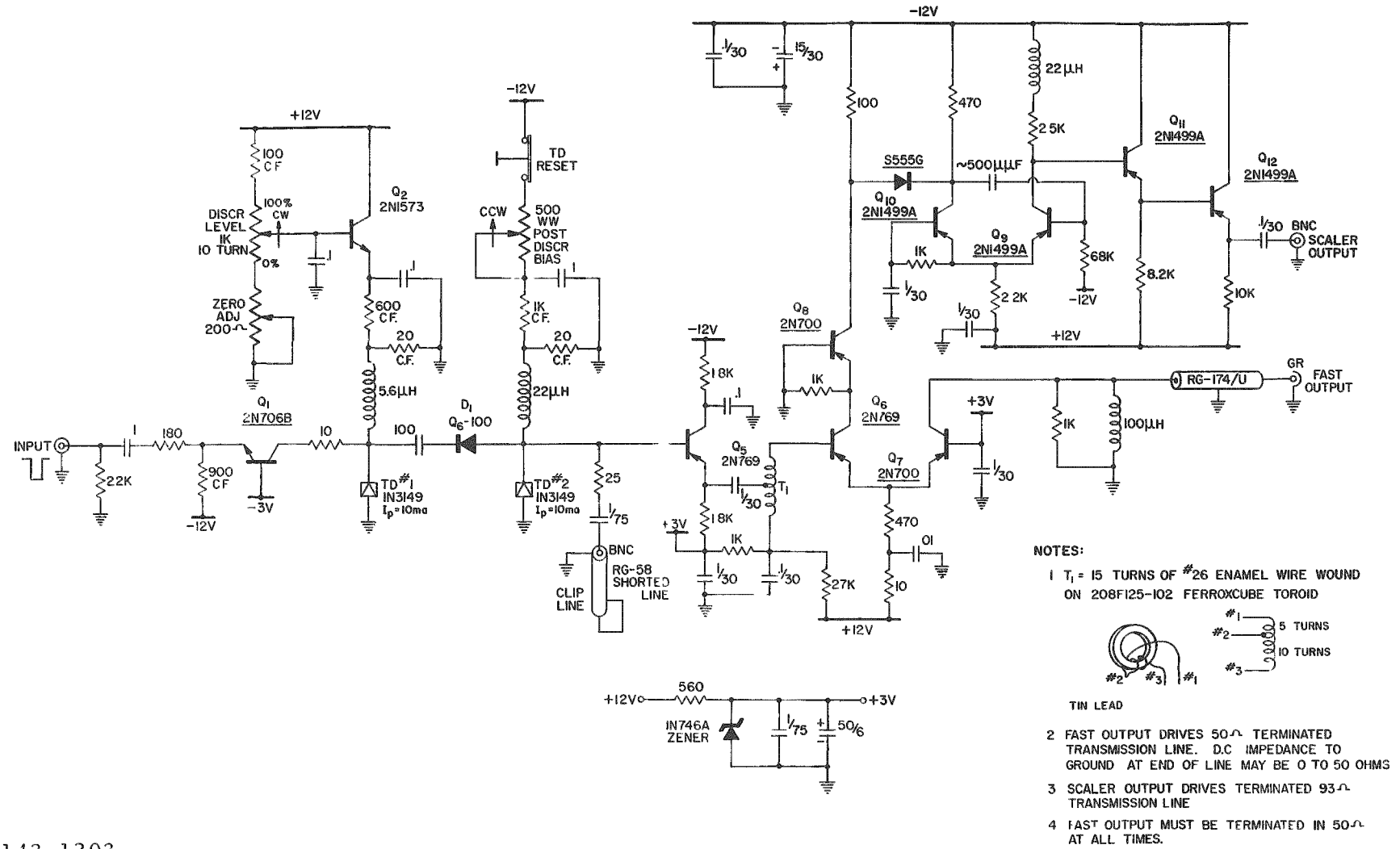

NOTES:

1 T_1 = 15 TURNS OF #26 ENAMEL WIRE WOUND ON 208F125-102 FERROXCUBE TOROID

#1 #2 5 TURNS #2 #3 10 TURNS #3 #1

TIN LEAD

2 FAST OUTPUT DRIVES 50Ω TERMINATED TRANSMISSION LINE. D.C IMPEDANCE TO GROUND AT END OF LINE MAY BE 0 TO 50 OHMS

3 SCALER OUTPUT DRIVES TERMINATED 93Ω TRANSMISSION LINE

4 FAST OUTPUT MUST BE TERMINATED IN 50Ω AT ALL TIMES.

143-1203

Fig. 19. Tunnel Diode Discriminator

The physical layout of the discriminator is identical with that of the coincidence circuit. There are two discriminators and three power supplies mounted on one $3\frac{1}{4}$-in rack panel.

4. 10-Mc Prescaler

A prescaler was originally incorporated into the beta channel in order not to prejudice the measurements through a dead time in the single beta-count channel, as mentioned above.

5. Other Scalers

Three scalers, ANL model No. S24A, are used for manual checkout. These units are remotely controlled for greater convenience with a dekatron timer, ANL Model No. 89B, through additional relays A single pushbutton thus resets all scalers, registers, and the timer, and restarts a count after a delay of 0 1 sec. The scaler inputs may be switched over from the manual scalers to an automatic system, described in a laboratory report (4) The latter system can be programmed for repeated counting at adjustable intervals; counts are punched out into IBM cards. The manual scalers, which are used chiefly for checkout routines (see next section), have been integrated with a dekatron timer, by means of a simple arrangement of relays and switches, so a single pushbutton resets three scalers and registers as well as the timer, and starts another count after an about 0 1-sec delay

B. Detector Signal Circuits

This circuitry includes the input mixer and splitter, linear amplifiers, pulse-height analyzers, and zero-crossing timing circuits

1. Analog Mixer and Splitters

This circuit is shown in Fig 20 The emitter follower bias resistor has a resistance of 2 2 kΩ and also terminates the input cable. A pulse which appears at input 1, or point A, will appear at point B attenuated by 50%, since point C is held fixed by the low-output impedance of the emitter follower. The same follows for a pulse which appears at input 2. The pulse is split at the output of a third emitter follower. Thus, a pulse appearing at either of the two inputs appears (50% attenuated) at both outputs

2. Amplifiers, Pulse-height Analyses, and Zero Crossers

The amplifiers, General Nuclear Corp. Model No. 108, are almost exact copies of the ORNL A-8 circuit. As the units when delivered contained a number of wiring mistakes and required fairly extensive

changes in layout before they could be used, a few revisions were made in the basic circuit. More damping, for instance, was added in the output loop to improve overloading characteristics at some expense in risetime. Different tubes of better power dissipation were used in the single-channel analyzer, resulting in a considerable improvement in stability. The zero-crosser circuit, delivered as a separate unit, was incorporated in the main chassis; this made it possible to remove some of the very crowded components from the zero-crosser subchassis and to replace the rather unsatisfactory negative bias supply of the latter with a tap into the negative supply available on the main chassis.

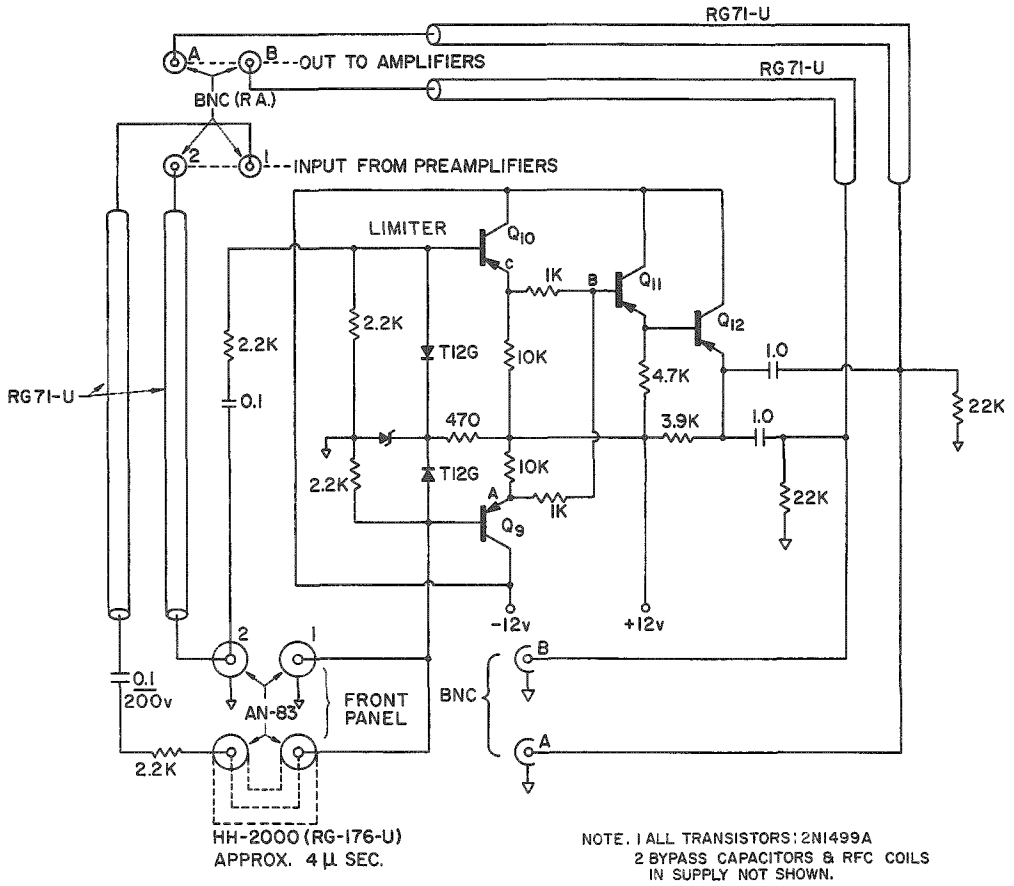

143-1349

Fig. 20. Mixer-splitter

The output pulses of the zero-crosser were sharpened by shunt-peaking and clipped very sharply through reduction of the coupling capacitor of the output trigger pair; the current through this circuit unit was at the same time increased so as to obtain output pulses of adequate height.

A number of diodes were replaced with diodes of better quality now available; resistors in some critical locations were replaced with precision wire-wound resistors and/or with resistors of higher wattage rating.

The clipping cables were separately jacketed in external shields to remove some echoes from the tail end of the pulses (for repeated input pulses such echoes are, of course particularly objectionable).

Another change which appeared to be desirable was to reduce the gain of the first loop of the amplifier. Many commercially available amplifiers, it appears, tend to have too much gain for scintillation applications, which means that input signals must usually be heavily attenuated. A reduction in gain obviously improves the feedback stability and, hence, seems advisable whenever the best possible stability is needed.

Through these various measures the stability of performance of the amplifiers was considerably improved.

An interesting and perhaps somewhat disappointing feature of operating these amplifiers with repeated pulses is that much of the overload stability is lost when repeated oscillations begin to appear at something like 20 to 50 times overload. This may well be due to the fact that the amplifier is necessarily very sensitive to the repetition frequency (250 kc for a 4-μsec delay), which may lead to, perhaps, forbidding difficulties if the pulse-repetition scheme is attempted in a counting problem for which considerable overloading is unavoidable.

A final change made in the circuits requires a brief exposition of two practical difficulties inherent in the operation of zero-crosser circuits:

a. The two adjustable parameters of the circuit, the threshold and the hysteresis, are interdependent, but vary individually with the age of active elements in the trigger circuit. As a result, the range over which the timing error falls within certain limits is necessarily smaller than the full range of input pulse heights. Since the error becomes large very rapidly for pulse heights below, say 10 v, it is expedient to keep the zero-crosser threshold well above this value, allowing some change as vacuum tubes weaken

b. In the present system, the timing error also becomes large near the high end of the pulse-height spectrum. As discussed by Fairstein et al.,[39] the zero-crossing point is the image of the time at which the input pulses rise to half their height; thus, any nonlinearity of amplifier gain (which may occur long before saturation limiting) will cause a systematic shift of the crossing point.

For these reasons, counting with the highest precision and stability calls for a more or less fixed window threshold, somewhere above the zero-crosser threshold, as well as a maximum window width

below the region of increasing timing error. In order to select different parts of spectra with the pulse-height analyzer, it is then expedient to provide an attenuator between amplifier output and analyzer input; such attenuators were incorporated in our equipment Furthermore, it was necessary to widen the maximum window from 10 to 20 v in order to accommodate the whole "high-energy" group, by rewiring the potentiometer-dividers controlling the window width

C. DC and AC Power Supplies

All the amplifiers, high-voltage supplies, and transistorized circuits receive their AC supply from a Sorenson Model No. FRLD 750 voltage regulator. This unit provides 0.35% distortion for a typical 2% line distortion and attenuates line transients by a factor of 8 in less than one cycle. Regulation accuracy is of the order of 0.5%, according to ratings by manufacturer. Additional pickup reduction was obtained by placing ferrite chokes in the DC supplies for the tunnel diode discriminators and the digital splitters.

The phototubes on the NaI(Tl) crystals are operated from Fluke Model 409A high-voltage supplies. These units are rated at 3 ma, 0.01% regulation for a 10-v change in line voltage and 0.02% stability per day after warmup. Since the phototube bleeders draw about $\frac{1}{4}$ ma each, a divider circuit was made up to supply both resistor strings from the same 409A. The divider shown in Fig. 21 was constructed to provide fine control of both tubes in common, as well as adjustment of each phototube voltage over a wide range. Ceramic rotary switches and low-temperature-coefficient (less than 50 ppm/°C) resistors and helipots were used throughout.

The gamma channel in the $\beta\gamma$ coincidence arrangement has a separate 409A providing current through another 300-kΩ helipot for fine gain control It is by means of these high-voltage controls that gains are modified in all gamma detectors to compensate for day-to-day variations

The two EMI-6255S phototubes in the beta channel draw their supply from a Fluke Model 405. This power supply readily provides the 2 ma and 2200 v required to obtain high gain, while maintaining 0.01% line regulation and 0.005% per hour, 0.05% per day stability after warmup. A divider which allows independent adjustment of each tube voltage, as well as the bleeders affixed to the base of each photomultiplier, are shown in Fig. 22

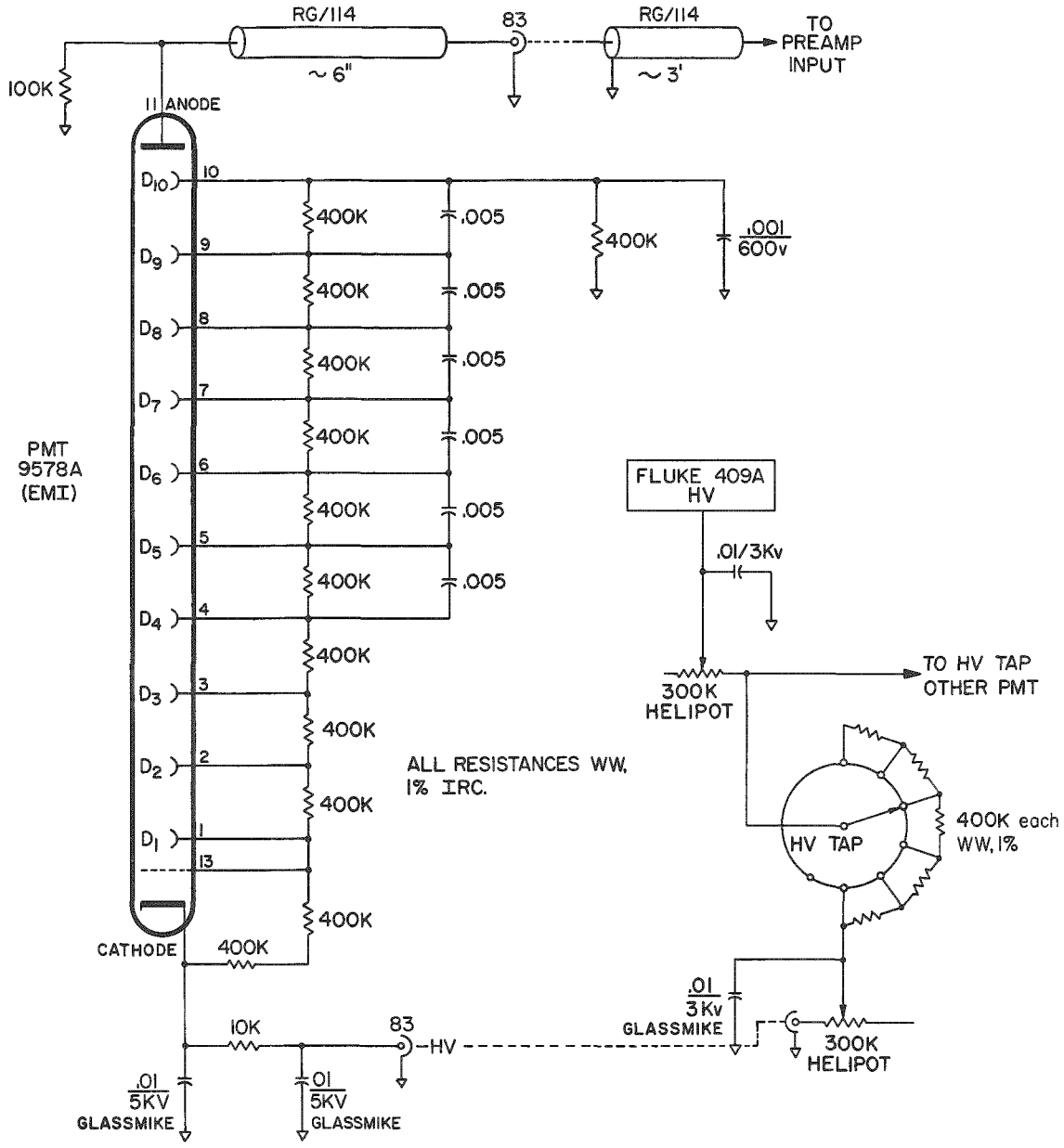

143-1348

Fig. 21. γ, NaI (Tl) Voltage-division System

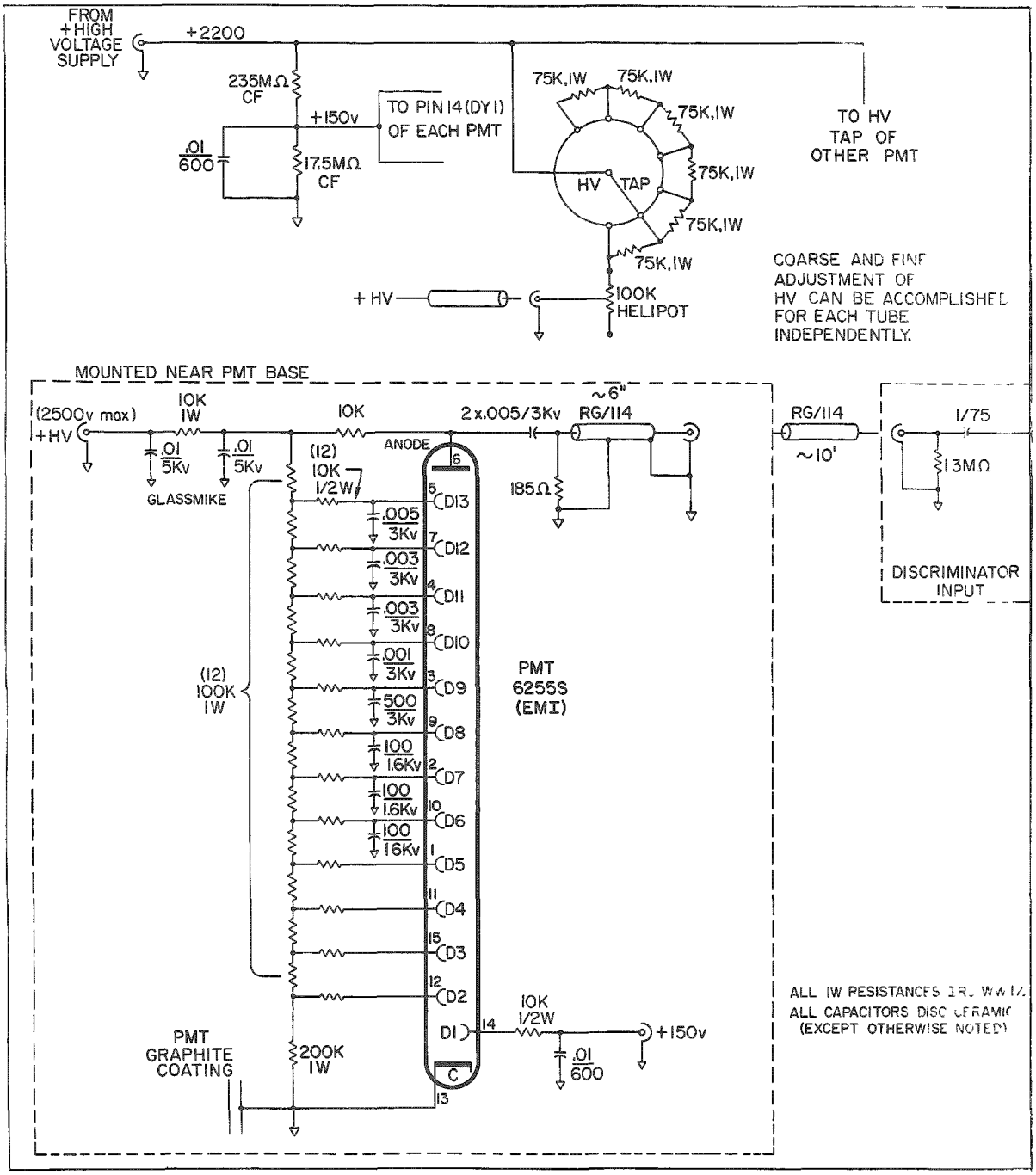

143-1350

Fig. 22. , Voltage-division System

VI. EQUIPMENT OPERATION

A. Daily Checkout

1. Gamma-Gamma

About 45 min to an hour each working day is devoted to a morning checkout of both the $\gamma\gamma$ and $\beta\gamma$ counting systems. The tests are designed to inspect for malfunctions, gain changes, timing shifts, and stability.

In order to establish continuity in operation, a check list is provided (see Fig. 23), which may be used to verify all settings. After a short period of experience, reference to the list no longer becomes necessary. The $\gamma\gamma$ mode is usually checked with the aid of the form in Fig. 24. A dual-trace oscilloscope is set to view the triggered coincidence AB input with the pulse generator. A check mark is placed when switching the low-high sequence provides pulses, as in Fig. 13 (l) and (m).

Next, by recording the number of counts in all three scalers for each pulse sequence, a fairly extensive test of the counting system is accomplished. It is important at this stage that the number of coincidence counts be equal to the number of counts in one of the two single channels (specifically, the lowest).

The next task is to check the location of the 0.85-Mev peak. This is carried out with the aid of a Mn^{54} source, which happens to have its single line at an energy just under the 0.855-Mev peak of Mn^{56}. The half-life of Mn^{54} is about 300 days. A brief discriminator bias curve is accumulated in the vicinity of the peak. This is obtained from first channel 1 with channel 2 switched out at the preamp and then for channel 2, thus establishing that the gain of each channel is identical to the desired extent, and that pulses from each crystal will overlap. Some typical spectra are portrayed in Figs. 25, 26, and 27. That there is essentially no less resolution when adding the two channels is indicated in Fig. 25.

A note should be added concerning the poor resolution displayed. For Mn^{54}, this is largely the result of poor geometry, since the radiation must penetrate a $\frac{1}{2}$-in. steel pipe and also is degraded by much scattering material. Although Mn^{56} is inside the steel pipe, it is dissolved within two liters of water and its spectrum is further penalized by scattering. Once the two channels are aligned, the total count with both channels switched on is obtained in order to evaluate overlap with better statistics. Normally, gain corrections of only 1% are necessary, and there are many days when no adjustments at all are required.

COUNTING SYSTEM CHECK LIST

Gamma-Gamma

1. PG Pulse Amplitude = _____ Polarity = _____ Attenuation = _____
   Decay Time = _____ Rise Time = _____ Relay = ON
   $\gamma\gamma$ HV = _____ -v; DC SW OFF $\beta\gamma$ HV: DC SW OFF
   β HV: DC SW ON
   Scalers: common/remote - MANUAL
   AMP A: Gain = _____ E = _____ % ΔE = _____ Mode: DIFF.
   B: _____ _____ % _____ DIFF.
   Coinc. A: F-1 = R F-2 = γ S = γ SW-7 = γ
   B: R NR R SW-5 = γ
   AB: R R NR
   Disc. 1: _____ % SW-4 = γ
   2: _____ % SW-3 = γ SW-8 = ON
   Prescaler: γ
   PA: 1 = PG 2 = PG
   SCOPE Test: Pulse Amplitude = _____ v; PW = _____ ns & _____ ns

2. Mn^{54} PG: Relay = OFF $\gamma\gamma$ HV: DC SW ON
   PA: 1 γ 2 PG for Ch. 1 test
   1 PG 2 γ for Ch. 2 test
   1 $\gamma\gamma$ 2 $\gamma\gamma$ for Ch. 1 + 2 test

3. Y^{88} Set AMP B Disc. to Y^{88} peak = _____ %

4. BG Set AMP B Disc. to Mn^{56} peak = _____ % Remove Sources; Set coinc.

5. AUTO SCALERS Scalers: Automatic; PA 1 = PG; Set 6 digit code; PA 2 = PG
   PG: Relay ON; Coinc. = 4-fold; $\gamma\gamma$ HV = DC SW OFF

6. Mn^{56} PG: Relay OFF $\gamma\gamma$ HV = DC SW ON
   Set 6 digit code PG 1 = $\gamma\gamma$ PG 2 = $\gamma\gamma$

Beta-Gamma

1. Mn^{54} $\gamma\gamma$ HV = DC SW OFF $\beta\gamma$ HV = DC SW ON
   PG 1 = $\beta\gamma$ β HV = DC SW ON
   Scalers = M or A

2. BG Remove sources; close plug; insert dummy scintillator.
   Check automatic scaler code (if used); Set Disc. Amp B to Mn^{56} peak.

3. Co^{60} Use integral disc. E = _____

4. Mn^{56} Use differential disc. E = _____ on Amp B

   Check:
   - 8 switches, especially SW 8 on β after Co^{60} test
   - $\beta\gamma$ & $\gamma\gamma$ HV
   - PA 1 & 2
   - Amp B settings
   - PG

Fig. 23

PG (HL)' 40 min = 144,000)
A 144 010
B 143 985
AB 143 978

COUNTING SYSTEM DAILY CHECKOUT

Date Feb. 21, 1963
Time 0900
By F. O.

Gamma-Gamma

1. A. Scope: Coinc. AB IP ✓ B. Scalers

	Disc.	H-L	L-H
A	10 %	722	722
B	33 %	722	722
AB	___	722	722

c/12 sec

2. Mn^{54}

	HV →	73.5%	___	___	___	67%	___	___	___
B Disc.	29	1671				1769			
	30	1816				1946			
	31	1903				2107			
	32	1972				2199			
	33	1882				2047			
	34	1836				1998			

c/12 sec

HV CH. 1: Old 5 x 73.5% New ___ Old HV 1020 V @ 80 % New HV ___ V @ ___ %
CH. 1: A 49; B 10 200; AB 0 — c/30 sec
HV CH. 2: Old 5 x 67 % New ___
CH. 2: +

Coinc. Pulses at 5½ % on A

3. Y^{88}

A 10 % 10245
B 33 % 10639
AB 146
c 60 sec { B 1.45 %; A 1.39 %; 2N 1.22 x 10^4 c/sec }
{ A ___ c/ B ___ min { B ___ %; A ___ %; 2N ___ x 10^4 c/sec }

Coinc.	3-Fold	2-Fold(A)	2-Fold(B)	2-Fold(F)	2-Fold(S)
A	✓	2031	1990	8011	2045
B	✓	2137	2160	12413	2124
AB	✓	2031	2159	7846	11

c/12 sec

4. BG — Plug IN, Water OUT

	Disc.	4-Fold	2-Fold(A)	2-Fold(B)
A	10 %	99	93	95
B	33 %	128	118	101
AB		2	93	101

cts / 1 min

H_2O ___ Plug ___ — cts / ___ min

5. Auto. Scalers: A 1, B 2, AB 6 — Scaler Channel 300, 301, 301 — PG cts / 10 sec

6. Mn^{56} @ 33% on B: 1471, 3186, 68.4 cts/sec — A 2.15 %, B 4.65 %

Beta-Gamma

1. Mn^{51} HV → 35.5 % ___ % ___ % ___ %

Disc. ΔE = 20%				
19	5610			
20	5757			
21	5872			
22	5785			
23	5538			

Old HV 1105 V @ 35.5 New HV 1105 V @ 35.5

2. BG Plug IN Dummy IN

Disc.	c/60 sec
15 %	51
21½ %	88
	1

3. Co^{60}

Disc.	c/30 sec
15 %	35741
32 %	2493 (integral)
	2242

ϵ_p = 90.0% σ_s = 3.14 %
N = 2.65 x 10^3 d/s
ϵ_p = 92.2% w/o Blocking (SW8)

4. Mn^{56}

E = 21½ % 95.2 %
ΔE = 20 % 1.97 %
N 4.2 x 10^3 d/s

RE-89 1 9 63

Fig. 24

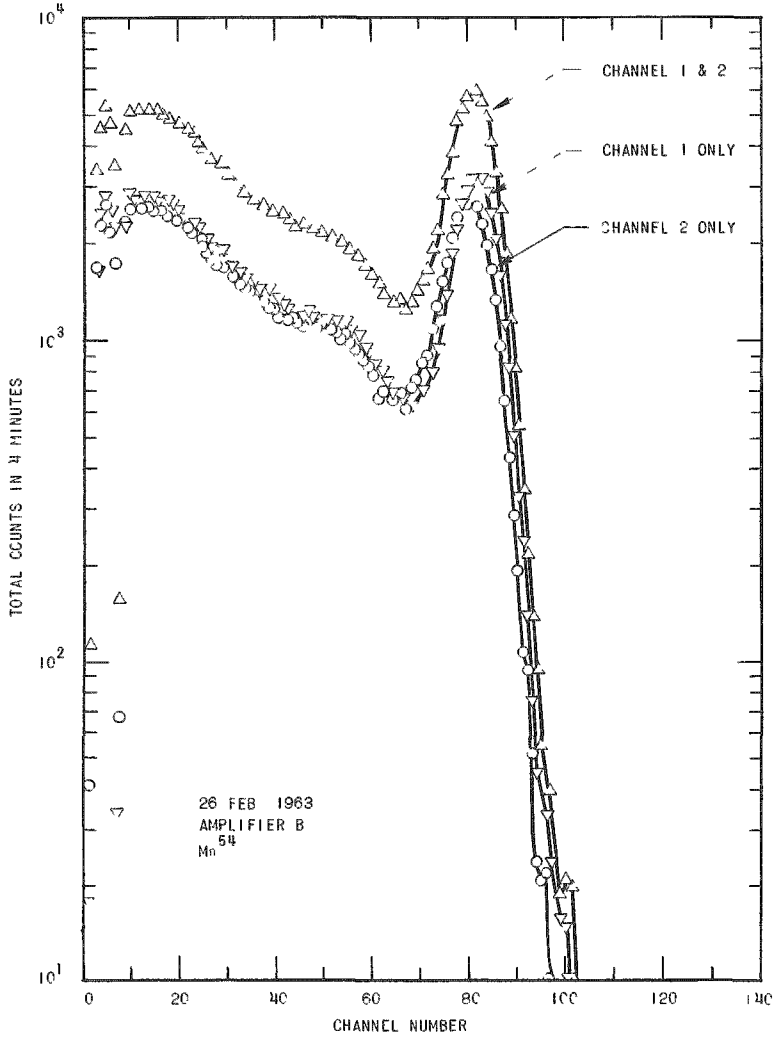

Fig. 25. Mn^{54} Spectra Used in Checkout

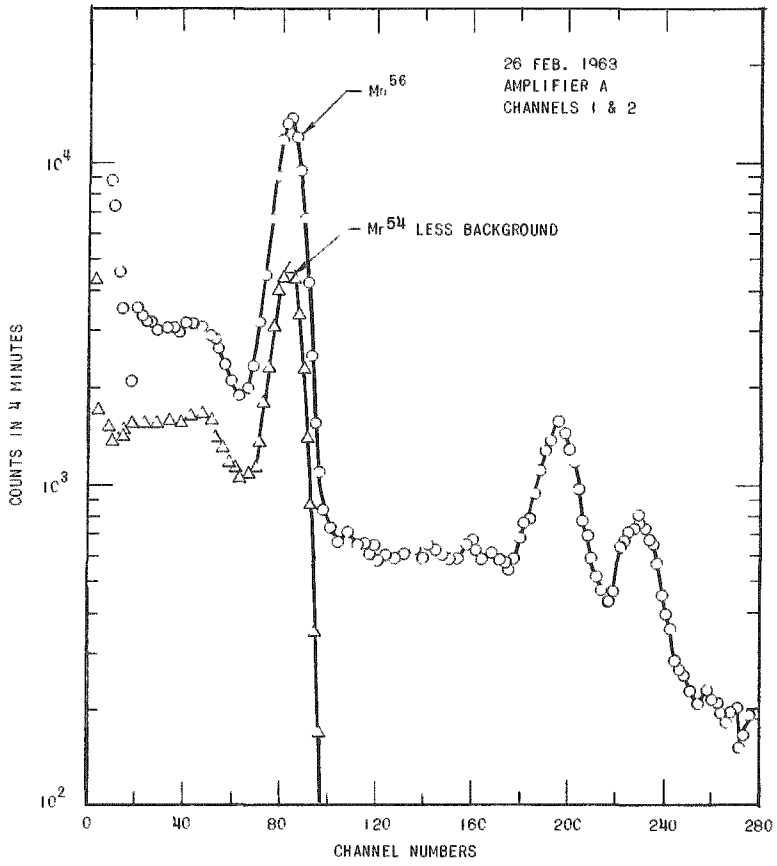

Fig. 26. Comparison of Mn^{54} and Mn^{56} Spectra (Mn^{54} Normalized in Pulse Height)

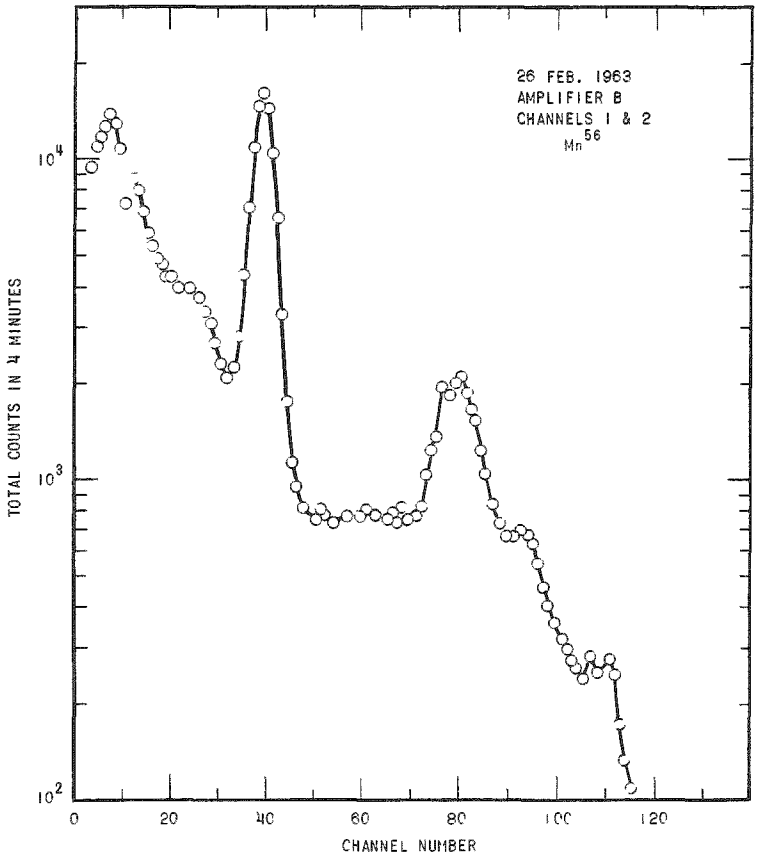

Fig. 27

Mn^{56} Spectrum in Amplifier B

One further test is made with the Mn^{54} source. As indicated in Fig. 26, the bias in analyzer A can be chosen as to avoid completely all counts due to the 0.85-Mev peak. When this bias is properly chosen, there should be no coincidences at all due to the Mn^{54} source (but a few from background). Accordingly, the channel A discriminator is lowered until the sudden onset of coincidence occurs, and this value is recorded. Normal operation of the high-energy channel A is at 8.0%, well above the $5\frac{1}{2}$% cut-off indicated.

In order to make an assessment of the coincidence-circuit operation, an Y^{88} source is placed in position for counting. This 100-day gamma source has a convenient coincidence between 0.91- and 1.85-Mev levels for about 90% of all decays. Only a small change in discriminator B location is required to obtain an optimum count rate. First, a 1-min run is made, the efficiencies and disintegration rate being calculated and compared with previous runs. A longer run may be made later during the day when convenient.

The next tests with the Y^{88} sample are carried out by switching various toggles located on the coincidence panels. By "3-Fold" is meant the imposition of a third coincidence requirement when, in fact, only

two pulses are entering the particular unit; there should be an immediate cessation of coincidences, as the check marks so attest.

If, in the final coincidence AB, either A or B input is placed in "not required" position, then there should be direct feedthrough of the single channel; this is the meaning of "2-Fold(A)" and "2-Fold(B)." There is a small difference in the dead times of the two coincidence output (~0.5 μsec), so that at very high count rates one can expect a discrepancy. This particular test has been very helpful in indicating some shortcomings which have now been corrected. At one time overloading of the amplifiers was poor, a situation especially noticeable with large background pulses. Since there was only 1-μsec deadtime in the direct output for singles, but almost 5 μsec for coincidences, extra single pulses were appearing. This has been remedied by better tuning of the amplifiers.

The remaining two Y^{88} tests determine features of fast and slow coincidence without the simultaneous fast-slow requirement. The number of AB counts in "2-Fold(F)" reflects the number of coincident pulses hitting the zero-cross circuit. This number should be equal to, but not much less than, the lowest count rate of the two single channels. There are six pulses at the zero cross for every one accepted in Channel B fast-slow coincidence, and 4:1 for Channel A. Channel B rate should be larger, since it needs higher gain in order to fire on 0.85-Mev events; Channel A pick-off triggers only on events above that energy.

When the fast channel is no longer required, then the number of counts in A and B under "2-Fold(S)" should agree, within statistics, or be not much more than the counts obtained with the results under "2-Fold(A)" or "2-Fold(B)" or be $\frac{1}{5}$ of a 60-sec count. A higher result in Channel B would indicate that a few pulses are rejected on the basis of timing. There are only 11 coincidences in AB result, instead of perhaps $\frac{1}{5}$ of 14, because the leading edges of the slow pulses are not properly timed for final AB coincidence; alignment is based on fast pulse appearance.

The fourth testing category is background. First of all, this ensures that there is no significant residual activity or sources in the area and that there is no electronic pickup from other equipment. The "4-Fold" test is made under standard operating conditions, whereas "2-Fold(A)" and "2-Fold(B)" again test for a feedthrough discrepancy. Space is set aside for recording the results of a longer background run when carried out on the manual console.

When the automatic equipment is to be used, a brief check is made with the pulse generator to ensure that pulses are going into the proper scaler. After a Mn^{56} sample has been inserted in the liquid counter, a computation is made to ascertain that counting efficiency is in the normal range.

Several summaries of test data are maintained. A quick glance at the Y^{88} efficiency summary provides a reliable indication of any trends in the single efficiencies or the disintegration rate. These are further supported by a log of "Mn^{54} counts in 30 sec" and the summary of Mn^{56} efficiencies.

2. Beta-Gamma

On those days that $\beta\gamma$ detection is to take place, a brief test series is conducted. A 20% window is used in order to obtain high efficiency at reasonably low background; thus, the peak counting rate occurs at a lower discriminator setting for analyzer B, even though the gain is about the same as for $\gamma\gamma$ counting. With the Mn^{56} source, the peak is maintained at the 21 $\frac{1}{2}$% level. A background check for 1 min is adequate to disclose possible spurious operation. An aliquot of Co^{60}, dissolved in a liquid scintillator, is maintained as a reference standard for efficiency. The disintegration rate and channel efficiencies are computed; in addition, the blocking pulse is removed from the $\beta\beta$ coincidence in order that a more valid measure of the true efficiency may be obtained, as well as assurance of correct operation.

Finally, when a Mn^{56} vial has been placed in the chamber, the results of an initial run are recorded as the final referee. A log of Co^{60} and Mn^{56} results is also maintained for this mode of operation. The computed disintegration rate for Co^{60} has been quite reproducible within counting statistics. Mn^{56} beta efficiency has been consistently in the order of 98% and the gamma efficiency around 1.9%.

B. Counting Routine

1. Intercalibration

Since the $\gamma\gamma$ system is not completely independent of efficiency in the computation of $N_A N_B / N_{AB}$, a procedure of intercalibration is carried out frequently. At present, this is done every day, but as results reach a reliable pattern, the intercalibration frequency will diminish to two or three times a week.

A $MnSO_4$ sample, irradiated in the CP-5 rabbit, is dissolved in a dilute aqueous solution at a specific activity intended to yield around 10^4 (d/s)/100 λ in the late afternoon. A 50-λ aliquot is quantitatively introduced to a liquid scintillation sample and 100 λ to 2,000 liters of distilled water. The pipettings are carried out with an ultramicroburet, or, more recently, with a pipet-buret with relative delivery accuracy better than 0.1%. Generally, three scintillation and three water samples are made. Specific details of the procedure are listed in Appendix F.

The samples are then counted according to a prescribed plan (see Table I) so as to yield about 10^5 coincidences for each sample in the course of approximately 2 hr. The $\gamma\gamma$ counting of three samples ordinarily takes about 1 $\frac{1}{2}$ hr and $\beta\gamma$ counting of three samples less than $\frac{1}{2}$ hr. The results are then sent to the computer, where the appropriate calculations are made; further information on the steps involved in handling this data are relegated to Appendix G.

Table I

Mn^{56} INTERCALIBRATION SCHEDULE

Initial Rates				$\gamma\gamma$ Standard Deviation (%)	Counting Time			$\gamma\gamma$ Total Coincidence Counts	Counting Time*			Total Counting Time** (min)
$\gamma\gamma$		$\beta\gamma$			101 min	102 min	103 min		201 min	202 min	203 min	
N (d/s x 10^{-4})	AB (c/s)	N (d/s)	$\beta\gamma$ (c/s)									
4	70	2×10^4	500	1/3	25	28	34	10^5	4	4	4	97
3.5	63	1.8×10^4	450	1/3	30	35	41	10^5	5	5	5	136
3	50	1.5×10^4	375	1/3	36	41	47	10^5	7	7	7	160
3	50	1.5×10^4	375	1/2	18	20	24	5×10^4	5	5	6	93
2.5	45	1.25×10^4	300	1/3	40	47	63	10^5	10	10	11	196
2.5	45	1.25×10^4	300	1/2	20	23	27	5×10^4	7	7	7	106
2	36	10^4	250	1/3	50	65	88	10^5	15	16	17	266
2	36	10^4	250	1/2	27	31	37	5×10^4	9	9	10	138
1.5	25	7.5×10^3	190	1/2	36	41	47	5×10^4	14	15	16	184

* In all cases total $\beta\gamma$ coincidence counts = 8×10^4 for 0.1% standard deviation.

** Includes 15 min for total sample-changing time.

It is necessary to flush out the $\gamma_1\gamma_1$ liquid counter with water at least twice in order to reduce residual activity to a small fraction. This requires about 5 min, including time for refilling with the next counting sample. Time for changing scintillation samples is about 1 min.

As shown in Appendix B, there remains, after computing the disintegration rate for $\gamma_1\gamma_1$ detection, a correction factor related to the true rate obtained in the $\beta\gamma$ coincidence apparatus. The specific activity is determined by dividing the weighted mean disintegration rate for each sample by its aliquot volume. The ratio of the $\gamma_1\gamma_1$ to $\beta\gamma$ specific activities is then obtained, and this result is divided by 4; division by 2 is required in order to adjust the result for the prescaling factor of 2 in $\beta\gamma$ counting; the other factor of 2 is used to correct the double efficiency factors in the $\gamma_1\gamma_1$ equations. The existing ratio of 1.23 is close to $\bar{\mu}(1+\alpha)V_{eff}/2.000$; this implies that $\bar{\mu}(1+\alpha) \approx 1.35$. A log of these results is kept current, and those data obtained since the last modification of the equipment have an rms spread of 0.67% for over 30 intercalibrations.

The relationship between 2.000 liters used in intercalibration versus the approximate 2 liters drawn from the bath is as follows: The liquid counter actually holds about 1.8 liters within the counting volume and

immediate tubing. The remaining liquid is retained in the tubing which passes through the shield and for the most part, in the beaker on top of the shield. Thus, there is an effective volume (V_{eff}) which is seen by the gamma scintillators, and this volume is quite insensitive to the exact amount of liquid remaining in the shielded beaker. When the intercalibration takes place, the same analysis holds true, but at this point it is important to dilute the activity to an exact volume; yet the result is applicable to V_{eff}.

2. Manganese Bath

It is intended that about 5 hr of each working day be devoted to counting samples derived from the manganese bath. With a 1-hr checkout and a 2-hr intercalibration, this is feasible; on days without an intercalibration, additional time may be devoted to the manganese bath. Usually, a manganese bath solution is counted for about one half-life (2.6 hr).

After at least 1 hr of stirring by a closed-loop pumping process, a sample of volume approximately 2 liters is withdrawn and then carried downstairs to the counting room. Information appropriate to decay corrections is recorded.

Some results based on a dilute concentration (25 g/l) of manganese sulfate activated by a 1-c Ra-α-Be source indicate an rms deviation of 1% for 5 runs.

The most significant counting efficiency to discuss is the number of coincidence counts/sec (referred to the start of actual counting) divided by the number of Mn^{56} disintegrations/sec in the sphere at saturation. This is 4×10^{-6} count/disintegration for a 640-liter manganese bath. From the intercalibration procedure, one learns that the efficiencies for counting 2 liters in the count rate doubler $\gamma\gamma$ system are $A \simeq 2 \times 0.026$; $B \simeq 2 \times 0.048$, $AB \simeq 2 \times 0.001$. There is a 5-10 min lag between sample withdrawal and commencement of counting.

3. Other Radioisotopes

Although the $\gamma\gamma$ counter is rather limited in terms of isotopes that can be counted, the $\beta\gamma$ system is quite versatile. Since timing by the zero-crosser is closely related to pulse height, one can only use the $\gamma\gamma$ mode without modification if the ratio of gamma energies is about 2 to 2.5:1. (This applies to Y^{88} and Na^{24}, for example.) One further restriction would be that it is best not to introduce long-lived radioisotopes into the counting chamber because of difficulty in flushing. On the other hand, a 1-in. source hole is available for counting external samples, although this suffers from attenuation by $\frac{1}{2}$-in. steel surrounding the NaI(Tl). By either bypassing the mixer-splitter (and repeater) or by changing gain, window, and zero-cross settings, any type of $\gamma\gamma$ detection may be carried out; in fact, by providing new inputs to the preamps, external detectors may be encompassed

The $\beta\gamma$ mode can accommodate a much wider range of active nuclides with a spread in disintegration rates. Again, keeping in mind the requirements of pick-off circuit adjustment, the γ channel has reasonable latitude for differential or integral settings. There is, however, little room for changes in NaI(Tl) distance to scintillation vial, although this feature may be added in the future. The background level of this channel is its main limitation. When set for a very broad region around the 0.85-Mev peak, γ background is about 1.5 c/s and coincidence background about 0.014 c/s. When opened up for Co^{60} counting (lower level around 0.6 Mev, integral setting), gamma background goes up to 2.2 c/s and coincidence rate by a factor of 10 (due to cosmic ray coincidences).

High intrinsic β efficiency (98% for Mn^{56}) and modest background (1.5 c/s) allows this single channel to be used even for noncoincident low-energy isotopes, such as C^{14}. One must first find a chemical form compatible with a liquid scintillator to obtain these high efficiencies, but experience, as indicated in the literature survey in Appendix C, has proven that almost any nuclide can be incorporated for internal liquid scintillation counting. Moreover, there are supplemental methods, such as use of gels, Cherenkov counting, and foil counting with a plastic scintillator.

For Cherenkov detection, we have dissolved active $MnSO_4$ in a counting vial filled with water and obtained 40% efficiency. In addition, we know from earlier experience that concentrations of 200 g/l, although slightly pink in solution, still approach that limiting value. Counting of Na^{24} (1.39 β max) has yielded 25% efficiency for an 11.8-ml solution containing 7 g of $NaNO_3$; we have also managed to count an aqueous solution of 0.3 g $NaNO_3$ with 96% efficiency when incorporated in a liquid scintillator.

A plastic scintillator, shaped in a cylinder not much larger than the scintillation vial, cut in two with a small recess for a 1-cm^2 foil, its plane lying on the horizontal axis between the two phototubes, provides 73% efficiency for a 5-mil manganese foil. Our efficiencies are equal to or better than those given by Loveridge,[5] which is basically the system upon which our setup is patterned. Some typical efficiencies from that reference are abstracted in Table II and compared with those we have obtained. It appears that an augmentation of internal scintillation sample efficiency is obtained from Cherenkov light generated in the glass and coupling fluid. If satisfactory seals can be made, we plan to use a liquid scintillator as coupling fluid in order to catch additional photons from long-range betas which escape at the walls of the scintillator vial.

Table II

COMPARISON OF BETA CHANNEL EFFICIENCIES

Isotope	Beta End-point Energy (Mev)	Our Results	Loveridge[5]
Mn^{56}	2.8 (50%) 1.1 (30%) 0.7 (20%)	98%	96%
P^{32}	1.7	99%	98%
Co^{60}	0.31	93%	85%
Na^{24}	1.4	98%	97%
Sc^{16}	0.36	95%	87%

4. Background and Environment

Nighttimes and weekends are usually reserved for background monitoring. When the automatic readout equipment is available, counting periods of about 2000 sec are chosen; the data are later inspected for spurious effects and then tallied to obtain the average for all three channels. Most of the time background is run for the $\gamma\gamma$ mode, but about once a week a $\beta\gamma$ run is made. With the automatic data, it is possible to observe the appearance of any residual activity not flushed out. For a long weekend, we often leave a fully active sample in the counter and follow its decay into background levels (Mn^{56} decays by a factor of 10^3 in a full day). The data are processed by the computer and subsequently plotted, thereby testing the long-term stability of the apparatus.

In order to preclude a systematic error, some backgrounds are obtained during the working day. These check well with overnight and weekend count rates.

Temperature and humidity are also recorded daily.

A review of one month's accumulated background information reveals the following:

$$\beta = 1.562 \pm 0.118 \text{ c/s}; \quad \gamma = 1.47 \pm 0.15 \text{ c/s}; \quad \beta\gamma = 0.015 \pm 0.001 \text{ c/s}$$

$$A = 1.58 \pm 0.17 \text{ c/s}; \quad B = 1.96 \pm 0.10 \text{ c/s}; \quad AB = 0.018 \pm 0.001 \text{ c/s}$$

The errors are rms values.

With a source yielding 10^5 neutrons/sec in a 200 g/l manganese solution, signal/background rates at the start of counting would thus be approximately:

A = 1.7/1 with signal/error = 16/1

B = 2.9/1 with 58/1

AB = 7/1 with 120/1 .

VII. DISCUSSION

A. Equipment Performance

1. Gamma-Gamma

An extensive series of tests have been carried out to determine the dependence of channel counts and coincidence ratio on various operating parameters. For several settings which straddle the normal operating region, disintegration rates have been obtained at statistics of 1/2% or better. Figures 28 and 29 demonstrate that plateaus exist in the neighborhood of the 0.845-Mev peak, which is set daily on each detector. Accordingly, changes in gain of ±5% in either detection channel may be tolerated between checkouts. Similar results obtain for changes in discriminator level or window width. To ensure reliability of coincidences, curves such as Fig. 30 have been run.

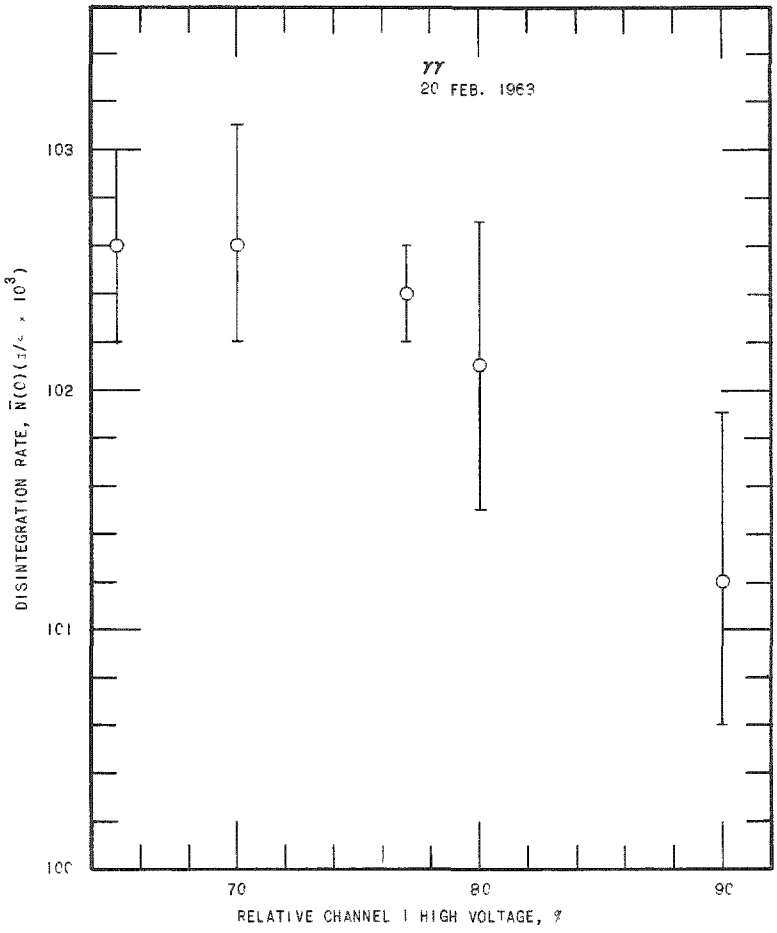

Fig. 28. γγ Disintegration Rate as a Function of Channel 1 High Voltage

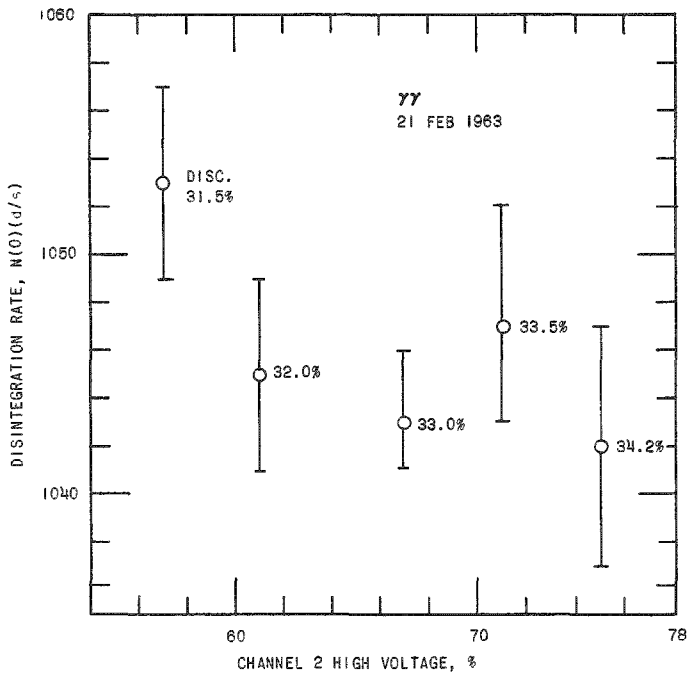

Fig. 29. $\gamma\gamma$ Disintegration Rate as a Function of Channel 2 High Voltage

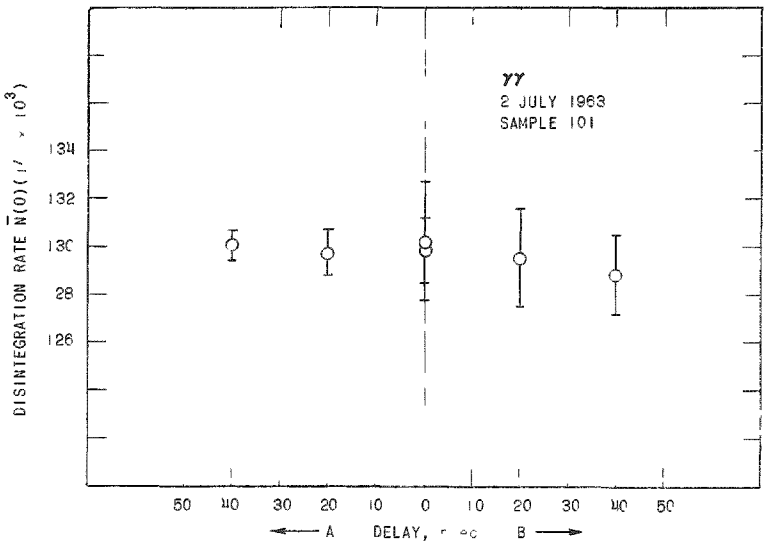

Fig. 30. $\gamma\gamma$ Delay Plateau

Other evaluations, such as variation in fluid volume, confirm that the liquid counter is primarily sensitive only to the 1.8 liters contained and is adequately isolated from the 200 ml in the tubing and beaker outside the shield (see Fig. 31). Thus, the exact quantity of liquid drawn from the manganese bath is not significant, permitting use of an effective volume for calculations.

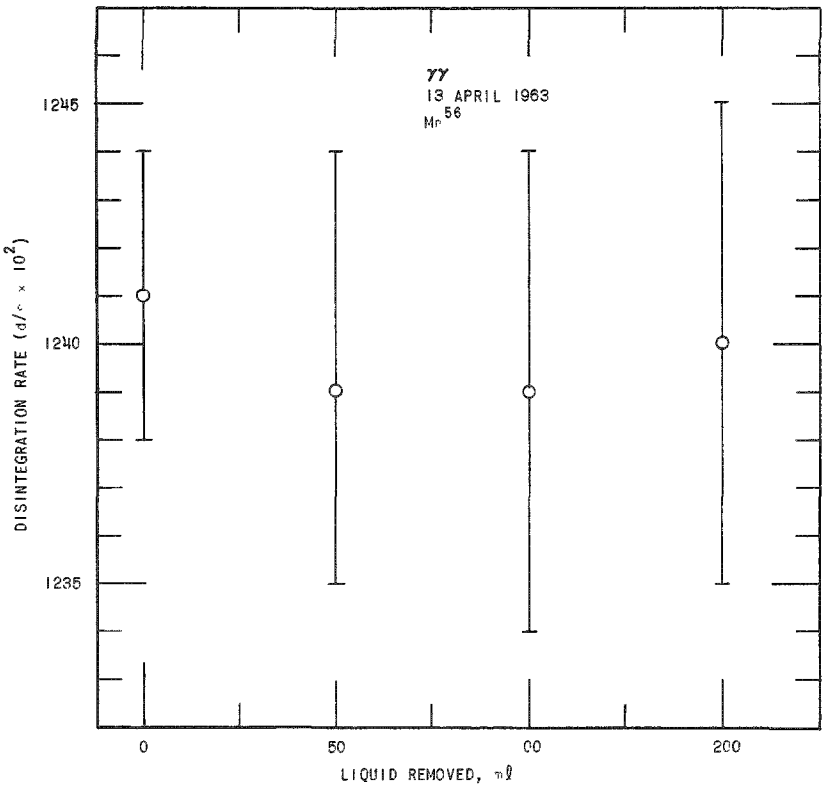

Fig. 31. Insensitivity of γγ Counter to Liquid Volume (Capacity 2.00 Liters)

An important test which is sensitive to many effects is the operating plateau obtained as a function of common high voltage, that is, the single supply which governs both channels. This corresponds to changing both detector gains simultaneously. The results of this investigation are revealed in Fig. 32. At this juncture it is apparent that a high-voltage supply with good regulation is needed and is employed.

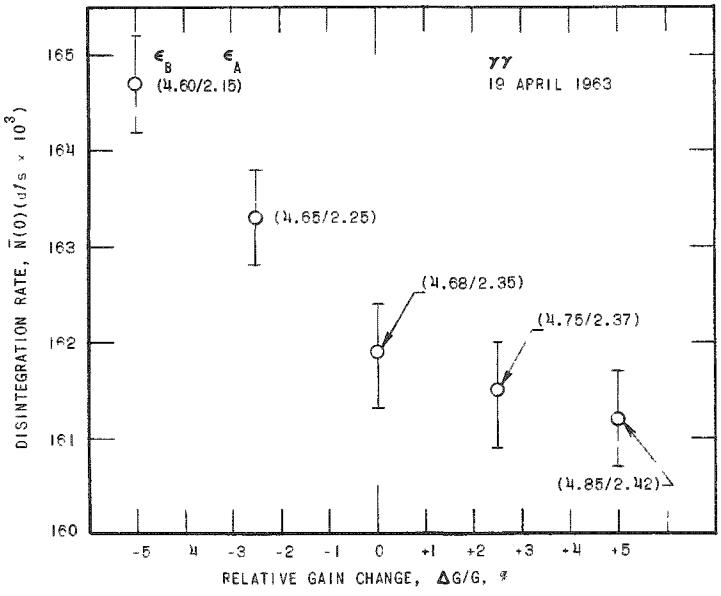

Fig. 32

Disintegration Rate as Affected by Changes in Common High Voltage

Possibly the most severe test of the system is obtained by allowing a very hot sample to decay over many half-lives until it reaches background level. This displays the adequacy of computer corrections based on assumptions made (see Appendices B and D), as well as the extent of stability over a full day or so. Figures 33 and 34 are the results; in Fig. 33 the slope is that of the characteristic Mn^{56} curve normalized only at the intersect with the ordinate. The computed weighted mean and probable error are drawn in Fig. 34. A similar set of decay curves for a sample from a solution weakly activated by a Ra-Be source is presented in Fig. 35.

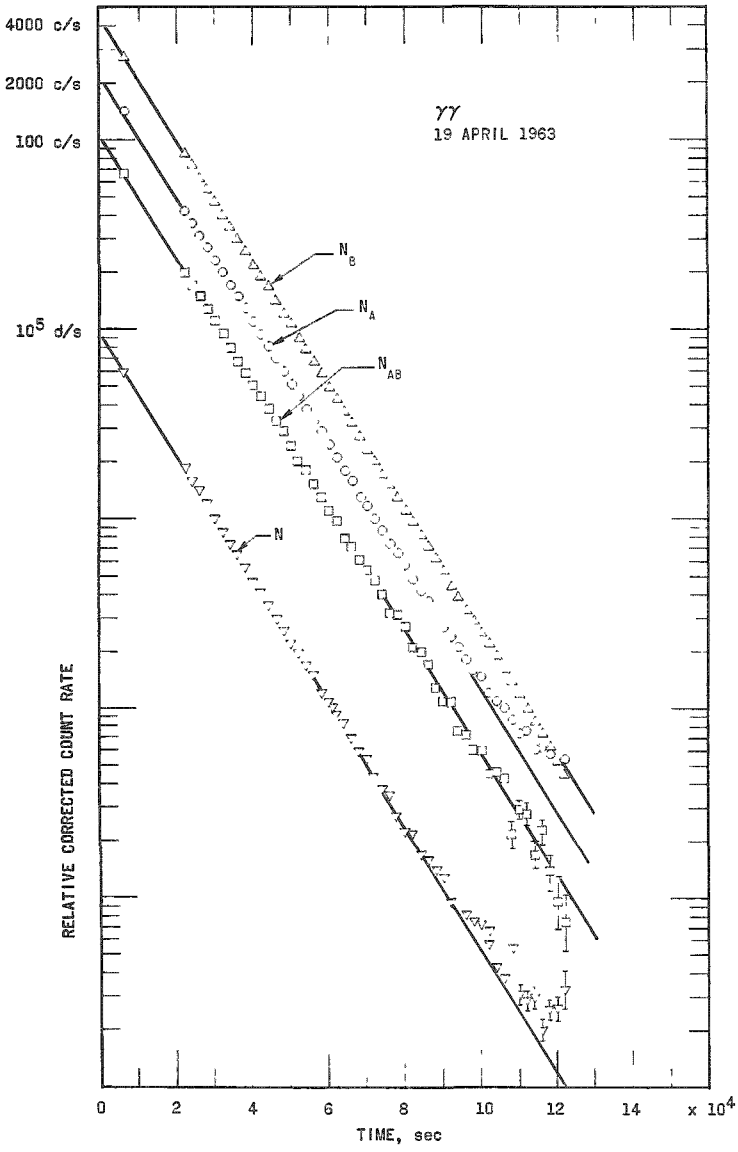

Fig. 33. γ γ Decay Curves for 12 Half-lives

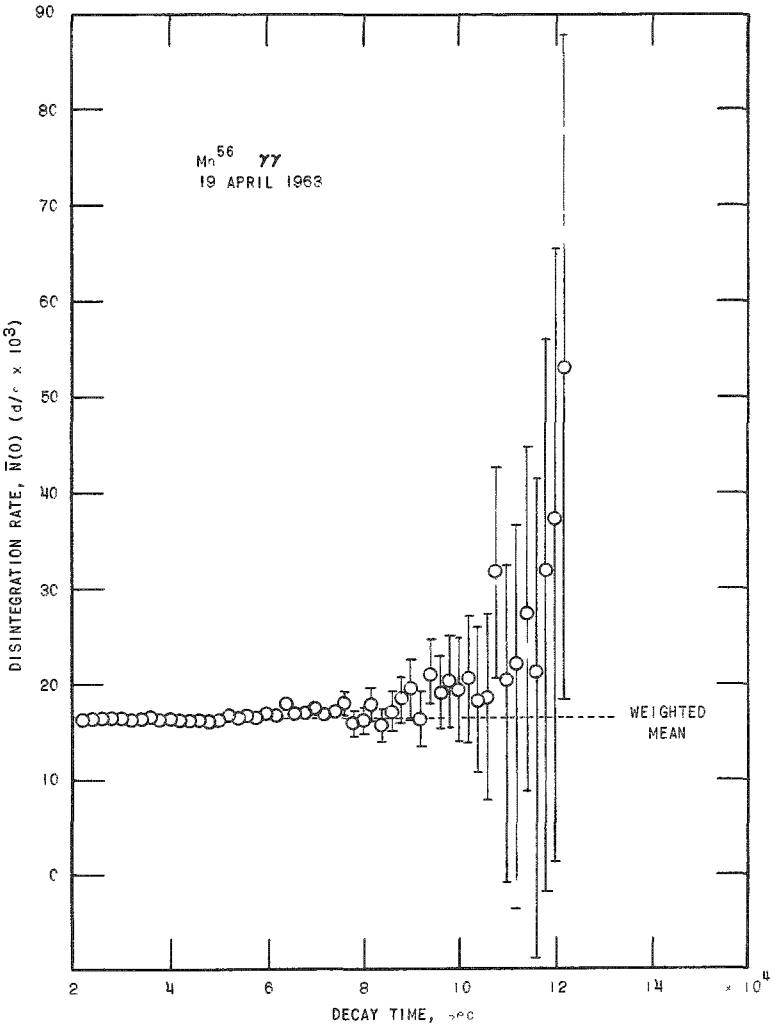

Fig. 34
Disintegration Rate Computed for Mn^{56} Sample Decaying for 10 Half-lives

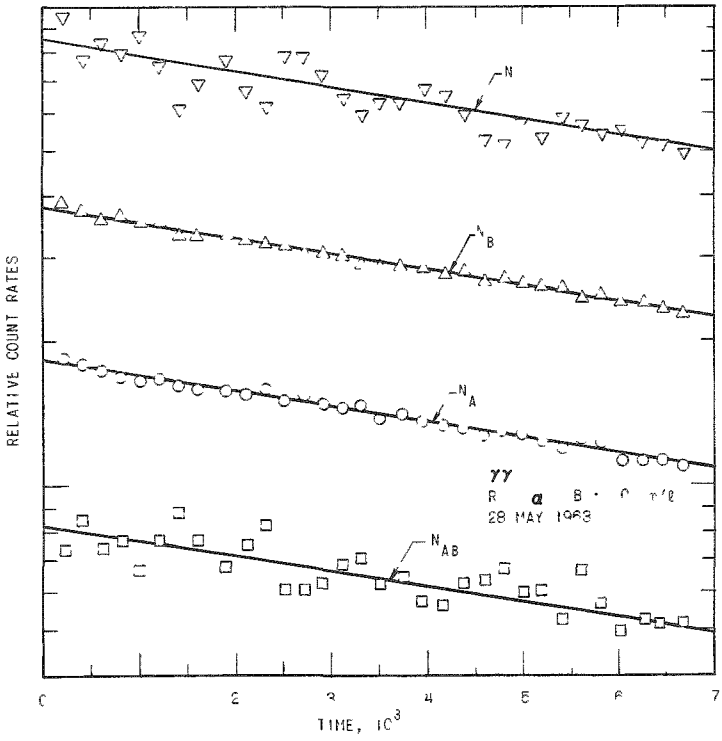

Fig. 35
Decay of 10-g/liter Manganese Bath Sample (Disintegration Rate Initially about 800 d/s)

When combined with information obtained from records of count rates of reference sources (300-day Mn^{54} and 90 day Y^{88}) and with the computed values of single-channel Mn^{56} efficiencies based on the coincidence equations (see Appendix D), these data provide assurance of long-term reproducibility in use.

2. Beta-Gamma

Similar functional curves have been obtained for the absolute system. The emphasis here has been in showing that fairly large fluctuations in beta or gamma efficiency could be tolerated while still leading to invariant disintegration rates for Mn^{56}. This may be accomplished by varying the high voltage (see Fig. 36), the discriminator level (see Figs. 37 and 38), the γ window width (see Fig. 39), and the delay (see Figs. 40 and 41). These indications of stability are sustained by a decay curve of almost 3 half-lives (see Figs. 42 and 43).

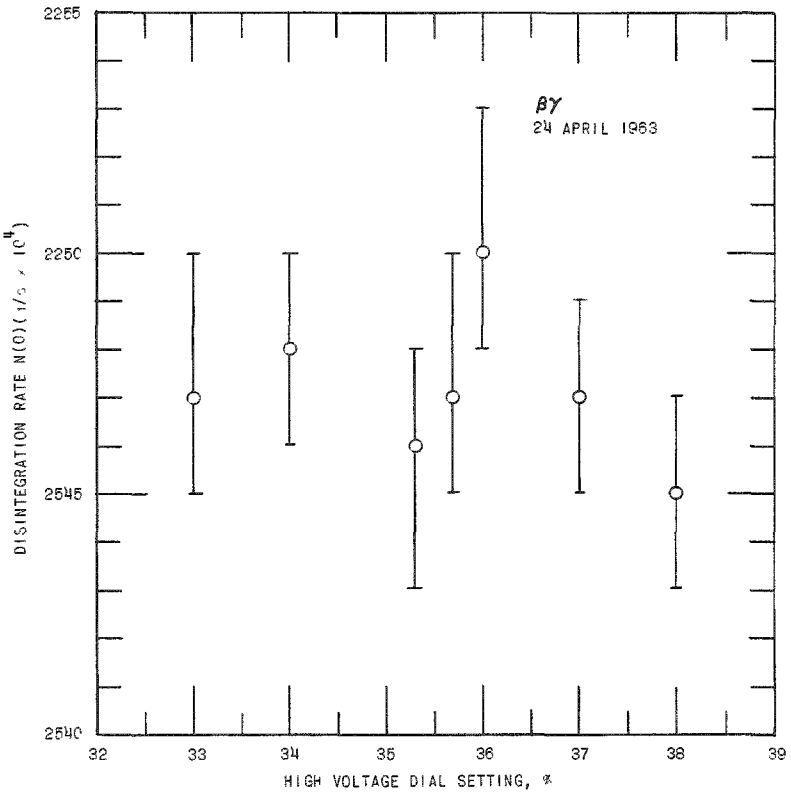

Fig. 36. $\beta\gamma$ Disintegration Rate in Vicinity of Normal γ High Voltage Setting

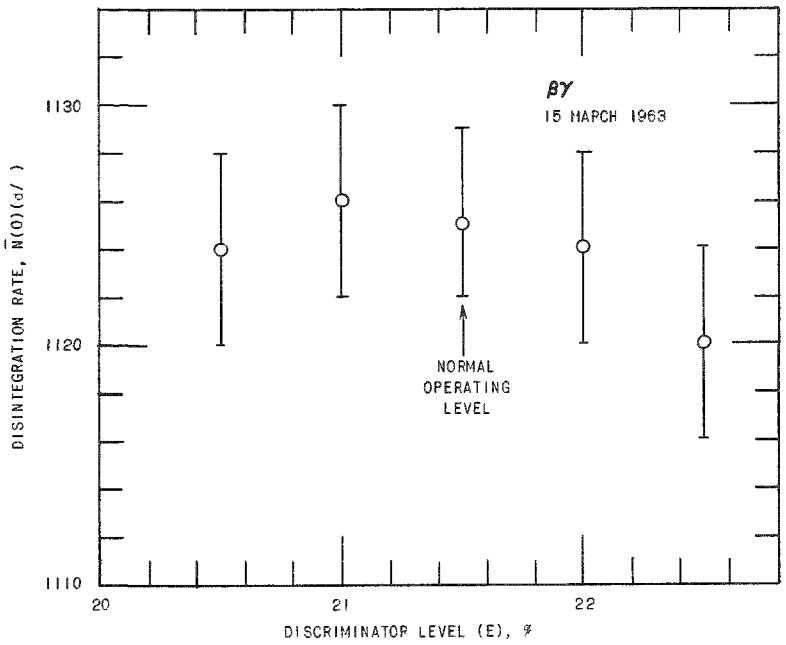

Fig. 37. βγ Discrimination Rate in Neighborhood of Normal Operating γ Discriminator Level.

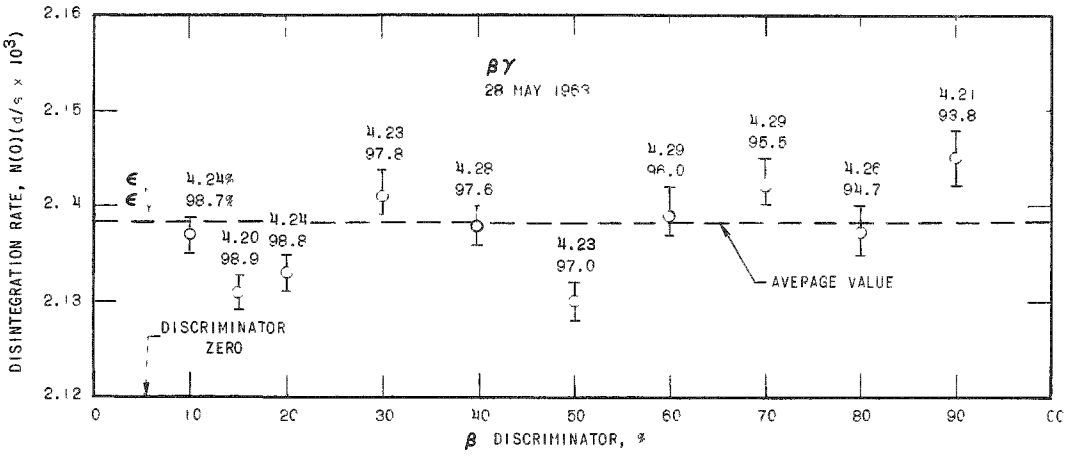

Fig. 38. βγ Disintegration Rate vs β Discriminator Level

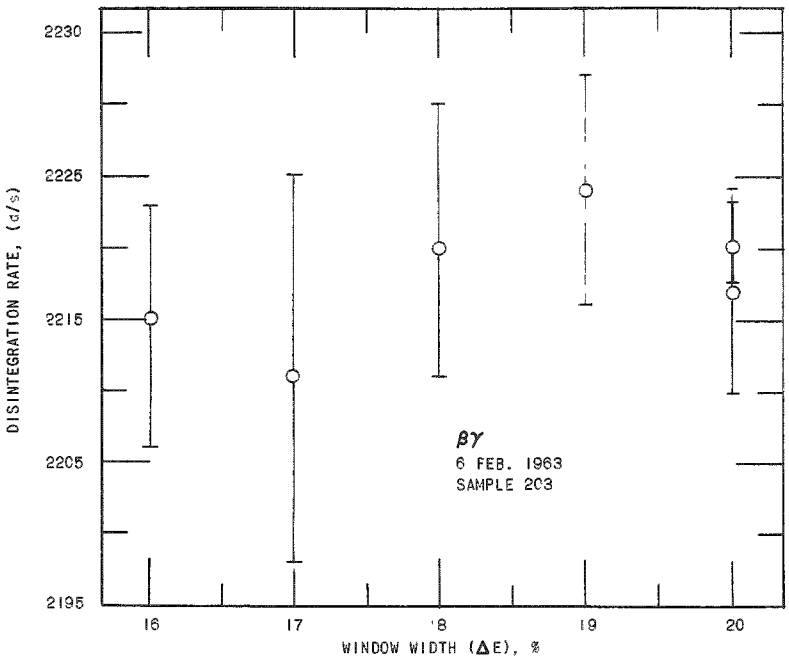

Fig. 39
$\beta\gamma$ Disintegration Rate as a Function of Channel-window Width

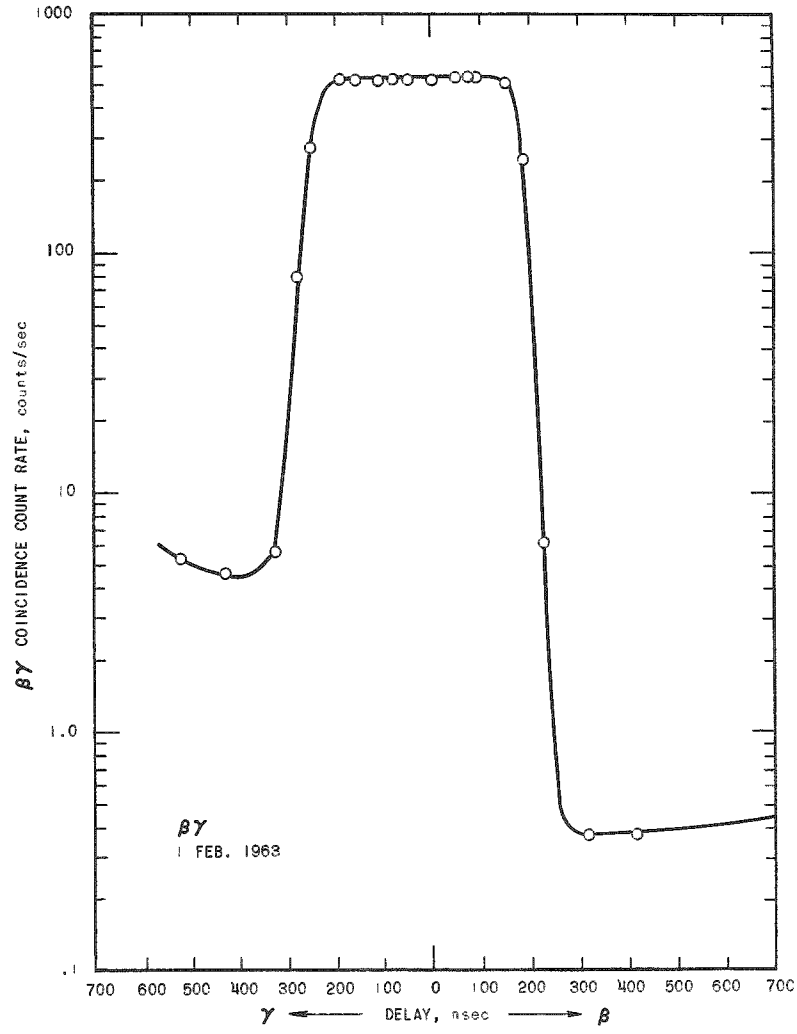

Fig. 40
$\beta\gamma$ Delay Curve

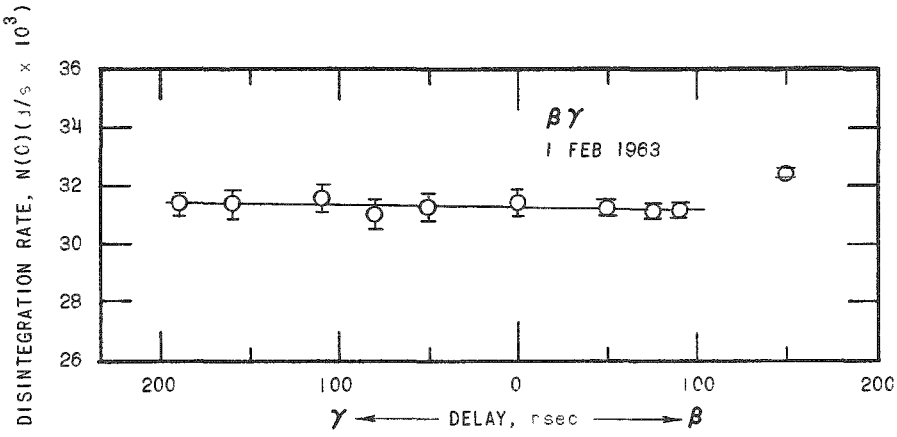

Fig. 41
$\beta\gamma$ Delay Plateau

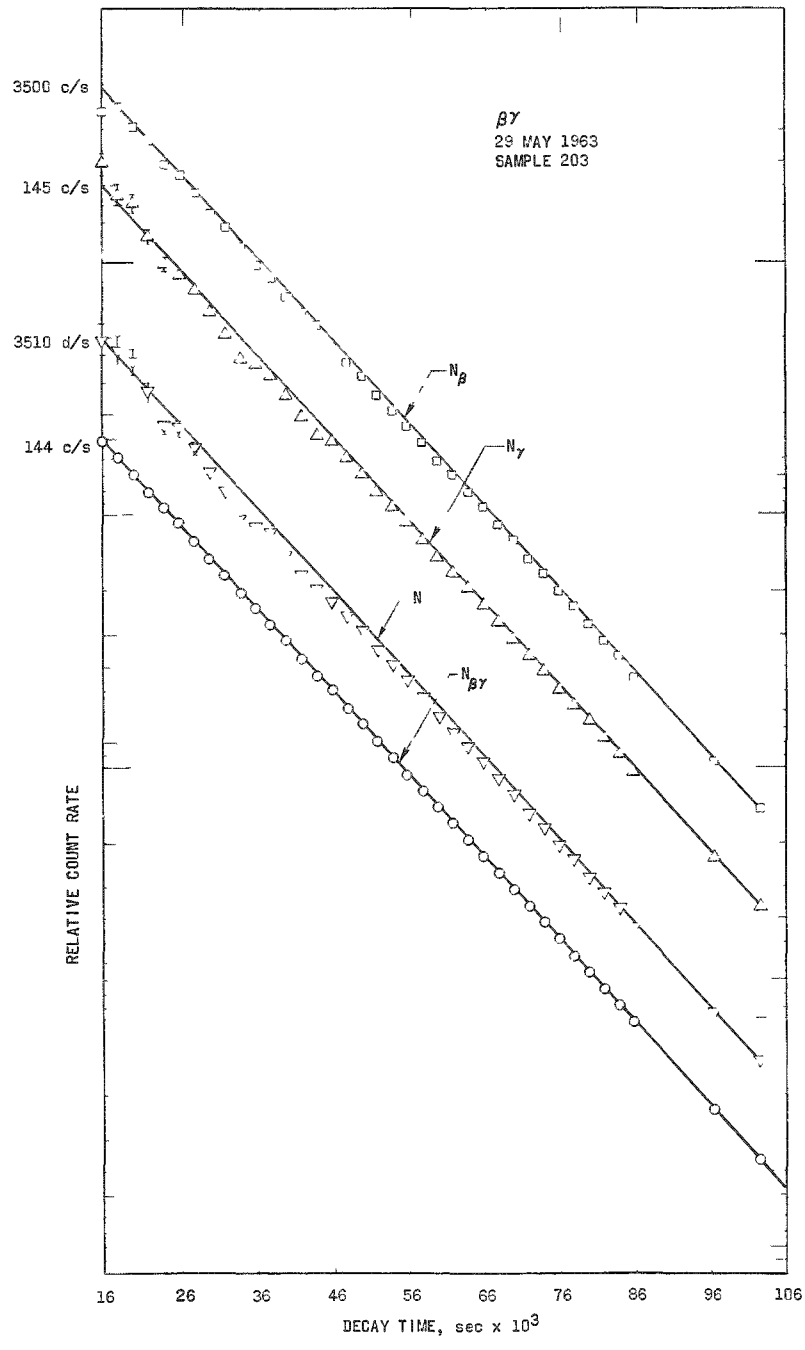

Fig. 42
Mn^{56} Decay in $\beta\gamma$ Coincidence System

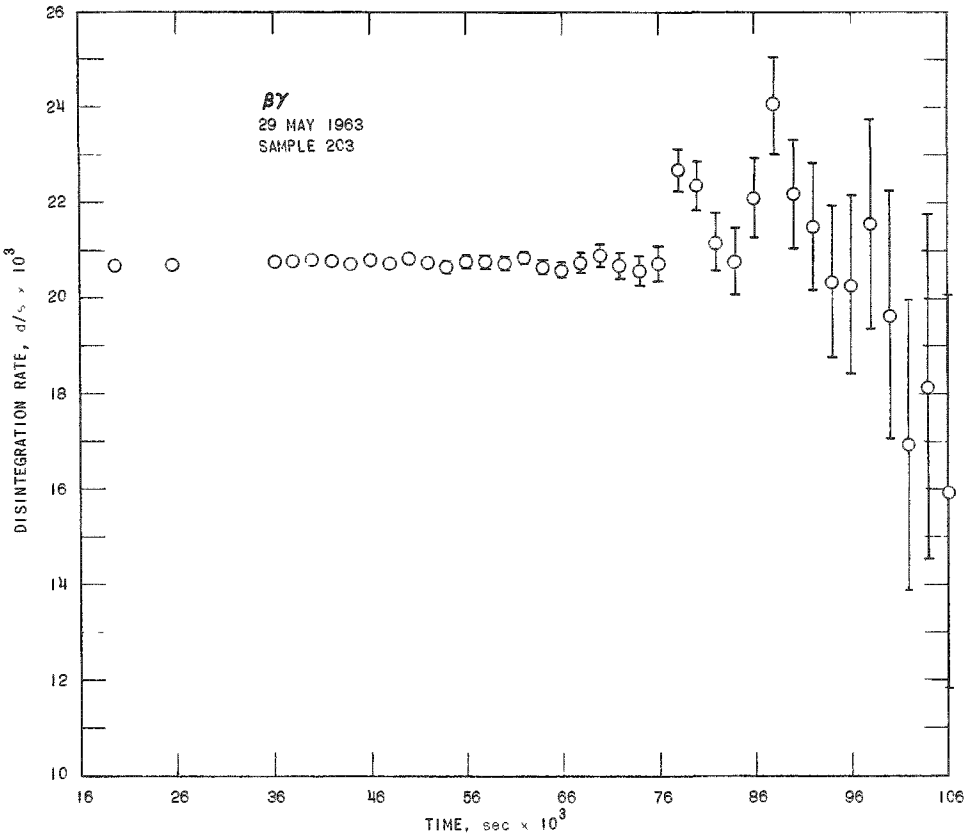

Fig. 43. Coincidence Rate Computed for $\beta\gamma$ Counting of Mn^{56} Decay

There is, in addition, proof that results are insensitive to aliquot volume in the range of normal use, or to other factors involved in sample preparation, such as liquid scintillator quenching and manganese concentration; however, a trial-and-error procedure was required to find the optimal procedure for irradiation, handling, dilution, and delivery. It is for this reason that an appendix is included with details of the steps involved.

To date, the main effort has been directed towards demonstrating the invariant character of beta-gamma operation. A lengthy program of comparison with $4\pi\beta$ counting is in progress. Careful correction is required for the crossovers involved in the Mn^{56} decay scheme.

Although liquid scintillators tend to deteriorate after months of storage, and although the Co^{60} betas have a rather low mean energy, consistent disintegration rates have been collected for such a reference sample.

The liquid scintillation system is rather versatile, as discussed earlier. There are occasions when thin deposits cannot be made with sufficient activity or when there are chemical difficulties in sample

preparation for $4\pi\beta$ proportional counting. In addition, with or without the aid of supplemental pulse-shape-recognition circuitry, it is possible to count and distinguish between betas, alphas, and fission fragments.[6] However, when large amounts of material are incorporated internally, one no longer benefits from lengthy regions of stability or from very high efficiency. In such cases, secondary calibrations are often essential, and proper consideration must be given to the effect of scintillation pulses caused by interactions originating from gamma emission, etc. Single-channel counting of charged particles is feasible with this equipment; in fact, for low-energy radiation, the 13-μsec deadtime may be removed, leaving only a 0.1-μsec paralysis caused by the prescaler.

Future uses of the equipment include neutron-yield measurements with Cf^{252} spontaneous fissions and thermal beam activations of U^{235} sources.

B. Comments on Design and Performance

In the course of designing, testing, improving, and operating the equipment described in this report, a number of alternative means of signal processing were seriously considered; at the same time, further potentially useful applications of the delay-mixing processing logic became apparent. Some brief observations on these matters may be appropriate here.

The first group of comments concerns the gamma-gamma electronics. As already mentioned, the system described in this report was specifically designed to make use of two available amplifier-single-channel analyzers of very good stability and overload characteristics. If amplifier specifications are unrestricted, the delay-mixing scheme would in principle allow one to use only a single amplifier and zero-crosser, with two pulse-height selectors. One could further replace the mixer-splitter input stage with a passive network, to improve the overall gain stability, and likewise replace the repeater with a passive network in the interest of economy and simplicity.

The design of possible passive networks for mixing (and splitting) pulses at the input of the amplifier (or amplifiers) must match output impedances of preamplifiers and input impedances of amplifiers to the impedance of available delay cables of adequate bandwidth, as well as to pulse cables which interconnect units. By proper location of the network, long interconnecting cables can be placed where they do not affect the pulse shape. Attenuation due to the network is not important, since enough total gain is always available in the amplifier and preamplifier. Distortion of pulse shapes, and appearance of small satellites due to distributed capacitances and inductances are, however, more serious, and would have to be eliminated by careful layout and compensating networks. This rather

laborious task would improve overall stability to the extent to which a purely passive element is more stable, in the long run, than any circuit component, however carefully designed, which includes active elements.

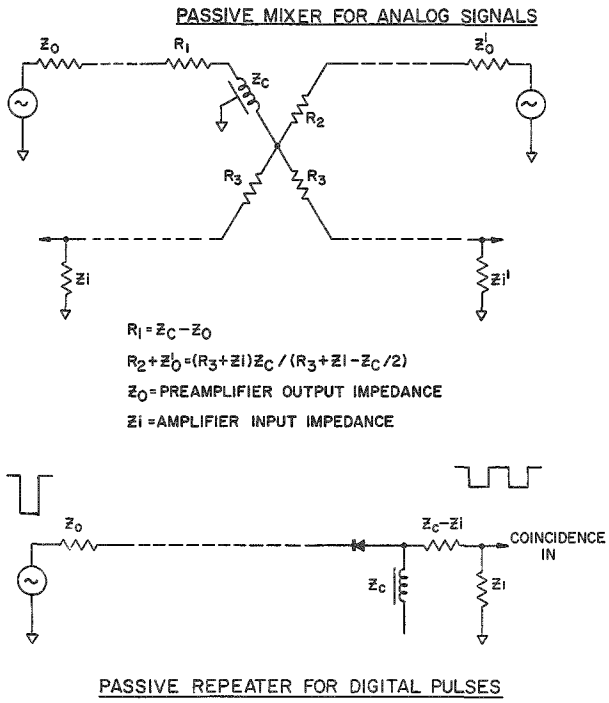

Fig. 44. Some Passive Network Concepts for Mixing, Splitting and Repeating

The splitting and repeating of the digital pulses at the output of the two pulse-height selectors could, similarly, be performed by passive elements; in this case, attenuation is apt to be more of a nuisance than distortion and small satellites. Two simple passive circuits, for input mixing and for output repeating, respectively, are shown, for the sake of illustration, in Fig. 44.

When the equipment is intended for very low count rates only, the zero-crossing circuit can be dispensed with; in that case, instead of using repeaters, the discriminator output may simply be lengthened to extend slightly beyond the delay, resulting in an overall system of great simplicity.

As concerns the choice of amplifier clipping and bandwidth, double differentiation clearly has the advantage of improving the return of the trace to the base line, while usually lengthening the necessary delay of the second pulse with respect to the first one. The delay, in turn, results in attenuation - which can be compensated by adjusting the high voltage on the photomultiplier whose output is delayed - and in distortion of the pulse shape. For this, as well as other reasons, a delay-mix system of count rate doubling may not be suitable when good pulse-height resolution is a prime requisite. On the other hand, when resolution is relatively unimportant, single delay-line clipping may be feasible; the pulse separation could then be reduced by a factor of two. Ultimately, pulses might be clipped very sharply, and delay times thus cut down to several hundred nanoseconds, allowing use of ordinary pulse cable for all delays throughout the system. The considerably better bandwidth of such cables would result in improved sharpness of timing, allowing coincidence gates to be narrowed to the point where the accidental/true coincidence ratio is insignificant at the highest practical count rates. The ultimate limit of clipping beyond which the resolution becomes inadequate is imposed only by the detector pulse rise time, since stable amplifiers of bandwidth up to 50 Mc have become available recently.

The addition of pulse doubling and sorting circuitry does not interfere with occasional use of the system, or parts of the system, without doubling, if a few switches are arranged to disable the doubling function. The gamma channel borrowed for the beta-gamma coincidence system described in this report illustrates one of many possible arrangements of this sort. Furthermore, part of the doubling circuitry may be combined with additional units to construct other useful systems, such as, for instance, a sum-coincidence spectrometer.

A modification of the delay-mix technique may be useful in liquid scintillation counting: when photomultipliers are used whose gain is not large enough to deliver single electron pulses directly to a discriminator (say, 200 mv), the anode signal from one tube may be slightly delayed and mixed with the signal from the other tube, the combined signal fed to a single amplifier and discriminator, the discriminator output split, one branch delayed, and both fed to a coincidence circuit (see Fig. 45). This stratagem, to be sure, results in an increase by a factor of three of the accidental coincidence rate; however, with pulses of 5-10-nsec width, accidentals would still be negligible at relatively high count rates. Further comments on liquid scintillation counting electronics are made below.

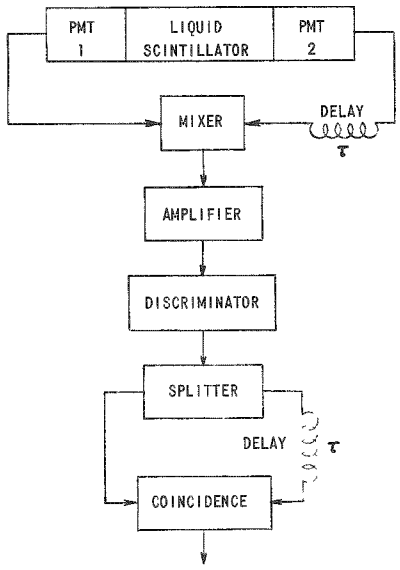

Fig. 45. Delay-mixing-splitting-repeating Technique Applied to Single-channel Liquid Scintillation Counting

The relative advantages of the delay-mix scheme in comparison with two separate single channels on each detector, followed by addition of appropriate outputs and coincidence, may now be briefly discussed. Although no performance figures have been obtained for the latter system, other tests show that channel gain in stability is by far the largest contributing factor to coincidence-ratio fluctuation. The addition of two more single-channel selectors, whose level and window must be absolutely stable, thus appears to be inherently less desirable than the addition of the relatively stable digital circuits which perform the time realignment; furthermore, frequent exact adjustment of four single channels may be something of a nuisance in the long run. On the other hand, this scheme would achieve slightly better resolution, for reasons mentioned above, and behave better under severe overloading. Whether a delay-mix system offers an economic advantage over a four-channel system is difficult to assess, as both relatively inexpensive, transistorized, single-channel analyzers and digital computer circuitry are becoming increasingly available. The delay-mixing system allows more scope for useful improvements,

such as anti-pileup circuits and self-contained pulse timing of zero-crossing or other type, which improve the accuracy of deadtime corrections.

We consider now some of the problems of the beta liquid scintillation counter. In principle, a single photomultiplier and fast discriminator are sufficient to count all events which result in the emission of at least two electrons from the photocathode within a time of the order of the transit time jitter of the tube and reject dark-current single electrons. This implies, however, that the light emitted by a scintillation is as efficiently collected by a single-tube-plus-reflector system as by two tubes, that the gain of the tube and the discriminator level are very constant, allowing reliable rejection of single electrons and acceptance of more than one electron, that no afterpulses occur, and that the dark-current, two-electron pileup is negligible in comparison with the desired signal count rate. In practice, it is found that light collection is never quite as efficient for single tubes as for two-tube arrangements, that fast, stable discrimination between single and multiple electrons is very difficult, that large light pulses result in afterpulses of multi-electron height, and that available phototubes of low time dispersion produce an appreciable two-electron pileup, even with a few-nanosecond pulse clipping. The last remark refers to room temperature; it turns out, however, that organic scintillators compatible with an appreciable admixture of aqueous solution become opaque when cooled to a temperature at which the dark current of the phototube is reduced significantly. Light couplers which would allow cooling the tube but not the scintillator again reduce the light-collection efficiency. An important reason, however, which makes a coincidence scheme an improvement over a simple pulse-addition scheme is the presence of numerous afterpulses following a large light pulse, due to beta particles near the upper end of the spectrum.

Such afterpulses, whether due to positive ion or to light feedback, are minimized by the venetian blind structure and opaque coating of the EMI 6255-S tubes used in our beta counter; other types of tubes presumably are not likely to give better results. Since the afterpulse rate increases rapidly with multiplication, relief might be sought through reduction of tube gain and wideband amplification between multiplier and discriminator.

For the record, an aborted earlier effort to obtain high efficiency and good stability for liquid counting is summarized. This was by means of Cherenkov-β/NaI(Tl)-γ coincidences. Five low-noise phototubes, each with gain capabilities of better than 4×10^7, were obtained from EMI. Dark currents ranged from 0.002 to 0.010 μa and proprietary "tritium ratings" were 90/8 to 90/20. The photocathodes protruded into a 1-in. annulus which surrounded a single 4 x 5-in. sodium iodide crystal (see Fig. 46). It has been previously determined that the maximum range for light collection from a manganous sulphate solution of 200 g/liter was about 1 cm. The light-absorbing distribution of the slightly pink solution are presented in

Fig. 47. Because there existed reasonable transmission in the ultraviolet, only quartz-faced photomultiplier tubes (EMI 6255S) were used, since Cherenkov light is emitted as $1/\lambda^3$ in this region. Operation was at room temperature with no anti-noise coincidence requirement.

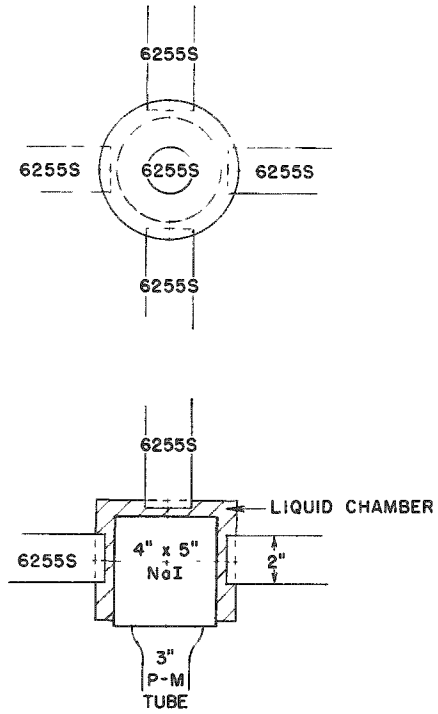

Fig. 46. Arrangement of Phototubes and NaI(Tl) Crystal for Mn^{56} Coincidence $\beta\gamma$ Counting with Cherenkov β Detection

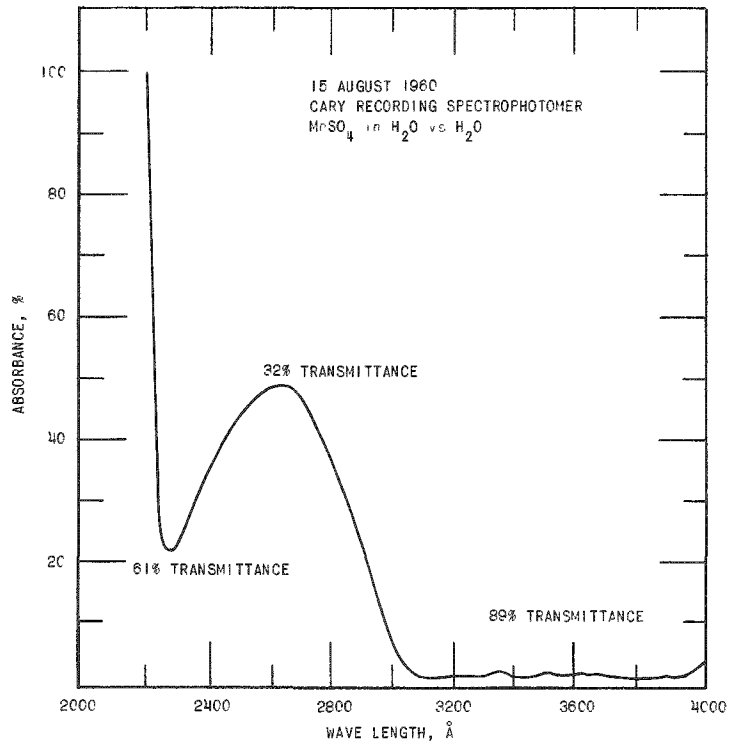

Fig. 47. Absorbance of Manganous Sulphate Solution (Approximate Rendition)

The efficiencies obtained at first appear relatively impressive; for a 1.8-liter solution we found:

beta: 2.4% with 4.9 c/s background for all tubes added.

gamma: 5.8% with 0.85 c/s background for a full-width window on the 0.85-Mev peak.

beta-gamma coincidences: 0.35% for 0.02 c/s background rate.

However, abandonment of this method was found necessary due to the poor stability distribution of the disintegration rates. In the vicinity of the beta bias setting, a slope of 3% disintegration rate per 10% beta amplitude change resulted. In Fig. 48 a steep slope for the Mn^{56} Cherenkov distribution indicates that there was no inherent region of plateau operation, as is the case for the present gamma-gamma coincidence mode. The

failure of efficiency terms to cancel is attributed largely to the fact that Cherenkov photons were collected from only 500 ml of the fluid at best. This leaves a large multiplicative factor to amplify residual efficiency dependent terms arising from the "poor geometry" situation presented here, as far as the coincidence equations (see Appendix A) are concerned.

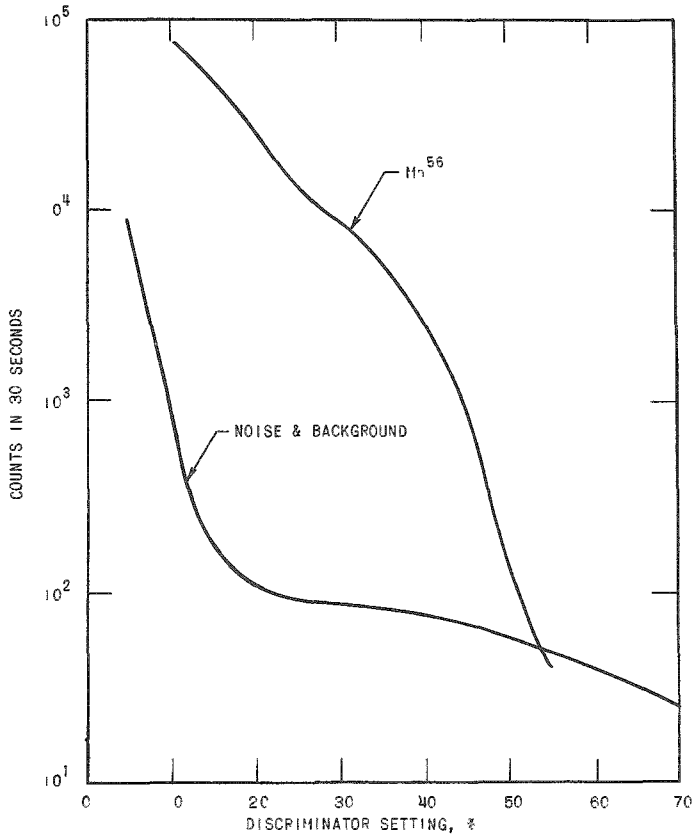

Fig. 48. Cherenkov Counter Integral Bias Curves

VIII. SUMMARY

It is now possible to obtain consistent results in the assay of radioactive $MnSO_4$ solutions, enabling extended measurements of neutron-source strengths which lead to rather weak activations. Although counting time to obtain a given level of statistical confidence is extended, systematic errors are less likely to affect the determination. Calibration procedures are still required, but as experience in operation develops these steps may be reduced at a faster rate than would be permitted for a comparable single-channel counting system. The gamma-gamma detection mode also allows a relatively large sampling of the manganese bath in a situation of relatively low background under all experimental conditions The utility of the count rate doubling technique as well as the $4\pi\ \beta$-γ system is demonstrated in terms of a facility for general-purpose detection, aside from its original application to Mn^{56}, and, furthermore, for some special situations whereunder other methods of radioassay are less effective.

Appendix A

GEOMETRY, GAIN STABILITY, AND DECAY-SCHEME DEPENDENCE OF COINCIDENCE COUNTING

I.

Gamma-gamma coincidence counting is frequently used to determine the absolute activity of radioactive sources which have a suitable decay scheme, the source decay rate being obtained as the coincidence ratio (product of single-channel counts to coincidence count), with certain corrections which involve the decay scheme, the counting geometry, and detection efficiencies of channels. These corrections, as will be shown, are known only when the decay scheme is known with sufficient accuracy and the source is essentially a point. For a large source, a precise, absolute activity measurement through coincidences is therefore impossible. However, coincidence counting still improves the accuracy of intercomparison of a number of such sources, as only a small part of the correction term mentioned above is influenced by single-channel count-rate variations due to electronic gain instability. Since gain variations of this sort cannot be reduced beyond a certain point, the coincidence ratio obtained with a large-sample gamma-gamma coincidence system is a more reliable measure of the relative activity of different samples, assayed over long periods, than the channel count which might be obtained without coincidences, to the extent that the gain-sensitive part of the correction term is small in comparison with unity. The gamma-gamma counting system described in this report takes advantage of this fact. The geometry and decay-scheme dependence of the correction term is presumably constant, and may therefore be found empirically by comparing coincidence ratios of aliquots of the same source measured by the gamma-gamma system and an absolute counter, in which the detection geometry may be optimized. The latter system may be for instance, a beta-gamma coincidence system, which has certain advantages over gamma-gamma counting chiefly related to the decay scheme. Arguments in support of these several assertions will now be given, both for a large-source gamma-gamma counting and for a beta-gamma counting.

II.

Consider, first, a gamma-gamma system of arbitrary geometry, in which an extended, homogeneous source is viewed by two scintillation detectors, attached to single channels with pulse-height selection, which deliver countable pulses to single scalers as well as suitably shaped pulses to a coincidence circuit and attached coincidence scaler. For the sake of simplicity, we assume that the source has a simple decay scheme of the Co^{60} type, and adopt the convention that γ_1 has higher, and γ_2 lower energy.

A decay which takes place at some source point S thus results in the absorption, at various points in the interior of either or both scintillators, of various photons, as the source photons are scattered and degraded (through Compton, pair production, and photoelectric interactions) in the source, in the scintillator, and elsewhere. A certain amount of light is thereupon generated in either or both scintillators, yielding a certain number of electrons at the photocathodes, and eventually in pulses of certain amplitudes in either or both channels. While the transformation of well-collimated incident gamma radiation into pulse height has been extensively studied both theoretically and experimentally,[37] the present situation further includes degradation in a medium surrounding the scintillator, and arbitrary rather than collimated incidence. This precludes any direct calculation of pulse-height spectra, even for relatively simple geometries. A certain amount of insight can, however, be gained by singling out different contributions to the spectra in both detectors from radiations emanating from a small volume dV near some arbitrary source point $S(r_s)$.

We consider now specifically that part of the pulse-height spectrum in one channel, say channel "a," which results from decays near the point S, and absorption by detector a of direct or degraded radiation of type 1. The number of such pulses per unit pulse height interval we denote by $N'_{1a}(h,r_s)\,dh$; as discussed above, this number is an implicit function of decay scheme, source geometry, and detector parameters, and an explicit function of the coordinate r_s. All quantities referring to such a point source will be designated here by primed symbols; the same quantities, referring to the whole source, by unprimed symbols. Integration over all pulse heights yields the intrinsic point-source detection probability:

$$W'_{1a} = \int_0^\infty N'_{1a}(r_s,h)\,dh \quad , \tag{A-1}$$

whereas a similar integration over the analyzer cut (assuming all pulses whose heights fall between h_1 and h_2 are accepted) yields the contribution to the channel count $(1/\eta)(dC'_{1a}/dV_S)$ per unit decay from point S, by γ_1 photons only, in channel a (η = source density). The ratio of channel count to intrinsic detection probability may now be defined as the electronic detection efficiency:

$$\epsilon'_{1a} = \frac{1}{\eta}\frac{dC'_{1a}}{dV_S}\Big/W'_{1a} \quad . \tag{A-2}$$

Alternatively, the electronic efficiency (which is the only part of the overall efficiency sensitive to electronic gain) may be defined in terms of the normalized point spectrum:

$$\epsilon'_{1a} = \int_{h_1}^{h_2} n'_{1a}(h,r_s)\, dh \quad ; \tag{A-3}$$

$$\eta'_{1a}(h,r_s) = N'_{1a}/W'_{1a} \quad . \tag{A-4}$$

Single absorption of the other gamma ray, ignored thus far, may be treated analogously. However, all or part of the energy of both gamma rays may be absorbed in one detector, which yields a further contribution to the observed spectrum. This sum spectrum, $N'_{sa}(h,r_s)dh$, with intrinsic detection probability

$$W'_{sa} = \int_0^{\infty} N'_{sa}(h,r_s)\, dh \quad , \tag{A-5}$$

may be written as a folding integral:

$$N'_{sa}(r_s,h)\, dh = dh \int_0^{\infty} N'_{1a}(r_s,h)\, N_{2a}(r_s,h-h_1)\, dh_1 \quad . \tag{A-6}$$

Substitution of Eq. (A-5) in Eq. (A-6) and integration, in reverse order, yield

$$W'_{sa} = \int_0^{\infty} N'_{1a}(r_s,h_1)\, dh_1 \int_0^{\infty} N'_{2a}(r_s,h-h_1)\, dh = W'_{1a}\, W'_{2a} \quad . \tag{A-7}$$

The probabilities defined above must now be corrected for sum loss:

$$\left(W'_{1a}\right)_t = W'_{1a}\,(1 - W'_{2a}) \quad . \tag{A-8}$$

Assuming that channel a brackets the photopeak of γ_1 and channel b the photopeak of γ_2, some counts appear in channel b due to the Compton tail of γ_1 photons absorbed in detector b, while the reverse is not the case (we have assumed that γ_1 photons are more energetic). Both channels, however, will sample the sum spectra. Coincidences can result only from the joint detection of 1 in a and 2 in b. The point-source channel counts and coincidence count per decay can now be written down:

$$\frac{1}{\eta}\frac{dC'_a}{dV_s} = \epsilon'_{1a}\,(W'_{1a})_t + C'_{sa} = \epsilon'_{1a}\, W'_{1a}\left\{1 - W'_{2a}\left[1 - (\epsilon'_{sa}/\epsilon'_{1a})\right]\right\} \quad ; \tag{A-9}$$

$$\frac{1}{\eta}\frac{dC'_b}{dV_s} = \epsilon'_{2b}\, W'_{2b}(1 - W'_{1b}) + \epsilon'_{1b}\, W'_{1b}\,(1 - W'_{2b}) + \epsilon'_{sb}\, W'_{1b}\, W'_{2b} \quad ; \tag{A-10}$$

$$\frac{1}{\eta}\frac{dC_{ab}}{dV_s} = \epsilon'_{1a}\, \epsilon'_{2b}\, W'_{1a}\, W'_{2b} \quad . \tag{A-11}$$

The spectrum which would be observed in channel a, for instance, from a point source at S only is the weighed sum of component spectra:

$$N'_{1a}(r_s,h)\, dh = \left\{N'_{1a}\,(1 - W'_{2a}) + N'_{2a}\,(1 - W'_{1a}) + N'_{sa}\right\} dh \quad ; \tag{A-12}$$

the total intrinsic detection probability for channel a is obtained by integrating Eq. (A-12) over all pulse heights:

$$W'_a = W'_{1a} + W'_{2a} - W'_{1a}\, W'_{2a} \quad . \tag{A-13}$$

From (A-9), (A-10), and (A-11), one obtains the point-source coincidence ratio

$$\frac{dC'_a\, dC'_b}{dC'_{ab}} = \eta\, dV_s\,(1 + \alpha') \quad , \tag{A-14}$$

where

$$\begin{aligned}\alpha' = {} & \left[(r'_{1b}\, W'_{1b}/W'_{2b}) - (W'_{2a} + W'_{1b})\right] \\ & - \left\{r'_{1b}\, W'_{1b}\,[1 + (W'_{2a}/W'_{2b})] - (r'_{sa}\, W'_{2a} + r'_{sb}\, W'_{1b})\right\} \\ & + W'_{1b}W'_{2a}\left\{1 + r'_{1b} - (r'_{sa} + r'_{sb}) + r'_{sa}\,[(r'_{sb} - r'_{1b}) + (r'_{1b}/W'_{1b})]\right\} \quad ;\end{aligned} \tag{A-15}$$

$$r'_{1b} = \epsilon'_{1b}/\epsilon'_{2b} \quad ; \quad r'_{sa} = \epsilon'_{sa}/\epsilon'_{1a} \quad ; \quad r'_{sb} = \epsilon'_{sb}/\epsilon'_{2b} \quad . \tag{A-16}$$

The leading term of α' in Eq. (A-15) is composed of the intrinsic detection efficiencies of either crystal for the radiation which is not wanted in that channel, and of the Compton tail contribution of γ_1 to channel b. Intrinsic detection probabilities are small for source points which are not too close to either detector, while the Compton tail can always be reduced through selection of a narrow channel, given reasonably good resolution. Thus, the coincidence ratio is certainly much less sensitive to channel gain or discriminator base-line shift than the individual counts. It may be added that the factor α' can always be made negligibly small for gamma-gamma coincidence counting with a point source by choosing suitable detector-source distances, i.e., reducing W' factors to less than the required fractional precision.

The observed counts due to a source of arbitrary size (and, again, simple decay scheme) may now be obtained through integration over the source volume:

$$C_a = \eta \int \epsilon'_{1a} W'_{1a} (1 - W'_{2a})\, dV_s + \eta \int \epsilon'_{sa} W'_{1a} W'_{2a}\, dV_s \quad ; \quad \text{(A-17a)}$$

$$C_b = \eta \int \left[\epsilon'_{2b} W'_{2b} (1 - W'_{1b}) + \epsilon'_{1b} W'_{1b} (1 - W'_{2b}) + \epsilon'_{sb} W'_{1b} W'_{2b} \right] dV_s \quad \text{(A-17b)}$$

$$C_{ab} = \eta \int \epsilon'_{1a} \epsilon'_{2b} W'_{1a} W'_{2b}\, dV_s \quad . \quad \text{(A-17c)}$$

Note that all terms under the integration sign are sensitive to source geometry. We may now write down integrals for component channel counts:

$$C_{1a} = N\epsilon_{1a} W_{1a} = \eta \int_{V_s} \epsilon'_{1a}(r_s)\, W'_{1a}(r_s)\, dV_s \quad ; \quad \text{(A-18)}$$

pulse-height spectra:

$$N_{1a}(h)\, dh = (\eta\, dh/N) \int_{V_s} N'_{1a}(r_s, h)\, dV_s \quad , \quad \text{(A-19a)}$$

$$N_{1a}(h)\, dh = (\eta\, dh/NW_{1a}) \int_{V_s} N'_{1a}(r_s, h)\, W'_{1a}(r_s)\, dV_s \quad ; \quad \text{(A-19b)}$$

and electronic and intrinsic detection efficiencies:

$$\epsilon_{1a} = \int_{h_1}^{h_2} N_{1a}(h)\, dh = (\eta/N) \int_{V_s} \epsilon'_{1a} [W'_{1a}(r_s)/W_{1a}]\, dV_s \quad ; \quad \text{(A-20a)}$$

$$W_{1a} = (\eta/N) \int_{V_s} W'_{1a}(r_s)\, dV_s \quad . \quad \text{(A-20b)}$$

In so many words, the whole-source counting efficiency, (Eq. A-20), as well as the whole-source component spectra, (Eq. A-19), are composed of appropriately weighed point-source efficiencies and component spectra (weights possibly including local source densities for nonuniform sources). Further defining certain integrals:

$$\eta \int \epsilon'_{1a} W'_{1a} W'_{2a}\, dV_s = I_{1a} \quad , \quad \text{(A-21a)}$$

$$\eta \int \epsilon'_{sa} W'_{1a} W'_{2a}\, dV_s = I_{sa} \quad , \quad \text{(A-21b)}$$

$$\eta \int \epsilon'_{1b}\, W'_{2b}\, W'_{1b}\, dV_s = I_{2b} \quad , \tag{A-21c}$$

$$\eta \int \epsilon'_{sb}\, W'_{2b}\, W'_{1b}\, dV_s = I_{sb} \quad , \tag{A-21d}$$

$$\eta \int \epsilon'_{1b}\, W'_{1b}\, W'_{2b}\, dV_s = I_{1b} \quad , \tag{A-21e}$$

$$\eta \int \epsilon'_{1b}\, W'_{1b}\, dV_s = \epsilon_{1b}\, W_{1b} \quad , \tag{A-21f}$$

$$\eta \int \epsilon'_{1b}\, W'_{2b}\, dV_s = \epsilon_{1b}\, W_{2b} = C_{1b}/N \quad , \tag{A-21g}$$

we obtain a coincidence ratio for extended sources:

$$C_a C_b / C_{ab} = N\bar{\mu}(1 + \bar{\alpha}) \quad , \tag{A-22}$$

where now

$$\bar{\alpha} = \left\{(\epsilon_{1b}W_{1b}/\epsilon_{2b}W_{2b}) - [(I_{1a}-I_{sa})/(N\epsilon_{1a}W_{1a}) + (I_{1b}+I_{2b}-I_{sb})/(N\epsilon_{2b}W_{2b})]\right\}$$

$$- [\epsilon_{1b}W_{1b}\,(I_{1a}-I_{sa})/N\epsilon_{1a}W_{1a}\epsilon_{2b}W_{2b}] + (I_{1a}-I_{sa})(I_{1b}+I_{2b}-I_{sb})/$$

$$N^2\epsilon_{1a}W_{1a}\epsilon_{2b}W_{2b} \quad , \tag{A-23}$$

and

$$\bar{\mu} = C_{1a}C_{2b}/N\eta \int (\epsilon'_{1a}W'_{1a})(\epsilon'_{2b}W'_{2b})\, dV_s \tag{A-24}$$

The factor $\bar{\alpha}$ in Eq. (A-22) is seen to be similar in structure to the analogous factor α' of the partial coincidence ratio due to radiations from one arbitrary point of the source [see Eq. (A-14)]. Its leading term is therefore still small, being essentially composed of averages of various kinds (W_{1a}, I_{1a} ...) of small quantities (W'_{1a}, ϵ'_{1a} ...) over the source volume. The factor $\bar{\mu}$, on the other hand, is the ratio of different kinds of averages of the same quantities, and should therefore not differ very much from unity.

As regards the sensitivity of the $\bar{\mu}$ factor to electronic instability, we may as a zero approximation assume that the normalized partial pulse-height spectra from different source points of either channel are roughly identical. Thus $\bar{\mu}$ becomes independent of electronic gain:

$$\bar{\mu}_0 = N\, W_{1a}W_{2b}/\eta \int W'_{1a}W'_{2b}\, dV_s \quad . \tag{A-25}$$

Actually, one would expect a certain amount of variation in the spectrum from different points of the source, both because of absorption and scattering by the source itself and because the resolution of the scintillation detector changes with the solid angle subtended by the detector at the source point. The equipment, however, is sensitive only to small regions of the pulse-height spectra in the vicinity of the respective channel windows; over such a region, differences between spectra from different source points should be relatively small. It may therefore be permissible to express the point efficiencies in terms of deviations from the whole source efficiencies:

$$\epsilon'_{1a}(r_s) = \epsilon_{1a}[1 + \Delta'_{1a}(r_s)] \quad ; \quad \epsilon'_{2b}(r_s) = \epsilon_{2b}[1 + \Delta'_{2b}(r_s)] \quad . \tag{A-26}$$

By inserting Eq. (A-26) in Eq. (A-24) and dropping small terms, a first-order approximation is obtained:

$$\bar{\mu}_1 = \bar{\mu}_0[1 + I_1 + I_2 - I_{12}] \quad , \tag{A-27}$$

where

$$I_1 = \frac{\eta}{N}\int \Delta'_{1a}(W'_{1a}/W_{1a})\,dV \quad ; \tag{A-28a}$$

$$I_2 = \frac{\eta}{N}\int \Delta'_{2b}(W'_{2b}/W_{2b})\,dV \quad ; \tag{A-28b}$$

$$I_{12} = \int(\Delta'_{1a} + \Delta'_{2b})\,W'_{1a}W'_{2b}\,dV \Big/ \int W'_{1a}W'_{2b}\,dV \quad . \tag{A-28c}$$

The three latter integrals, which constitute the electronic gain-sensitive part of the factor $\bar{\mu}$, are source-volume averages of the deviations of limited regions of single-point-channel pulse-height spectra from the whole-source spectra. In I_1 and I_2 these deviations are weighted in such a way that the contribution from the most strongly deviating spectra - from more distant points - is depressed. On the other hand, in I_{12} the deviations are weighted more evenly, for points close to detector 1, which have a large W'_{1a}, W'_{2b} should be small, and vice versa. The relative magnitudes of $I_1 + I_2$ and I_{12} should depend on the actual geometry; the above weighting considerations would lead one to expect a net small positive contribution. (Similar considerations govern the gain-insensitive part, $\bar{\mu}_0$, which may be larger than unity by a substantial amount.) Note that the intrinsic efficiencies W' necessarily change very strongly over a source which is contiguous to the two detectors, since W' factors include solid angles subtended by the detector at the source point, and still more strongly due to absorption.

To sum up, the gamma-gamma coincidence ratio for a simple decay scheme, extended source, and pulse-height selection in both channels can be written symbolically as

$$\frac{C_a\, C_b}{C_{ab}} = N\, \bar{\mu}_0 (W_i) \left[1 + \bar{I} (\Delta_i') + \bar{\alpha} (r_i W_i)\right] \quad , \qquad \text{(A-29)}$$

where $\bar{\mu}_0(W_i)$ is entirely independent of electronic gain, $\bar{I}(\Delta_i')$ is a small positive term consisting of three integrals which are weighted averages of differences $\Delta_i' \epsilon_i'$ of channel electronic efficiencies over the source, and $\bar{\alpha}$ (r_i, W_i) is a small negative term which is mainly a function of ratios r_i of electronic efficiencies and of intrinsic efficiencies W_i.

III.

We now extend these remarks to include complex decay schemes, in order to show that branching information appears in the factor $\bar{\alpha}$ but not elsewhere (this is primarily of importance in absolute assays of sources whose decay scheme is not known with the required precision). For the present discussion, we specifically consider gamma-gamma coincidences as above; the situation is, however, entirely analogous for beta-gamma coincidences.

Suppose that the daughter nuclide has m levels, and let the fractional beta decay directly into each of these levels be denoted by p_0, $p_i \cdots p_m$ (including a possible ground-state transition). Let the relative intensity of gamma radiation connecting the ith and jth such levels be denoted q_{ij}. Note that, given n_i branches in the decay of the ith level,

$$\sum_{i=0}^{m} p_i = 1 \quad ; \quad \sum_{j=1}^{n_i} q_{ij} = 1 \quad ; \quad \sum_{i_1 j} p_i q_{ij} = 1 \quad . \qquad \text{(A-30)}$$

Consider, now, the cascade $r \to s \to 0$, for instance, and let counter channel a be adjusted to count $r \to s$ and channel b to count $s \to 0$ gammas. Again, let W_{rsa} represent the intrinsic detection probability of counter a for $r \to s$ radiation (point-source geometry is assumed, for the sake of simplicity). We may now write down the channel count rates (neglecting Compton-tail effects and sum effects):

$$C_a = N \epsilon_{rsa}\, W_{rsa} (1 - W_{soa}) \left\{ p_r + \sum_{i=r+1}^{m} p_i Q_{ia} \right\} \quad ; \qquad \text{(A-31a)}$$

$$C_b = N \epsilon_{sob}\, W_{sob} \left\{ p_s q_{so} + (1 - W_{rsb}) \left[p_r + \sum_{i=r+1}^{m} p_i Q_{ib} \right] \right\} \quad ; \qquad \text{(A-31b)}$$

$$C_{ab} = N \epsilon_{rsa}\ \epsilon_{sob}\ W_{rsa}\ W_{sob} \left\{ p_r + \Sigma\ p_i\ Q_{iab} \right\} \quad , \qquad \text{(A-31c)}$$

where

$$Q_{ia} = q_{ir}\ (1 - W_{ira}) + \sum_{j=1}^{n_i} q_{ij} q_{jr}\ (1 - W_{ija})\ (1 - W_{jra}) + \qquad \text{(A-32a)}$$

$$+ \sum_{j=1}^{n_i} \sum_{\ell=1}^{n_j} q_{ij} q_{j\ell} q_{\ell r}\ (1 - W_{ija})\ (1 - W_{j\ell a})\ (1 - W_{\ell ra}) + \ldots \quad ; \qquad \text{(A-32b)}$$

$$Q_{ib} = q_{ir}\ (1 - W_{irb}) + \sum_{j=1}^{n_i} q_{ij} q_{jr}\ (1 - W_{ijb})\ (1 - W_{jrb}) + \ldots \quad ;$$

$$Q_{iab} = q_{ir}\ (1 - W_{ira} - W_{irb}) + \sum_{j=1}^{n_i} q_{ij} q_{jr}\ (1 - W_{ija} - W_{ijb})(1 - W_{jra} - W_{jrb}) + \ldots . \qquad \text{(A-32c)}$$

(levels are labelled from the bottom up, as customary).

We now may make use of relations (A-30) and write the coincidence ratio

$$\frac{C_a C_b}{C_{ab}} \quad N\ (1 - W_{soa}) \left(1 - \sum_{k \neq r}^{n_i} p_k + \sum_{i\ r=1}^{n_i} p_i Q_{ia} \right)$$

$$\left[\left(1 - \sum_{k \neq r}^{n_i} p_k \right) \left(1 - \sum_{t=1}^{n_s} q_{st} \right) + (1 - W_{rsb}) \left(1 - \sum_{k \neq r}^{n_i} p_k + \sum_{i=r+1}^{n_i} p_i Q_{ib} \right) \right] \Big/$$

$$\left(1 - \sum_{k \neq r}^{n_i} p_k + \sum_{i=r+1}^{m} p_i Q_{iab} \right) \qquad \text{(A-33)}$$

Evidently, all branching information can be lumped in a correction term $\bar{\alpha}$:

$$C_a C_b / C_{ab} = N\ (1 - \bar{\alpha}) \quad ;$$

$$\bar{\alpha} = W_{soa} + \sum_{k \neq r}^{m} p_k - \sum_{i=r+1}^{m} p_i Q_{ia} \ldots . \qquad \text{Q.E.D.}$$

IV.

These various considerations may now be illustrated by applying them to the physical situation described in the present report. The Mn^{56} spectrum may for these purposes be simplified: all transitions to the 0.8-Mev level are lumped as one transition of approximately 2-Mev energy; the relative strength of the direct beta emission to the 0.8-Mev level is labelled p and hence the strength of all higher levels is (1 - p). Adopting the designations 0.8 Mev = "2," 2 Mev = "1," and looking for "2" with channel b and for "1" with channel a, one finds count rates (from a point source) in the above notation:

$$\frac{1}{\eta}\frac{dC'_a}{dV} = (1-p)\left[W'_{1a}(1-W'_{2a})\,\epsilon'_{1a} + W'_{1a}W'_{2a}\epsilon'_{sa}\right] \quad ;$$

$$\frac{1}{\eta}\frac{dC'_b}{dV} = (1-p)\left[W'_{2b}(1-W'_{1b})\,\epsilon'_{2b} + W'_{1b}(1-W'_{2b})\epsilon'_{1b} + W'_{1b}W'_{2b}\epsilon'_{sb}\right]$$

$$+ pW'_{2b}\epsilon'_{2b} \quad ;$$

$$\frac{1}{\eta}\frac{dC'_{ab}}{dV} = (1-p)\,W'_{1a}W'_{2b}\epsilon'_{1a}\epsilon'_{2b} \quad .$$

Hence, a coincidence ratio (from a point source)

$$\frac{dC'_a dC'_b}{\eta\, dV dC_{ab}} = (1-p)\left[1-W'_{2a}(1-r_{sa})\right]\left[1-W'_{1b}\left(1-r_{sb}+\frac{1-W_{2b}}{W_{2b}}r_{12b}\right)+\frac{p}{1-p}\right]$$

$$= 1-\bar{\alpha} \quad ; \quad \bar{\alpha} = W'_{2a} + W'_{1b} \ldots .$$

is obtained. Thus far, each detector was associated with one channel only. The pulse-distribution scheme results in an input, into each channel, of a mixed pulse-height spectrum, composed of the point spectra of both detectors at some source point. The symmetric arrangement of the detectors allows one, however, to consider two source points at a time, located symmetrically with respect to a central plane normal to the common axis through the detectors. The combined spectra in each detector from two such points are now identical and have 4 times the strength of the single-channel-single-detector system discussed above. After integration (over one-half of the source volume), one thus finds total source count rates twice as strong as previously, and hence also twice the coincidence ratio. No other differences result from the use of any count-rate-doubling pulse distribution scheme. This conclusion will still hold for the whole-source-coincidence ratio and count rates.

It may further be instructive to obtain a rough estimate of the relative magnitude of the factor $\bar{\mu}_0$, through which mainly the coincidence ratio differs from the decay rate of the sample, for the source geometry shown in Fig. 2 of the text. Let the whole source volume be split into two annular regions V_1 and V_2 around each detector plus a "plug" V_0 between detectors. The intrinsic detection efficiencies may then be roughly estimated in terms of average values over these regions as sums $\Sigma W_{ij} V_j$, where $W_{11} \doteq W_{22}$, $W_{10} = W_{20}$, and $W_{12} = W_{21} \ll W_{11}$; furthermore, $V_1 = V_2$. This yields

$$\bar{\mu}_0 = (\Sigma W_{1i} V_i)(\Sigma W_{2k} V_k)/(\Sigma W_{1j} W_{2j} V_j)(V_0 + 2V_1)$$

$$\doteq W_{11} V_1 \left[1 + (W_{10} V_0 / W_{11} V_1) + (W_{12}/W_{11})\right]^2 / \left[2W_{12} + (W_{10}^2 V_0 / W_{11} V_1)\right] (V_0 + 2V_1) \quad .$$

Dropping the small terms,

$$\bar{\mu}_0 \doteq \left(\frac{V_0}{V_0 + 2V_1} \right) \left(1 + \frac{W_{11} V_1}{W_{10} V_0} \right)^2 \quad .$$

For the present case, $V_1 \approx V_0$; further, $W_{11} \approx W_{10}$. With these rough approximations,

$$\mu_0 \approx 4/3 \quad .$$

This value turns out to agree rather well with a scaling factor of 1.35 obtained by calibration.

V.

We consider now briefly the corresponding case of beta-gamma coincidence. Once more, it will be expedient to restrict the discussion at first to a simple decay scheme in which all beta transitions reach an excited level of the daughter nuclide, and hence are in cascade with a single gamma transition (see Fig. 49 for a simplified version of Mn^{56} decay scheme). We specify that a photomultiplier is used in the beta channel; this photomultiplier may be coupled to a liquid scintillator containing the source, to a plastic scintillator surrounded by the source, or simply exposed to the Cherenkov radiation from the source. As a result of source activity near some source point S with coordinate r_s, a certain pulse-height distribution develops at the anode of the multiplier; these pulses are put into the beta-counting channel through an integral discriminator. The details of the beta-particle energy to voltage pulse transformation are again of no specific interest here; it is worth observing, however, that the nature of the beta spectrum will cause a cutoff in the intrinsic efficiency which depends only on which one of the three energy-into-light conversion mechanisms mentioned above is used: highest for Cherenkov radiation, lowest for liquid

scintillator-distributed sources. Angular correlations are averaged out, except for Cherenkov detection (which method anyway is not, as will be demonstrated, capable of sufficient accuracy to warrant angular correlation corrections).

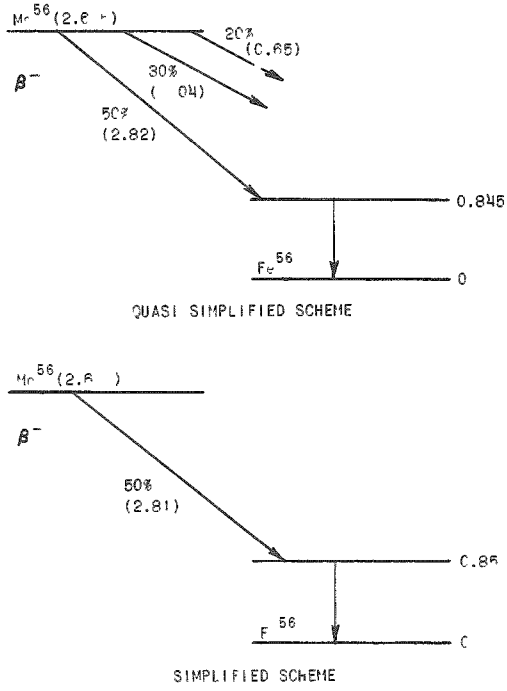

Fig. 49. Abridged Mn^{56} Decay Schemes

As before, we consider intrinsic and electronic detection efficiencies separately. Let a beta decay occur in a small volume near point S of the source; the beta channel count then comes to

$$\frac{1}{\eta}\frac{dC'_b}{dV} = W'_{\beta b}\,(1 - W'_{\gamma b})\,\epsilon'_{\beta b} + (1 - W'_{\beta b})\,W'_{\gamma b}\epsilon'_{\gamma b} + W'_{\beta b}W'_{\gamma b}\epsilon'_{sb} \quad . \tag{A-34}$$

The first term includes detection of the beta ray in the beta detector and escape of the associated gamma ray; the second term escape of the beta ray, but stopping of the associated gamma in the beta detector; the third stopping of both radiations in the beta detector. For large beta-decay energy and integral discrimination at low bias,

$$\epsilon'_{sb} \doteq \epsilon'_{\beta b} \quad , \tag{A-35}$$

since the only difference in $\epsilon'_{\beta b}$ and ϵ'_{sb} could be due to those rare events when beta detection alone does not yield pulses of sufficient height to pass the discriminator. (Such events are rare when the channel gain in the beta channel is large enough to bring pulses due to

a few electrons emitted by the photocathode past the discriminator and when the beta-decay energy is high enough to yield more than this number of photoelectrons from most beta particles stopped in the scintillator.) Thus,

$$\frac{1}{\eta}\frac{dC_b'}{dV} \doteq W_{\beta b}'\epsilon_{\beta b}' \left\{1 + [(1 - W_{\beta b}')\, W_{\gamma b}'\epsilon_{\gamma b}'/W_{\beta b}'\epsilon_{\beta b}']\right\} \qquad \text{(A-36)}$$

to a very good approximation, subject to the stated conditions. The gamma count similarly comes to

$$\frac{1}{\eta}\frac{dC_a'}{dV} = W_{\gamma a}'\epsilon_{\gamma a}' + W_{\gamma b}'W_{\delta a}'\epsilon_{\delta a}' \quad . \qquad \text{(A-37)}$$

The first term again comprises all gamma rays emitted by the point source which were stopped and detected in the gamma detector, the second those relatively rare events when the gamma is stopped in the beta detector, and the latter interaction - Compton scattering or pair production - results in one or more secondary photons δ which in the aggregate yield a detectable pulse in the gamma channel. The second term thus involves an integration over the beta detector. (In the same sense, the first term may contain a small contribution from secondary radiation due to gamma scattering elsewhere - the source holder, shield, etc.) A further possible contribution to the gamma-channel count, from bremsstrahlung, may be safely neglected as long as there are no media of high atomic number exposed to direct beta radiation The coincidence count then comes to

$$\frac{1}{\eta}\frac{dC_{ab}'}{dV} = W_{\gamma a}W_{\beta b}'\epsilon_{\gamma a}'\epsilon_{\beta b}' + (1 - W_{\beta b}')\, W_{\gamma b}'W_{\delta a}'\epsilon_{\gamma b}'\epsilon_{\delta a}'$$

$$+ W_{\gamma b}'W_{\delta a}'W_{\beta b}'\epsilon_{\delta a}'\epsilon_{\beta b}' \quad . \qquad \text{(A-38)}$$

The point coincidence ratio in turn may be written, after some expedient rearrangement and dropping of second-order terms, as

$$\frac{1}{\eta}\frac{dC_a'dC_b'}{dC_{ab}\,dV} = 1 + \Delta' \quad ; \qquad \text{(A-39)}$$

$$\Delta' = [W_{\gamma b}'(1 - W_{\beta b}')/W_{\beta b}'](\epsilon_{\gamma b}'/\epsilon_{\beta b}') \quad . \qquad \text{(A-40)}$$

The correction term Δ' can be made negligibly small by increasing $W_{\beta b}'$ as much as possible, while keeping the scintillator volume small so as to keep $W_{\gamma b}'$ small. The value of $W_{\beta b}'$ may be made large through good light collection and photocathode conversion efficiency. The conditions specified above, large beta-decay energy and high channel gain, are, of course, most important of all

Proceeding again from the point source to the whole source, one arrives, after some steps similar to the foregoing, at a coincidence ratio

$$\frac{C_a C_b}{C_{ab}} = \eta \frac{\int W'_{\beta b} \epsilon'_{\beta b} dV \left[\int W'_{\gamma a} \epsilon'_{\gamma a} dV + \int W'_{\gamma b} W'_{\delta a} \epsilon'_{\delta a}\, dV\right]}{\int W'_{\gamma a} W'_{\beta b} \epsilon'_{\gamma a} \epsilon'_{\beta b} dV + \int W'_{\gamma b} W'_{\delta a} W'_{\beta b} \epsilon'_{\delta a} \epsilon'_{\beta b} dV} \quad . \quad \text{(A-41)}$$

In this expression, the small point-source correction term Δ' has been dropped, in accordance with the foregoing discussion. Note, however, that terms in $\epsilon'_{\delta a}$, which cancel to first order in Eq. (A-40), do not cancel in Eq. (A-41). For an extended source, it is therefore necessary to make $\epsilon'_{\delta a}$ small, which can usually be done through appropriate pulse-height discrimination in the gamma channel (difficulties may arise only in cases where there is a fairly complex decay scheme). With this further proviso, the second terms in the numerator and denominator of (A-41) may be dropped. Furthermore, recalling that the source volume V_s is relatively small and that both intrinsic and electronic beta-channel detection efficiencies are large, the point-source beta count may be expressed, similarly to the gamma-gamma case treated earlier, in terms of relatively small deviations ν' of the point efficiencies from the whole-source efficiency:

$$W'_{\beta b} \epsilon'_{\beta b} = W_b \epsilon_b + \nu' \quad , \quad \text{(A-42)}$$

where

$$\eta \int W'_{\beta b} \epsilon'_{\beta b} dV = \eta W_b \epsilon_b V_s = N W_b \epsilon_b \quad \text{(A-43)}$$

and

$$\int \nu' \, dV = 0 \quad . \quad \text{(A-44)}$$

Inserting Eq. (A-43) in Eq. (A-41), and dropping small second-order quantities, one finally obtains

$$C_a C_b / C_{ab} = N(1-k) \quad ; \quad \text{(A-45)}$$

$$k = (\eta / N \epsilon_b W_b \epsilon_a W_a) \int \nu' W'_{\gamma a} \epsilon'_{\gamma a} dV \quad . \quad \text{(A-46)}$$

If the gamma detector is not too close to the source, the variation of the gamma-channel efficiency over the source volume should also be relatively small; we may then put

$$W'_{\gamma a} \epsilon'_{\gamma a} = W_a \epsilon_a + \lambda' \quad . \quad \text{(A-47)}$$

Hence, Eq. (A-46) is replaced by

$$k' = (\eta / N W_b \epsilon_b W_a \epsilon_a) \int \nu' \lambda' \, dV \quad . \quad \text{(A-46')}$$

Thus, it is apparent that the correction k can be readily reduced to insignificance, and an absolute measurement of the decay rate of any source which meets the specifications discussed above is feasible with high precision through beta-gamma coincidence counting. More complex decay schemes do not change this conclusion, as may be seen from the brief exposition of such decay schemes for the gamma-gamma coincidence case.

To sum up, it has been shown that absolute beta-gamma coincidence counting requires either (a) high beta-channel efficiency and low detection efficiency of the beta detector for gamma rays, with a quasi-point source; or (b) high beta-channel efficiency, low gamma-detection efficiency in the beta detector, plus low detection efficiency in the gamma channel for photons emitted through gamma interactions in the beta detector, and a fairly uniform gamma detection geometry. Some of these requirements may be redundant if others can be met to a high degree (for instance, if ν' can be made very small, λ' need not be very small, or vice versa)

Appendix B

CORRECTIONS FOR DEAD TIME AND COINCIDENCE RESOLVING TIME

The matter of correcting the coincidence equations for dead-time and resolving-time effects has been recently covered in the literature. We present here, however, a somewhat simpler derivation of essentially the same result, at least to first order; furthermore, the entire correction evolves in one step.

In Fig. 50, we have illustrated the time relationships involved in pulse events which require attention. First of all, events of higher order (three pulses occurring in one dead-time sequence) are neglected. Moreover, we assume nice square pulse shapes. We also assume that DD-2 effects accentuated by a single-channel analyzer tend to wash out, that is, pulses knocked above the window are compensated by pulses kicked downstairs (valid only in double differentiation mode). There are also complex effects of pile-up on time of zero cross that are ignored. We will further omit consideration of an accidental (or chance) coincidence being spoiled by the dead time of a preceding pulse on the grounds that both of these circumstances are in themselves to be kept to the order of 10% or less.

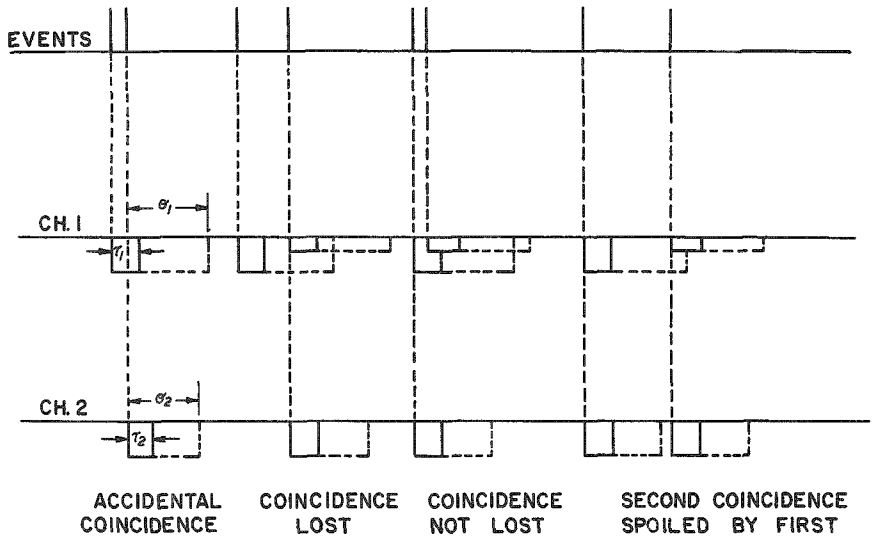

Fig. 50. Timing of Events and Pulses Which Lead to Gains or Losses in Coincidence Count Rate

From an experimental point of view, the main item of interest is to find a relationship between the disintegration rate N and the three counting rates C_i. We shall make use of known fixed dead times and resolving times, and also find that we must know the channel efficiencies.

Let us define the following quantities:

p_i = probability of an event being detected in i^{th} channel at amplitude proper for i^{th} discriminator

$\bar{p}_i$ = probability of not detecting the p_i event

c_i = efficiency without regard to pile-up effect

θ_i = longest dead time, generally the discriminator or otherwise imposed

T_i = coincidence resolving time

C_i = observed count rates

$p_i(\theta_i)$ = probability of an event p_i occurring during θ_i

N = true disintegration rate

$\Theta_i = 1 - \theta_i C_i$ = dead-time loss factor (first-order approximation)

The following three equations are derived on the basis of Fig. 50:

$(\theta_1 > \theta_2) \qquad (\tau_i \leq \theta_i) \qquad (\theta_{12} > \theta_1)$

$$C_1 = p_1 N - p_1 p_1(\theta_1) N = p_1 N [1 - p_1(\theta_1)] \quad ; \tag{B-1}$$

$$C_2 = p_2 N - p_2 p_2 (\theta_2) N = p_2 N [1 - p_2(\theta_2)] \quad ; \tag{B-2}$$

$$C_{12} = N \{p_1 p_2 + [p_1 \bar{p}_2 p_2(\tau_1)\bar{p}_1 + p_2 \bar{p}_1 p_1(\tau_2)\bar{p}_2] - [p_1 \bar{p}_2 p_1(\theta_1 - \tau_1)p_2 + p_2 \bar{p}_1 p_2(\theta_2 - \tau_2)p_1] - p_1 p_2 p_1(\theta_1)p_2\} \{1 - p_1 p_2(\theta_{12} - \theta_2)N\} \quad . \tag{B-3}$$

If we set $p_i = \epsilon_i$ and approximate $p_i(\theta_i)$ as $\epsilon_i \theta_i N$, these expressions may be rewritten as

$$C_1 = \epsilon_1 N(1 - \epsilon_1 \theta_1 N) \equiv \epsilon_1 \Theta_1 N \quad ; \tag{B-4}$$

$$C_2 = \epsilon_2 N(1 - \epsilon_2 \theta_2 N) = \epsilon_2 \Theta_2 N \quad ; \tag{B-5}$$

$$\begin{aligned} C_{12} = {} & N\{\epsilon_1\epsilon_2 + [\epsilon_1(1 - \epsilon_2)\epsilon_2\tau_1 N(1-\epsilon_1) + \epsilon_2(1 - \epsilon_1)\epsilon_1\tau_2 N(1 - \epsilon_2)] \\ & -[\epsilon_1(1 - \epsilon_2)\epsilon_1(\theta_1 - \tau_1)N\epsilon_2 + \epsilon_2(1 - \epsilon_2)\epsilon_2(\theta_2 - \tau_2)N\epsilon_1] \\ & - \epsilon_1\epsilon_2\epsilon_1\theta_1 N\epsilon_2\} \{\epsilon_1\epsilon_2[1 - \epsilon_1\epsilon_2(\theta_{12} - \theta_1)N]\} \\ = {} & \epsilon_1\epsilon_2 N\{1 + N[(1 - \epsilon_2)(1 - \epsilon_1)(\tau_1 + \tau_2) - \epsilon_1(1 - \epsilon_2)(\theta_1 - \tau_1) \\ & - \epsilon_2(1 - \epsilon_1)(\theta_2 - \tau_2) - \epsilon_1\epsilon_2\theta_1]\} \{1 - \epsilon_1\epsilon_2 N(\theta_{12} - \theta_1)\} \quad , \end{aligned} \tag{B-6}$$

and finally

$$\frac{C_1C_2}{C_{12}} = N \frac{\Theta_2}{(1+N\tau_g)\Theta_{12}} \quad . \tag{B-7}$$

where we define an effective gate time

$$\tau_g \equiv (1-\epsilon_2)(1-\epsilon_1)(\tau_1+\tau_2) - \epsilon_1(1-\epsilon_2)(\theta_1-\tau_1) - \epsilon_2(1-\epsilon_1)(\theta_2-\tau_2)$$
$$- \epsilon_1\epsilon_2\theta_1 \quad . \tag{B-8}$$

It is important to note that the dead times are often the dominant factor in the coincidence correction. In fact, by setting a rather long paralysis it is possible to choose operating conditions such that the correction factor tends to cancel; this is especially useful in that dead times are often relatively easy to set and are relatively rigid. One should observe that second-order effects have been neglected in both the numerator and denominator of (B-7).

Let us examine some special conditions of operation. If Channel 1 has an efficiency close to unity, while the other channel is somewhat less, then

$$\frac{C_1C_2}{C_{12}} \cong \frac{N\Theta_1\Theta_2}{\{1-N[\epsilon_1\theta_1-(1-\epsilon_2)\tau_1]\}\Theta_{12}} \tag{B-9}$$

When the coincidence resolving time $\tau_1 \ll \theta_1$, we then see that the residual correction is chiefly the dead-time loss for the inefficient channel. This important conclusion may be used with great advantage in 4π β-γ counting.

If both channel efficiencies are rather small, then

$$\frac{C_1C_2}{C_{12}} \cong \frac{N\Theta_1\Theta_2}{\{1+N[(\tau_1+\tau_2)-\epsilon_1\theta_1-\epsilon_2\theta_2]\}\Theta_{12}} \tag{B-10}$$

In this case the dead-time losses in the single channels are generally small and the accidentals tend to be offset by deadtime losses in the coincidence channel. Thus, the measure of relative chance coincidence must be diminished by the effect of imposed paralysis, another feature which may be used to advantage. In a repeating scheme such as reported here, a deadtime > 4.1 μsec is required to avoid single-channel accidental coincidences.

The above results agree in the first order with the more elaborate formulae of Gandy,[9,10] who has experimentally verified his work; e.g., there is only a 0.1% discrepancy in N for a 10% dead-time loss.

A computer program now needs to be provided only with three parameters for each isotope: the two dead times and the effective gate time, although a more extensive code could be set up to make use of the daily efficiencies computed by taking the coincidence rate and dividing by the singles. In our situation, there are only small effects for modest changes in the efficiency due to some change in experimental conditions.

Having wired in dead times of the order of 13 μsec, we calculate the following results:

For 2300 disintegrations/sec, the correction factor is 0.7%, where $\epsilon_1 = 0.98$, $\epsilon_2 = 0.026$, $\tau_1 = 0.125$ μsec and $\tau_2 = 0.275$ μsec; yet dead-time losses in the high-efficiency channel would be 8.5%. We must use $\tau_g = -12.8$ μsec.

For the same disintegration rate but with $\epsilon_1 = 0.042$, $\epsilon_2 = 0.092$, and $\tau_1 = \tau_2 = 0.09$ μsec, we have a factor of 0.7% when channel 2 loss is 1%; here $\tau_g = -0.155$ μsec

Note that $\Theta_{i2} = 0$ if $\theta_i \geq \theta_{i2}$

Appendix C

LITERATURE SURVEY

Mn^{56}

Manganese-56 is a particularly useful radioisotope in absolute calibration of neutron sources. It has a convenient half-life (2.577 ±0.003 hr);[11] a high thermal activation cross section (13.2 ± 0.1 b),[12] a resonance integral of 11.7 ± 1.5 b;[13] good solubility in water (520 g/l as $MnSO_4$);[14] relatively high atomic density; a natural abundance of 100%[14] for Mn^{55}; high-energy radiation in decay, and cascades adaptable to coincidence counting.[15] A monograph on the radiochemistry of manganese is available.[16] The internal conversion coefficient is quite small.[17]

The decay scheme of Mn^{56} is presented in Fig. 1. Branching ratio data among several investigators[3,18,19] differ widely, so that any counting requiring detailed knowledge of these ratios would be unlikely to approach 1% in precision.

Some research reports discussing the use of Mn^{56} are by De Juren in absolute calibration of neutron sources;[20-22] Richmond and Gardner;[23] Geiger and Whyte;[34] Macklin;[24] and Axton and Cross in 4π β counting.[25]

Liquid Scintillation Counting

One of the primary sources of information of liquid scintillation counting is derived from the 1958 Northwestern symposium.[26] Data concerning the miscibility of organic salts (such as of manganese) may be obtained from Loveridge;[5] from Packard Instrument Co. technical bulletins;[6,27] Myers;[28] Ronzio;[29] Horrocks;[30] and Hayes.[31] A useful monograph on organic scintillation detectors has been written by Schram.[32]

Absolute Counting

A recent and thorough discussion of absolute counting techniques, especially coincidence methods, has been written by Gandy,[7] who includes a comprehensive bibliography. Gandy has also written two articles published in the "International Journal of Applied Radiation and Isotopes" exhaustively covering diode time and accidental coincidence corrections.[9,10] Some earlier significant works are by Steyn[33] on 4π β liquid scintillation/γ coincidence calibration; Campion,[8] who uses a 4π proportional counter for the β detector in coincidence with the γ channel; and Putnam,[35] who applies corrections for complex decay schemes. The International Atomic Energy Agency has devoted an entire symposium to "Metrology of Radionuclides": the proceedings are available in book form.[36]

Appendix D

DATA COLLECTION AND PROCESSING

Data may be collected on either punched cards or transcribed onto forms. The format for these operations is indicated in the accompanying illustrations. Since there are factors which are common to either method of data accumulation, certain parameters must be provided. Those which are rarely changed are the dead times, coincidence gate time, decay constant, and their respective errors, as well as probable error associated with the counting time and decay time. Parameters associated with each particular set of data are: data, sample withdrawal time, total number of data points, backgrounds, and errors in the background values. Each count must, of course, include identification, time counting started, counting time, and total number of counts in each channel. When an irradiated sample from the manganese bath is counted, pertinent information (in particular, the withdrawal time) is recorded on a chart such as in Fig. 51.

If the counting results must be taken down by hand, then it is transcribed onto a form such as in Fig. 52. The card types listed A, B, G, and F follow the format of Fig. 53. Card types A and B list the fundamental parameters; card G contains arbitrary identification of the problem set, date, sample-withdrawal time, number of F cards following, format identification (for handwritten data), and backgrounds with error estimates; card F has the actual data taken directly from the scalers with the essential chronology. The form in Fig. 52 has space for aliquot volume and other data characteristic of a particular run to be recorded, but this information is not carried over to the computer program.

Data automatically read out is punched directly onto cards of type E, shown in Fig. 53. The cumulative time and count time are in seconds. The "Code" has two purposes: (1) The last three columns are used to identify the channels in which the pertinent data are recorded, the other three channels being ignored by the computer program. When, for example, 126 is set into the code, then the machine program looks for A, B, AB (or β, γ, $\beta\gamma$) in that permutation of the three channels. (2) The other three columns (67, 68, and 69) can be used for any type of run identification; such usage is indicated in Table III.

Since the cumulative time is obtained from a constantly running meter which recycles every 100,000 sec, it is expedient to inform the computer that the clock-meter correspondence is punched on card type D. The meter can be reset to zero each day. Generally, for all the data accumulated in one day, it is necessary to put in one type C card advising of a "clock change" forthcoming in a D-type card immediately following in the deck. Accordingly, a typical stack of cards for automatic collection of data might consist of the following: one each of cards A and B followed by a C and D, and then any number of E cards. If a run with a different

RE-73 8/27/63 Ra-Be Irradiation History

Name of Run _____ Date _____

TIME	DATE	ITEM	INITIALS
_____	_____	Source inserted	_____
_____	_____	Source withdrawn	_____
_____	_____	Short collimator inserted	_____
_____	_____	Long collimator inserted	_____
_____	_____	Start pump	_____
_____	_____	Stop pump	_____
_____	_____	Liquid Level_____(Pump off)	_____
_____	_____	Temperature_____	_____
_____	_____	Liquid Level_____(Pump off)	_____
_____	_____	Temperature_____	_____
_____	_____	Add_____ml H_2SO_4	_____
_____	_____	Add_____ml H_2O_2	_____
_____	_____	Add_____ml H_2SO_4	_____
_____	_____	Add_____ml H_2O_2	_____
_____	_____	Draw sample 1	_____
_____	_____	Draw sample 2	_____
_____	_____	Draw sample 3	_____
_____	_____	Draw sample 4	_____
_____	_____	Draw sample 5	_____
_____	_____	Check clocks (_____=_____)	_____
_____	_____	Returned_____samples to sphere	_____
_____	_____	_____	_____
_____	_____	_____	_____

. . . . . .

COMMENTS:

Fig. 51

704 INPUT DATA

FORM II

COST CODE 44111-02-111-303

PROGRAM PROBLEM RE 258 ORIGINATOR A. DE VOLPI ( ) DATE PAGE OF

A													
B	PROBLEM NUMBER	DATE	SWT	NO. OF CARDS	FORMAT	B_A	$\sigma(B_A)$	B_B	$\sigma(B_B)$	B_{AB}	$\sigma(B_{AB})$		
G	3 4				-1								
	CARD NO.	SWT	START TIME	COUNT TIME	TOTAL COUNTS CH. A(β)	TOTAL COUNTS CH. B(γ)		TOTAL COUNTS CH. AB($\beta\gamma$)		PARAMETER	VARIABLE	ALIQUOT	
F													

PUNCH COLUMNS 1-60 ONLY FOR "F" CARDS

Fig. 52

704 INPUT DATA

FORM II

COST CODE _____

PROGRAM | PROBLEM RE 258 | ORIGINATOR | DATE | PAGE | OF

CARD TYPE

	1	2	3	4	5	6	7	8
A	τ_{RA}	τ_{RB}	τ_{ig}		$\sigma(\tau_{RA})$	$\sigma(\tau_{RB})$		
B	$\varphi(\tau_g)$	$\rho(\lambda)$	$\varphi(\tau_c)$	$\varphi(\tau_D)$				
C	CLOCK CHANGE	PROBLEM NUMBER	DATE	SWT	TIME FIRST CARD	TIME FINAL CARD	B_A	$\sigma(B_A)$	B_B	$\sigma(B_B)$	B_{AB}	$\sigma(B_{AB})$
D	METER TIME	CLOCK TIME										
E	CARD NO.	CUMULATIVE TIME	COUNT TIME	CH. 1	CH. 2	CH. 3	TOTAL COUNTS CH. 4	CH. 5	CH. 6	CODE		
F	CARD NO.	SWT	START TIME	COUNT TIME		CH. A	TOTAL COUNTS CH. B	CH. AB				
G	PROBLEM NUMBER		DATE	SWT	NO. OF CARDS	FORMAT	B_A	$\sigma(B_A)$	B_B	$\sigma(B_B)$	B_{AB}	$\sigma(B_{AB})$

AMD 9 61

Fig. 53

sample of the same isotope made up from the same irradiation, then a new C card and again any number of E cards may follow. It is not until there is some change of parameter or background that cards A and B need be reinserted in the deck. Manual operation requires similar handling of the cards.

TABLE III

CARD PUNCH CODE

	Liquid $\gamma\gamma$	Scintillation $\beta\gamma$	Parameter
0	-	-	-
1	Testing	Testing	HV - 1 channel
2	Stability	Stability	HV - common
3	Parameter Evaluation	Parameter Evaluation	Gate width
4	Intercalibration	Intercalibration	Discriminator
5	BG	BG	Delay
6	Concentration	-	-
7	A/F	-	-
8	N/F	-	-
9	Miscellaneous	Miscellaneous	Miscellaneous

SAMPLE NUMBER CODE: 34.xxxx

Manganese : 0001-0999	Liquid $\gamma\gamma$ { Mn Bath : 001-0099 / Rabbit : 0101-0199
Other Isotopes: 1001-	
	Scintillation $\beta\gamma$ Rabbit : 0201-0299
	Y^{88} (Cold) : 1001
	Y^{88} (Hot) : 1002
	Co^{60} : 2001
	Ni^{63} : 3001
	C^{14} : 3501
	Cs^{137} : 2501
	Al^{28} : 4001
	Au^{198} : 5001
	Na^{24} : 6001

In order to support the data obtained on cards and to provide supplementary information, a "data summary" sheet (not shown) is maintained. On this is written sample information, special variables, clock and running time data, and comments.

A summary follows of the equations handled by the IBM 704 program 1198/RE 258 (made up by G. Jensen of the Applied Mathematics Division). Briefly, first-order corrections are applied for dead-time losses, coincidence gains and losses, backgrounds, counting time, and decay time. A typical output (for a single card of data) is reproduced in Fig. 54. The first three calculations are of the corrected single-channel count rates at the time indicated. N is simply the disintegration rate referred to the time indicated. N(0) contains the value of N adjusted to the sample-withdrawal time. The output also reports the counting efficiencies. To simplify plotting, the errors are given in terms of their upper and lower limits. The computation of errors is actually one of the most useful features of the program. All errors are given as probable errors (0.6745 x standard error). About 68 data cards (type E or F) may be processed per minute of machine time.

```
1198/RE 258, DECAY CORRECTIONS FOR COINCIDENCE COUNTING
PROBLEM 34.0101, DATE 2.263, MANUAL FORM INPUT
BACKGROUND COUNT RATES/B(A) = 1.58000, B(B) = 1.96000, B(A,B) = 0.01800

 N(A) CALCULATIONS
CARD NUMBER   TIME          MEDIAN        UPPER LIMIT     LOWER LIMIT
        1.    1006.     0.1079E 04     0.1079E 04     0.1078E 04
 N(B) CALCULATIONS
CARD NUMBER   TIME          MEDIAN        UPPER LIMIT     LOWER LIMIT
        1.    1006.     0.2427E 04     0.2428E 04     0.2426E 04
 N(A,B) CALCULATIONS
CARD NUMBER   TIME          MEDIAN        UPPER LIMIT     LOWER LIMIT
        1.    1006.     0.5060E 02     0.5071E 02     0.5050E 02
 N CALCULATIONS
CARD NUMBER   TIME          MEDIAN        UPPER LIMIT     LOWER LIMIT
        1.    1006.     0.5173E 05     0.5185E 05     0.5162E 05
 N(0) CALCULATIONS
CARD NUMBER   TIME          MEDIAN        UPPER LIMIT     LOWER LIMIT
        1.    1006.     0.9101E 05     0.9121E 05     0.9081E 05
 EPSILON (B) CALCULATIONS
CARD NUMBER   TIME          MEDIAN        UPPER LIMIT     LOWER LIMIT
        1.    1006.     0.4691E-01     0.4907E-01     0.4476E-01
 EPSILON (A) CALCULATIONS
CARD NUMBER   TIME          MEDIAN        UPPER LIMIT     LOWER LIMIT
        1.    1006.     0.2085E-01     0.2298E-01     0.1872E-01
```

Fig. 54. Typical Computer Results for Mn^{56} Decay Corrections

Definitions

C_i = total counts in Channel i

t_c = counting time, sec

t_D = decay time

τ_{Ri} = dead time for channel i, sec (i = A,B)

i = A, B, and AB or β, γ, and $\beta\gamma$ unless restricted to A,B only

τ_g = coincidence gate time in seconds

B_i = background for channel i

λ = decay constant, sec^{-1}

$\sigma(\ )$ = probable error (0.6745 x standard error) for quantity in parenthesis

N_0 = disintegration rate computed

$\overline{N_0}$ = weighted mean of N_0

w_j = weighting factor for j^{th} value of N_0

$\Delta(\ )$ = probable error due to Poisson statistics

$\delta(\ )$ = probable error due to propagation of systematic errors

R_{0i} = uncorrected count rates

R_i = corrected count rates

ϵ_i = channel efficiencies

Computations

$$R_i = R_{0i}/(1 - R_{0i}\tau_{Ri}) \tag{D-1}$$

$$R_{0i} = C_i/t_c \tag{D-2}$$

$$R_{AB} = R_{0AB} - \tau_g R_A R_B \tag{D-3}$$

$$N_i = \lambda t_c\,(R_i - B_i)/(1 - e^{-\lambda t_c}) \tag{D-4}$$

$$\epsilon_A = N_{AB}/N_B \tag{D-5}$$

$$\epsilon_B = N_{AB}/N_A \tag{D-6}$$

$$N = N_A N_B/N_{AB} \tag{D-7}$$

$$N_0 = Ne^{\lambda t_D} \tag{D-8}$$

$$\sigma(C_i) = 0.6745\sqrt{C_i} \tag{D-9}$$

$$\sigma(R_i) = \sigma(C_i)/t_c \tag{D-10}$$

$$\sigma^2(R_i) = [\sigma^2(R_{0i}) + R_{0i}^4\,\sigma^2(\tau_{Ri})]/(1 - R_{0i}\,\tau_{Ri})^4 \quad ; \quad (i = A,B) \tag{D-11}$$

$$\sigma^2(R_{AB}) = \sigma^2(R_{0AB}) + (\tau_g R_{0A} R_{0B})^2 \{[\sigma(\tau_g)/\tau_g]^2 + [\sigma(R_{0A})/R_{0A}]^2 + [\sigma(R_{0B})/R_{0B}]^2\} \tag{D-12}$$

$$\sigma^2(N_i) = \sigma^2(R_i) + \sigma^2(B_i) + \sigma^2(e^{-\lambda t_c}) \tag{D-13}$$

$$\sigma^2(e^{-\lambda t_c}) = e^{-2\lambda t_c}\{[\lambda\sigma(t_c)]^2 + [t_c\,\sigma(\lambda)]^2\} \tag{D-14}$$

$$\sigma^2(N) = \Delta^2(N) + \delta^2(N) \tag{D-15}$$

$$\Delta^2(N) = N^2(2\epsilon_A\epsilon_B - \epsilon_A - \epsilon_B + 1)/C_{AB} \tag{D-16}$$

$$\delta^2(N) = N^2\{[\delta(N_A)/N_A]^2 + [\delta(N_B)/N_B]^2 + [\delta(N_{AB})/N_{AB}]^2\} \tag{D-17}$$

$$\delta^2(N_i) = \sigma^2(B_i) + \sigma^2(e^{-\lambda t_c}) + \delta^2(R_i) \tag{D-18}$$

$$\delta^2(R_{AB}) = (\tau_g R_{0A} R_{0B})^2 \{[\sigma(\tau_g)/\tau_g]^2 + [\sigma(R_{0A})/R_{0A}]^2 + [\sigma(R_{0B})/R_{0B}]^2\} \tag{D-19}$$

$$\delta^2(R_i) = R_{0i}^2\,\sigma^2(\tau_{Ri})/(1 - R_{0i}\,\tau_{Ri})^2 \quad (i = A,B) \tag{D-20}$$

$$\sigma^2(\epsilon_i) = \Delta^2(\epsilon_i) + \delta^2(\epsilon_i) \quad (i = A,B) \tag{D-21}$$

$$\Delta^2(\epsilon_i) = \epsilon_i^2(1 - \epsilon_i)/C_{AB} \tag{D-22}$$

$$\delta^2(\epsilon_A) = [\delta(N_{AB})/N_{AB}]^2 + [\delta(N_B)/N_B]^2 \tag{D-23}$$

$$\delta^2(\epsilon_B) = [\delta(N_{AB})/N_{AB}]^2 + [\delta(N_A)/N_A]^2 \tag{D-24}$$

$$\sigma^2(N_0) = e^{2\lambda t_D}\,\sigma^2(N) + N^2\,\sigma^2(e^{\lambda t_D}) \tag{D-25}$$

$$\sigma^2(e^{\lambda t_D}) = e^{2\lambda t_D}\{[\lambda\,\sigma(t_D)]^2 + [t_D\,\sigma(\lambda)]^2\} \tag{D-26}$$

$$\overline{N_0} = \sum_{j=1}^{n} N_{0j}\,w_j \Big/ \sum_{j=1}^{n} w_j \tag{D-27}$$

$$w_j = 1/\sigma^2(N_{0j}) \tag{D-28}$$

$$\sigma^2(\overline{N_0}) = 1 \Big/ \sum_{j=1}^{n} w_j \tag{D-29}$$

Appendix E

Mn^{56} DECAY TABLES

Because of the universal usefulness of Mn^{56} counting, some computer-produced decay tables are included in this appendix (Tables IV and V).

Table VI provides an estimate of the counting time required to obtain an equal number of counts when several samples are being counted in the same day. For example if the first sample yields a certain number of counts in 30 min, then it will require 34.5 min to obtain the same number of counts once again, 41 min for the third run, and so on. No provision has been made for background counting or time for changing samples, etc Table VI computations are valid only to a few per cent. One may interpolate for intermediate times.

TABLE IV

Mn^{56} $e^{-\lambda t}$ $\lambda = 0.0044829\ min^{-1}$

Minutes	0	1	2	3	4	5	6	7	8	9
00.	1.00000	.99553	.99107	.98664	.98223	.97783	.97346	.96911	.96477	.96046
10.	.95616	.95188	.94763	.94339	.93917	.93497	.93079	.92662	.99999	.91835
20.	.91424	.91015	.90608	.90203	.89800	.89398	.88998	.88600	.88204	.87809
30.	.87416	.87025	.86636	.86249	.85863	.85479	.85096	.84716	.84337	.83960
40.	.83584	.83210	.82838	.82468	.82099	.81732	.81366	.81002	.80640	.80279
50.	.79920	.79562	.79207	.78852	.78500	.78148	.77799	.77451	.77105	.76760
60.	.76416	.76075	.75734	.75395	.75058	.74723	.74388	.74056	.73724	.73395
70.	.73066	.72739	.72414	.72090	.71768	.71447	.71127	.70809	.70492	.70177
80.	.69863	.69551	.69240	.68930	.68622	.68315	.68009	.67705	.67402	.67101
90.	.66800	.66502	.66204	.65908	.65613	.65320	.65028	.64737	.64447	.64159
100.	.63872	.63586	.63302	.63019	.62737	.62456	.62177	.61899	.61622	.61346
110.	.61072	.60799	.60527	.60256	.59986	.59718	.59451	.59185	.58920	.58657
120.	.58395	.58133	.57873	.57614	.57357	.57100	.56845	.56591	.56337	.56085
130.	.55835	.55585	.55336	.55089	.54842	.54597	.54353	.54110	.53868	.53627
140.	.53387	.53148	.52910	.52674	.52438	.52204	.51970	.51738	.51506	.51276
150.	.51046	.50818	.50591	.50364	.50139	.49915	.49692	.49469	.49248	.49028
160.	.48809	.48590	.48373	.48157	.47941	.47727	.47513	.47301	.47089	.46879
170.	.46669	.46460	.46252	.46045	.45839	.45634	.45430	.45227	.45025	.44823
180.	.44623	.44423	.44225	.44027	.43830	.43634	.43439	.43244	.43051	.42858
190.	.42667	.42476	.42286	.42097	.41908	.41721	.41534	.41349	.41164	.40980
200.	.40796	.40614	.40432	.40251	.40071	.39892	.39714	.39536	.39359	.39183
210.	.39008	.38833	.38660	.38487	.38315	.38143	.37973	.37803	.37634	.37465
220.	.37298	.37131	.36965	.36799	.36635	.36471	.36308	.36145	.35984	.35823
230.	.35663	.35503	.35344	.35186	.35029	.34872	.34716	.34561	.34406	.34252
240.	.34099	.33947	.33795	.33644	.33493	.33343	.33194	.33046	.32898	.32751
250.	.32604	.32459	.32313	.32169	.32025	.31882	.31739	.31597	.31456	.31315
260.	.31175	.31036	.30897	.30759	.30621	.30484	.30348	.30212	.30077	.29942
270.	.29808	.29675	.29542	.29410	.29279	.29148	.29017	.28887	.28758	.28630
280.	.28502	.28374	.28247	.28121	.27995	.27870	.27745	.27621	.27497	.27374
290.	.27252	.27130	.27009	.26888	.26768	.26648	.26529	.26410	.26292	.26174

TABLE IV (Contd.)

Mn^{56} $e^{-\lambda t}$ $\lambda = 0.0044829\ min^{-1}$

Minutes	0	1	2	3	4	5	6	7	8	9
300.	.26057	.25941	.25825	.25709	.25594	.25480	.25366	.25252	.25139	.25027
310.	.24915	.24804	.24693	.24582	.24472	.24363	.24254	.24145	.24037	.23930
320.	.23823	.23716	.23610	.23505	.23399	.23295	.23191	.23087	.22984	.22881
330.	.22778	.22677	.22575	.22474	.22374	.22274	.22174	.22075	.21976	.21878
340.	.21780	.21682	.21585	.21489	.21393	.21297	.21202	.21107	.21013	.20919
350.	.20825	.20732	.20639	.20547	.20455	.20363	.20272	.20182	.20091	.20002
360.	.19912	.19823	.19734	.19646	.19558	.19471	.19384	.19297	.19211	.19125
370.	.19039	.18954	.18869	.18785	.18701	.18617	.18534	.18451	.18368	.18286
380.	.18204	.18123	.18042	.17961	.17881	.17801	.17721	.17642	.17563	.17485
390.	.17406	.17329	.17251	.17174	.17097	.17021	.16944	.16869	.16793	.16718
400.	.16643	.16569	.16495	.16421	.16348	.16274	.16202	.16129	.16057	.15985
410.	.15914	.15843	.15772	.15701	.15631	.15561	.15491	.15422	.15353	.15284
420.	.15216	.15148	.15080	.15013	.14946	.14879	.14812	.14746	.14680	.14614
430.	.14549	.14484	.14419	.14355	.14290	.14227	.14163	.14100	.14036	.13974
440.	.13911	.13849	.13787	.13725	.13664	.13603	.13542	.13481	.13421	.13361
450.	.13301	.13242	.13183	.13124	.13065	.13007	.12948	.12890	.12833	.12775
460.	.12718	.12661	.12605	.12548	.12492	.12436	.12381	.12325	.12270	.12215
470.	.12161	.12106	.12052	.11998	.11945	.11891	.11838	.11785	.11732	.11680
480.	.11628	.11576	.11524	.11472	.11421	.11370	.11319	.11268	.11218	.11168
490.	.11118	.11068	.11019	.10969	.10920	.10871	.10823	.10774	.10726	.10678
500.	.10630	.10583	.10536	.10488	.10442	.10395	.10348	.10302	.10256	.10210
510.	.10164	.10119	.10074	.10029	.09984	.09939	.09895	.09850	.09806	.09762
520.	.09719	.09675	.09632	.09589	.09546	.09503	.09461	.09419	.09376	.09334
530.	.09293	.09251	.09210	.09169	.09128	.09087	.09046	.09006	.08965	.08925
540.	.08885	.08846	.08806	.08767	.08727	.08688	.08650	.08611	.08572	.08534
550.	.08496	.08458	.08420	.08382	.08345	.08308	.08270	.08233	.08197	.08160
560.	.08123	.08087	.08051	.08015	.07979	.07943	.07908	.07872	.07837	.07802
570.	.07767	.07733	.07698	.07663	.07629	.07595	.07561	.07527	.07494	.07460
580.	.07427	.07394	.07360	.07328	.07295	.07262	.07230	.07197	.07165	.07133
590.	.07101	.07069	.07038	.07006	.06975	.06944	.06913	.06882	.06851	.06820

TABLE IV (Contd.)

Mn^{56} $e^{-\lambda t}$ $\lambda = 0.0044829\ min^{-1}$

Minutes	0	1	2	3	4	5	6	7	8	9
600.	.06790	.06759	.06729	.06699	.06669	.06639	.06610	.06580	.06551	.06521
610.	.06492	.06463	.06434	.06405	.06377	.06348	.06320	.06292	.06263	.06235
620.	.06208	.06180	.06152	.06125	.06097	.06070	.06043	.06016	.05989	.05962
630.	.05935	.05909	.05882	.05856	.05830	.05804	.05778	.05752	.05726	.05701
640.	.05675	.05650	.05625	.05599	.05574	.05549	.05525	.05500	.05475	.05451
650.	.05426	.05402	.05378	.05354	.05330	.05306	.05282	.05259	.05235	.05212
660.	.05189	.05165	.05142	.05119	.05096	.05074	.05051	.05028	.05006	.04983
670.	.04961	.04939	.04917	.04895	.04873	.04851	.04829	.04808	.04786	.04765
680.	.04744	.04722	.04701	.04680	.04659	.04638	.04618	.04597	.04577	.04556
690.	.04536	.04515	.04495	.04475	.04455	.04435	.04415	.04396	.04376	.04356
700.	.04337	.04317	.04298	.04279	.04260	.04241	.04222	.04203	.04184	.04165
710.	.04147	.04128	.04110	.04091	.04073	.04055	.04037	.04019	.04001	.03983
720.	.03965	.03947	.03930	.03912	.03894	.03877	.03860	.03842	.03825	.03808
730.	.03791	.03774	.03757	.03740	.03724	.03707	.03690	.03674	.03658	.03641
740.	.03625	.03609	.03593	.03576	.03560	.03545	.03529	.03513	.03497	.03482
750.	.03466	.03450	.03435	.03420	.03404	.03389	.03374	.03359	.03344	.03329
760.	.03314	.03299	.03284	.03270	.03255	.03241	.03226	.03212	.03197	.03183
770.	.03169	.03155	.03140	.03126	.03112	.03099	.03085	.03071	.03057	.03043
780.	.03030	.03016	.03003	.02989	.02976	.02963	.02949	.02936	.02923	.02910
790.	.02897	.02884	.02871	.02858	.02846	.02833	.02820	.02808	.02795	.02782
800.	.02770	.02758	.02745	.02733	.02721	.02709	.02696	.02684	.02672	.02660
810.	.02649	.02637	.02625	.02613	.02602	.02590	.02578	.02567	.02555	.02544
820.	.02532	.02521	.02510	.02499	.02487	.02476	.02465	.02454	.02443	.02432
830.	.02421	.02411	.02400	.02389	.02378	.02368	.02357	.02347	.02336	.02326
840.	.02315	.02305	.02295	.02284	.02274	.02264	.02254	.02244	.02234	.02224
850.	.02214	.02204	.02194	.02184	.02174	.02165	.02155	.02145	.02136	.02126
860.	.02117	.02107	.02098	.02088	.02079	.02070	.02061	.02051	.02042	.02033
870.	.02024	.02015	.02006	.01997	.01988	.01979	.01970	.01961	.01953	.01944
880.	.01935	.01927	.01918	.01909	.01901	.01892	.01884	.01875	.01867	.01859
890.	.01850	.01842	.01834	.01826	.01817	.01809	.01801	.01793	.01785	.01777
900.	.01769	.01761	.01753	.01746	.01738	.01730	.01722	.01715	.01707	.01699

TABLE V-A

Mn^{56} $e^{\lambda t}$ $\lambda = 0.0044829\ min^{-1}$

Minutes	0	1	2	3	4	5	6	7	8	9
00.	1.00000	1.00449	1.00901	1.01354	1.01809	1.02267	1.02726	1.03188	1.03651	1.04117
10.	1.04585	1.05055	1.05527	1.06001	1.06477	1.06956	1.07436	1.07919	1.08404	1.08891
20.	1.09380	1.09871	1.10365	1.10861	1.11359	1.11859	1.12362	1.12867	1.13374	1.13883
30.	1.14395	1.14909	1.15425	1.15944	1.16465	1.16988	1.17514	1.18042	1.18572	1.19105
40.	1.19640	1.20177	1.20717	1.21260	1.21805	1.22352	1.22902	1.23454	1.24008	1.24566
50.	1.25125	1.25687	1.26252	1.26819	1.27389	1.27962	1.28536	1.29114	1.29694	1.30277
60.	1.30862	1.31450	1.32041	1.32634	1.33230	1.33828	1.34430	1.35034	1.35640	1.36250
70.	1.36862	1.37477	1.38095	1.38715	1.39338	1.39964	1.40593	1.41225	1.41859	1.42497
80.	1.43137	1.43780	1.44426	1.45075	1.45727	1.46382	1.47039	1.47700	1.48364	1.49030
90.	1.49700	1.50372	1.51048	1.51727	1.52408	1.53093	1.53781	1.54472	1.55166	1.55863
100.	1.56563	1.57267	1.57973	1.58683	1.59396	1.60112	1.60832	1.61554	1.62280	1.63009

TABLE V-B

Mn^{56} $1/(1-e^{-\lambda t})$ $\lambda = 0.0044829\ min^{-1}$

Minutes	0	1	2	3	4	5	6	7	8	9
00.		223.575	112.036	74.8582	56.2692	45.1160	37.6806	32.3698	28.3868	25.2889
10.	22.8108	20.7832	19.0937	17.6641	16.4388	15.3769	14.4479	13.6281	12.8995	12.2476
20.	11.6610	11.1302	10.6478	10.2073	9.80355	9.43214	9.08933	8.77194	8.47725	8.20290
30.	7.94687	7.70738	7.48289	7.27202	7.07358	6.88650	6.70983	6.54274	6.38445	6.23430
40.	6.09168	5.95604	5.82687	5.70373	5.58620	5.47391	5.36652	5.26371	5.16521	5.07074
50.	4.98006	4.89296	4.80921	4.72865	4.65108	4.57634	4.50429	4.43478	4.36768	4.30286
60.	4.24022	4.17964	4.12103	4.06430	4.00934	3.95609	3.90447	3.85439	3.80580	3.75863
70.	3.71282	3.66831	3.62504	3.58297	3.54205	3.50223	3.46347	3.42572	3.38895	3.35312
80.	3.31820	3.28414	3.25093	3.21853	3.18690	3.15603	3.12588	3.09644	3.06768	3.03956
90.	3.01209	2.98522	2.95895	2.93324	2.90810	2.88349	2.85940	2.83581	2.81272	2.79009
100.	2.76793	2.74622	2.72493	2.70407	2.68362	2.66356	2.64388	2.62459	2.60565	2.58707

TABLE V-C

Mn^{56} $\qquad \lambda t \Big/ \left(1-e^{-\lambda t}\right)$ $\qquad \lambda = 0.0044829\ min^{-1}$

Minutes	0	1	2	3	4	5	6	7	8	9
00.	1.00000	1.00226	1.00450	1.00675	1.00900	1.01125	1.01351	1.01578	1.01804	1.02031
10.	1.02258	1.02486	1.02714	1.02942	1.03171	1.03400	1.03629	1.03859	1.04089	1.04319
20.	1.04550	1.04781	1.05012	1.05244	1.05476	1.05708	1.05941	1.06174	1.06407	1.06641
30.	1.06875	1.07109	1.07344	1.07579	1.07814	1.08050	1.08286	1.08523	1.08759	1.08996
40.	1.09234	1.09471	1.09709	1.09948	1.10186	1.10425	1.10665	1.10905	1.11145	1.11385
50.	1.11626	1.11867	1.12108	1.12350	1.12592	1.12834	1.13077	1.13320	1.13563	1.13807
60.	1.14051	1.14295	1.14540	1.14785	1.15030	1.15276	1.15522	1.15768	1.16015	1.16262
70.	1.16509	1.16757	1.17005	1.17253	1.17502	1.17751	1.18001	1.18250	1.18500	1.18750
80.	1.19001	1.19252	1.19503	1.19755	1.20007	1.20259	1.20512	1.20765	1.21018	1.21272
90.	1.21526	1.21780	1.22035	1.22290	1.22545	1.22801	1.23057	1.23313	1.23569	1.23826
100.	1.24084	1.24341	1.24599	1.24857	1.25116	1.25375	1.25634	1.25894	1.26153	1.26414

TABLE VI

COUNTING TIME* TO OBTAIN EQUAL NUMBER OF COUNTS: Mn^{56}

Δt_0 = initial counting interval

t_0 = starting time of initial counting interval

t_n = starting time of nth counting interval

Δt_n = counting time required starting at t_n to obtain equal counts as obtained in Δt_0 at t_0

$$e^{-\lambda \Delta t_n} = 1 - \left[e^{\lambda t_n} \left(1 - e^{-\lambda \Delta t_0} \right) \right]$$

t_n \ Δt_0	5	10	15	20	25	30	40	50	60
30	5.3	10.3	17.2	23.5	28	34.5	46	58	70
60	6.5	12.2	20	26.5	33.5	41	54	68	83
90	7.3	15.5	23	31.2	38.5	47	63	79	97
120	8.5	17.5	26	35.5	45	54	73	95	116
150	10	20.5	30.5	41.5	52	63	86	112	139
180	11.3	23.2	35	48	61.5	74	102	133	169
210	13	27	40.2	55.5	71	87	121	162	208
240	15	31	47	65	83	103	142	199	263
270	17	35.2	55	76	97.5	122	178	251	351
300	19.5	40.5	64	89	117	148	222	321	537
330	23	48	75	106	140	181	284	483	
360	25.5	55.7	88	126	169	223	388		

*All figures in minutes

Appendix F

SAMPLE PREPARATION

We present next an outline of procedures used in preparation of samples for intercalibration. The chief effort is directed towards preparing a set of liquid scintillator and 2-liter samples which may be reproducibly compared on the basis of delivered aliquot. A delicate balance has been reached so that the entire procedure is fully compatible. A short irradiation time in the CP-5 rabbit is necessary to avoid enhancement of high-energy neutron reactions; at the same time, the sample must not be too hot to handle by ordinary procedures. Only a small amount of powder may be irradiated in order to maintain a dilute ($\simeq$2.5 g/l) solution of high specific activity. Some peroxide and sulphuric acid must be added to retard the Szilard-Chalmers process. (An excess of $SO_4^=$ ion is made available, and MnO_2 already formed is promptly and efficiently reduced by the H_2O_2; this is a very important step in attaining reproducibility.)

Alcohol must be mixed in a high proportion with the aqueous solution in order to encourage the manganese-water molecular systems to remain in the liquid volume rather than to attach by surface tension effects to the walls of glassware, especially the scintillation vials. One effect of adsorption is to reduce geometry to 2π for a large fraction of the active manganese.

The solution is dispensed at a 1-ml capacity ultra-microburet,* and care is taken to maximize relative delivery accuracy. Normally, three scintillation samples are made up with about 50 λ of solution, and about 100 λ are given to the three 2-liter samples of water. These are the only quantitative steps required. The exact solution delivered is recorded to the nearest 0.1%, and the volume of the water sample is 2.000 $\pm$ 0.0005 liters by a thin-neck volumetric flask.

Preparation of these 6 samples requires about $1\frac{1}{2}$ hr and cleaning of glassware an additional $1\frac{1}{2}$ hr.

Preparation of Mn^{56} Samples

A. Irradiation

1. A Teflon vial is cleaned with doubly distilled H_2O and dried with acetone (CP).

2. 25 $\pm$ 5 mg of $MnSO_4 \cdot H_2O$ powder (CP) into the Teflon irradiation vial.

*Gilmont Ultramicro Buret, Manostat Corporation, 26 N. Moore St., New York 13

3. The sample is irradiated at CP-5 rabbit at 6 AM + 1 hr for 20 + 5 sec on day of use.

4. The vial is brought to D-316 by Special Materials handlers by ~9:30 AM.

5. The vial is checked with standard meter and the dilution factor determined (to yield ~10^4 d/s in liquid scintillator at ~11:00 AM). Present dilution formula is 18.8 ml:120 mr = x ml: daily reading in mr @ ~9:30.

B. Liquid Scintillator

1. p-dioxane scintillator consists of 1000 mg naphthalene(CP), 100 mg PPO (scintillator grade) and 10 ml p-dioxane (CP).

2. Cells are cleaned by rinsing with ethanol, washing in soapy H_2O, triple rinsing with distilled H_2O, and dried with ethanol.

3. $MnSO_4 \cdot H_2O$ powder emptied into ~10 ml distilled H_2O (according to dilution factor) with 12 (drops/100 ml) of conc H_2SO_4 and 12 drops/100 ml 30% H_2O_2.

4. 2 ml of $MnSO_4 \cdot H_2O$ solution mixed with 10 ml of ethanol.

5. Ultra-microburet tip is coated with silicone grease. Start of delivery is always based on liquid at tip with dial cranked several turns in ejection direction in order to take up gear slack. End of delivery is based on retrieval of solution from tip to midway up capillary tube and then return to tip again to take up gear slack. Interpolate 0.05 λ on dial reading.

6. Solution drawn into 1 ml capacity ultra-microburet should be at least 100 λ beyond calculated total delivery volume; the first 50 λ are discarded, and then ~50 λ are delivered into each liquid scintillator vial (already filled with p-dioxane scintillator).

7. Vial is topped off: ~11.8 ml scintillator total.

8. Usually 3 samples are made up.

9. Allow at least 2 full days to lapse before reusing vials: old solution can be dumped into drain after 1 or 2 days.

10. Care must be taken not to draw solution from region mercury sulfate formed in ultra-microburet.

C. Two-liter Sample

1. A two-liter polyethylene, bottle is washed in distilled H_2O and dried with acetone (CP). Allow at least 2 full days to lapse before reusing a bottle.

2. Add a total amount of water determined carefully from a standard volumetric flask to be 2.000 ± 0.0005 liters of distilled H_2O + 12 drops each H_2SO_4 and 30% H_2O_2 at 70-78°F.

3. ~100 λ are delivered from ultra-microburet into partly filled 100-ml beaker, using the same delivery techniques as in liquid scintillator sample. The solution in the beaker is then poured into the polyethylene bottle, and the beaker is rinsed 10 times with H_2O solution. The remaining H_2O solution is used to fill bottle.

4. The solution is thoroughly mixed in bottle and placed in an acid basket for toting.

5. Usually 3 samples are made up.

6. Old solution can be dumped into drain after 1 or 2 days.

7. Care must be taken not to draw solution from region where mercury sulfate has formed in ultra-microburet.

REFERENCES

1. R. D. Edge, Neutron Experiments with a Sensitive Szilard-Chalmers Detector, Austral. J. Phys., 9, 429-435 (1956).

2. D. C. Borg et al., Selective Radioactivation and Multiple Coincidence Spectrometry in the Determination of Trace Elements in Biological Material - Measurement of Manganese, Intl. J. Appl. Rad. and Iso., 110, 10-29 (1961).

3. P. Kienle and R. E. Segel, Decay of Co^{56} and Mn^{56}, Phys. Rev. 114, 1554-1560 (1959).

4. K. E. Plumlee and M. T. Wiggins, Automatic Foil Activity Counting Facility and Data-reduction Program, ANL-6628 (Oct 1962).

5. B. A. Loveridge and A. M. Thomas, Liquid Scintillation Counting of Aqueous Solutions, AERE-R2942 (1960).

6. D. L. Horrocks, Liquid Scintillation Counting of Inorganic Radioactive Nuclides, Packard Technical Bulletin, Packard Instrument Co., LaGrange, Ill. (March 1961).

7. A. Gandy, Préparation et é talonnage des sources radioactives de referénce, International Atomic Energy Agency, Vienna (1961).

8. P. J. Campion, The Standardization of Radioisotopes by the Beta-Gamma Coincidence Method Using High Efficiency Detectors, Intl. J. Appl. Rad. and Iso., 4, 232-248 (1959).

9. A. Gandy, Mesure Absolue de l'Activité des Radionuclides par las Méthode des Coincidences Béta-Gamma à l'Aide de Détecteurs de Grande Efficacité. Etude des Coincidences Instrumentaks, Intl. J. Appl. Rad. and Iso., 11, 75-91 (1961).

10. A. Gandy, Mesure Absolue de l'Activité des Radionuclides par la Méthode de Coincidences Béta-Gamma à l'Aide de Détecteurs de Grande Efficacité- Corrections de Gemps Morts, Intl. J. Appl. Rad. and Iso., 13, 501-513 (1962).

11. B. S. Dzhelepov and L. K. Peker, Decay Schemes of Radioactive Nuclei, Academy of Sciences of the USSR Press, Moscow (1958) (In Russian).

12. J. W. Meadows and J. F. Whalen, Thermal Neutron Absorption Cross Sections by the Pulsed Source Method, Nucl. Sci. and Eng., 9, 132-136 (1961).

13. V. B. Klimentov and V. M. Griazev, Some Neutron Resonance-Absorption Integrals, J. Nucl. Energy, 9, 20-27 (1959).

14. C. D. Hodgeman, (Editor), Handbook of Chemistry and Physics, Chemical Rubber Publishing Co., Cleveland, Ohio (1958).

15. Strominger et al., Table of Isotopes, Rev. Mod. Phys., 30, 585-904 (1958).

16. G. W. Leddicotte, The Radiochemistry of Manganese, National Academy of Sciences (NAS-NS-3018) OTS, Wash., D. C. (1960).

17. M. E. Rose, Internal Conversion Coefficients, North Holland Publishing Co., Amsterdam (1958).

18. Cook, C. Sharp, Gamma Radiation Following the Decay of Mn^{56} and the Energy Levels of Fe^{56}, Nucl. Phys., 7, 480-487 (1958).

19. L. V. Groshev et al., Investigation of Gamma Rays Emitted from Vanadium, Manganese, Cobalt, and Aluminum Nuclei after Thermal Neutron Capture, Atomnaya Energiya, 3, 187-203 (1957).

20. J. A. DeJuren et al., Absolute Calibration of the National Bureau of Standards Photoneutron Standard: I, J. Research Natl. Bur. Standards, 55, No. 2 (Aug 1955).

21. J. DeJuren and J. Chin, Absolute Calibration of the National Bureau of Standards Photoneutron Standard: II. Absorption in Manganese Sulphate, ibid., 55, No. 6 (Dec 1955).

22. R. Caswell et al., Recent Developments in Neutron Source Standardization, Symposium on Neutron Detection, Dosimetry, and Standardization, Paper SM-36/80 (International Atomic Energy Agency Symposium held Dec 1962 at Harwell, U. K.).

23. R. Richmond and B. J. Gardner, Calibration of Spontaneous Fission Neutron Sources, AERE R/R 2097 (1957).

24. R. L. Macklin et al., Manganese Bath Measurements of η of U^{233} and U^{235}, Nucl. Sci. and Eng., 8, 210-220 (1960).

25. E. J. Axton and P. Cross, The Establishment of an Absolutely Calibrated Neutron Source, Reactor Science and Technology, 15, 22-27 (1961).

26. C. G. Bell, Jr. and F. N. Hayes, (Editors), Liquid Scintillation Counting, (Proceedings of a conference held at Northwestern University, August 20-21, 1957), New York, Pergamon Press (1958).

27. E. Rapkin, Liquid Scintillation Measurement of Radioactivity in Heterogeneous Systems, Packard Technical Bulletin, Packard Instrument Company, LaGrange, Illinois (July 1960).

28. L. S. Myers and A. H. Brush, Counting of Alpha and Beta Radiations in Aqueous Solutions by the Detergent-Anthracene Scintillation Method, UCLA-484 (July 28, 1961).

29. A. R. Ronzio, Metal Loaded Scintillator Solutions, Intl. Jour. Appl. Rad. and Iso., 4, 196-200 (1959).

30. D. L. Horrocks and M. H. Studier, Determination of the Absolute Disintegration Rates of Low Energy Beta Emitters in a Liquid Scintillation Spectrometer, Anal. Chem., 33, 615-620 (1961).

31. F. N. Hayes, Liquid Solution Scintillators, LA-1639 (May 12, 1954).

32. E. Schram and R. Lombaert, Organic Scintillation Detectors. Counting of Low-energy Beta Emitters, Elseview Publishing Co., New York (1963).

33. J. Steyn and Haasbroek, The Application of Internal Liquid Scintillation Counting to a 4π β-γ Coincidence Method for the Absolute Standardization of Radioactive Nuclides, Proc. 2nd UN Intl. Conf. on Peaceful Uses of Atomic Energy, Geneva, Switzerland, 21, 95 (1958).

34. K. W. Geiger and G. N. Whyte, Absolute Standardization of Radioactive Neutron Sources. I. Activation of Manganese Bath, Can. J. Phys., 37, 256-262 (1959).

35. J. L. Putman, Limitations and Extensions of the Coincidence Method for Measuring the Activity of $\beta\gamma$ Emitters, AERE-I/M-26 (1953).

36. Metrology of Radionuclides, International Atomic Energy Agency, Vienna (1960).

37. G. D. O'Kelly, (Editor), Applications of Computers to Nuclear and Radiochemistry, Proceedings of a Symposium, Gatlinburg, Tenn., October 1962, NAS-NS-3107, Office of Technical Services, Dept. Commerce, Washington 25, D. C.

38. R. J. Epstein, Proceedings of "Argonne Accelerator Users' Group Meeting," Argonne National Laboratory, Argonne, Ill., Nov 9-10, 1962, p. 28.

39. E. Fairstein et al., A Pulse Crossover Pickoff Gate for Use with a Medium-speed Coincidence Circuit, ORNL-2480 (1958).

ACKNOWLEDGMENTS

The authors are indebted to a large number of the personnel of the Reactor Physics Group, both staff and technicians, for assistance in this project. Some of those closely involved are Fred Ozer and Mike Fontana, who operate the equipment daily; June Hamilton, who prepares the active samples; Vic Burke and Gerry Lowe, now no longer with this project; Ed Kimont, who provides able direction of manpower; Clare Kotora, in charge of shop construction; Roland Armani, who is cooperating in an intercomparison program; the late Stephan Kaufmann, who had always encouraged the authors' endeavors; and the many staff members who have helped with irradiations of samples in times of need: Karl Plumlee, Ed Bennett, Jack Haugsnes, and Quincy Baird.

Very valuable advice and some samples of low-energy beta emitters have been given freely by Don Horrocks of the Chemistry Division.

Jerri Jensen of Applied Mathematics Division is responsible for programming of the coincidence equations and following through on the reams of data which have passed through her hand, first in the form of raw data and back to the authors in the form of neat results.

We also take this opportunity to express our appreciation to Bill Kaiser's group for packaging NaI(Tl) crystals and providing phototubes.